Université du Québec
Institut National de la Recherche Scientifique
Centre Énergie, Matériaux et Télécommunications

Fiber-optics reconfigurable temporal intensity optical pulse shaping using chromatic dispersion: methods and applications

Par

Jeong Hyun Huh

Thèse présentée pour l'obtention du grade de
Doctorat en Télécommunication, Ph.D.

Jury d'évaluation

Président du jury et examinateur interne	Jinyang Liang INRS-EMT, Canada
Examinateur externe	Shulabh Gupta Carleton University, Canada
Examinateur externe	Joshua Schwartz Trinity University, USA
Directeur de recherche	José Azaña INRS-EMT, Canada

REMERCIEMENTS

To begin, I would like to deeply thank my parents, Mr. Huh, Bong Moo and Ms. Hwang, Soon Young, for their love and support throughout my life. They have always believed in me and they always provide me with wise advice. I also thank my brother and sister, Jeung Jae and Haeri, for their positive influence on me.

I have been extremely fortunate since I joined the UOP group and I would like to express my biggest gratitude to Prof. José Azaña who gave me the opportunity to work with him and who has supported me throughout my Ph.D study. His great leadership and valuable lessons encouraged me persevere and guided me to the right path. It has been such an honor to work with a great scientist and kind person like him.

I would like to thank my dear group members : Reza Ashrafi, Maurizio Burla, María del Rosario Fernández Ruiz, Hamed Pishvai Bazargani, Reza Maram, Bo Li, Lei Lei, Luis Romero Cortés, Mohamed Seghilani, Xiao-Zhou Li, Jinwoo Jeon, Benjamin Crockett, Sai krishna reddy, Saket Kaushal, and Robin Helsten. Thank you for your warm friendship and support.

Additionally, I would like to thank my friends in Korea, Canada, and the UK for their friendship and help, as well as the staff from the INRS-EMT for their support.

I truly appreciate the evaluation committee for my Ph.D. Thesis: Prof. Jinyang Liang, Prof. Joshua Schwartz, and Prof. Shulabh Gupta. Thank you for your time and efforts in reviewing my Thesis.

Finally, I thank the Natural Sciences and Engineering Research Council of Canada (NSERC), le Fonds Québécois de la Recherche sur la Nature et les Technologies (FQRNT), and Institut National de la Recherche Scientifique – Énergie, Matériaux et Télécommunications (INRS-EMT), for providing the funding which allowed me to undertake this Ph.D. research.

ABSTRACT

Optical pulse shaping methods have been developed over the past decades as a key enabling technology for ultrafast science and technology. These techniques enable precise synthesis and control of the temporal shape of optical pulses with durations down to the femtosecond regime, allowing high-speed processing of optical signals without the need of an optical to electrical converter (OEC), as well as generation of ultrafast arbitrary optical waveforms according to user specifications. The latter is of great interest for a broad range of applications, including ultrafast optical telecommunication and information processing, spectroscopy, nonlinear fiber optics, and high-field physics, among many others. The focus of this thesis is on picosecond pulse shaping, and the methods at the core of the work are mainly based on linear photonics signal processing since this approach provides not only simple configurations but also higher energy efficiency than nonlinear photonics signal processing and superior noise performance.

In a linear optical pulse shaper, arbitrary waveforms are typically synthesized based on a direct Fourier-domain technique, where the spectrum of a short optical pulse is re-shaped according to the Fourier transform of the target temporal waveform. A customized optical filter is used for this purpose, with a linear spectral response that is simply obtained from the relationship between the input optical spectrum and the target. However, the direct Fourier-domain synthesis method has two critical limitations: First, the maximum duration of the generated pulses is limited by the finest frequency resolution of the pulse shaper or filter, typically below ~10 GHz and shorter than 100 ps for the maximum duration. Moreover, the spectral coverage of the output pulse is dictated by the target pulse duration and as such, for synthesis of long temporal waveforms, a large portion of the input pulse spectrum, i.e., its energy, may need to be filtered out. Thus, the energy efficiency of the process is severely reduced for the synthesis of longer pulse durations, an issue that can be of critical importance for many applications, particularly those that exploit nonlinear effects.

The photonic implementation of the spectral filtering stage is another main topic of research. Previously reported photonic signal processors are usually designed to perform a specific function with none or very limited programmability. For general-purpose signal generation and processing, however, a photonic signal processor should be able to perform multiple functions with high reconfigurability. The design concept of the most widely used reconfigurable optical pulse shaper is based on free-space optical processing. In this approach, the spectral components of an incident optical pulse are first decomposed angularly (e.g., by bulk-optics diffraction gratings), focused, and then linearly modulated by spatial amplitude and/or phase masks. By using programmable spatial light modulators (SLMs) or acoustic-optic modulators (AOMs), reconfigurable optical pulse shapers have been successfully demonstrated with resolutions well into the femtosecond range. Central constraints of this approach include the need for an efficient coupling between fiber and free-space optics, and the requirement for multiple spatially-separated modulation points, which translate into a relatively lossy and bulky configuration. In addition, the approach is constrained by the limited update rate of SLMs, typically below the kHz range for liquid-crystal SLMs and a few tens of kHz for acoustic-optic modulators (AOMs).

The main objective of this Thesis is to develop linear optics methods for high-speed reconfigurable temporal intensity optical pulse shaping systems in order to overcome the limitations of conventional approaches and explore innovative applications. Generally, the proposed techniques in this Thesis are based on fiber-optics dispersion-induced frequency-to-time mapping (FTM) combined with spectral amplitude and/or phase modulation of either coherent or incoherent light

waves. Dispersion induced FTM is the time-domain analogue of spatial-domain Fraunhofer diffraction in the far-field, where the input signal's frequency components are linearly distributed along the time-domain by the mere process of linear chromatic dispersion. In Chapter 2, a novel linear-optics method for reconfigurable optical pulse shaping based on dispersive FTM is proposed for overcoming the above-mentioned critical limitations of the direct Fourier-domain technique. This method can provide a greatly increased flexibility to achieve a desired pulse duration, independently of the frequency resolution of the linear spectral shaping stage, while enabling an optimization of the energy efficiency of the shaping process for any target pulse duration. High-quality parabolic optical pulses with a temporal duration ranging from ~25 ps to ~400 ps are generated using the proposed optical pulse shaping method, and these are utilized for realization of an optically programmable time-lens (an important basic building block for temporal optical signal processing) through nonlinear cross-phase modulation (XPM). In Chapter 3, an all-fiber simple configuration is demonstrated for fully arbitrary (including asymmetric) programmable picosecond optical pulse shaping in the picosecond regime. The method is based on multi-level phase-only filtering, which is programmed directly in the time domain using a single high-speed electro-optic phase modulator. This time-domain optical pulse shaper provides the unique, additional capability of achieving high-speed pulse-shape update rates into the sub-GHz range, and solid potential for integration. Chapter 4 deals with an incoherent light temporal shaping system where the temporal shape of the output waveform is determined by the cross-correlation between the spectrum of a broadband incoherent light and a temporal intensity modulation pattern, exploiting the concept of dispersion-induced time-spectrum convolution. The process is specifically designed and developed for demonstration of a practically relevant application, namely reconfigurable real-time identification of optical spectrum patterns, e.g., for dynamic spectroscopy or related uses. This operation is implemented by simply programming the temporal modulation signal to match the target spectral pattern and, in the proof-of-concept experiments, near-infrared spectral pattern recognition is achieved directly in the optical domain without the need for any further numerical post-processing at an update rate of 650 kHz, over a bandwidth of 1.5 THz with a spectral resolution of ~12 GHz. The conducted research can provide useful guidelines for practical realization of dispersion-based optical pulse shaping technologies as well as contribute to the development of novel fiber-optics photonics signal processors and their numerous applications.

RÉSUMÉ

A. Introduction

Les méthodes de mise en forme des impulsions optiques ont été développées au cours des dernières décennies comme une technologie clé pour la science et la technologie ultra-rapides [1,2]. Ces techniques permettent une synthèse et un contrôle précis de la forme temporelle des impulsions optiques avec des durées allant jusqu'au régime femtoseconde, ce qui permet un traitement à grande vitesse des signaux optiques sans avoir besoin d'un convertisseur optique-électrique (OEC, pour 'optical to electrical converter'), ainsi que la génération de formes d'ondes optiques arbitraires ultra-rapides selon les spécifications de l'utilisateur. Ce dernier est d'un grand intérêt pour une large gamme d'applications, y compris les télécommunications optiques ultra-rapides et le traitement de l'information, la spectroscopie, la fibre optique non linéaire et la physique de champ élevé, parmi tant d'autres [1,2]. L'accent de cette thèse est mis sur la mise en forme des impulsions picosecondes, et les méthodes au cœur du travail sont principalement basées sur le traitement linéaire du signal photonique puisque cette approche fournit non seulement des configurations simples mais aussi une meilleure efficacité énergétique et des performances supérieures en matière de bruit.

Dans un générateur d'impulsions optiques linéaires, les formes d'ondes arbitraires sont généralement synthétisées sur la base d'une technique directe du domaine de Fourier, où le spectre d'une impulsion optique courte est refaçonné en fonction de la transformée de Fourier de la forme d'onde temporelle cible. Un filtre optique personnalisé est utilisé à cette fin, avec une réponse spectrale linéaire qui est simplement obtenue à partir de la relation entre le spectre optique d'entrée et celui de la cible. Cependant, la méthode de synthèse directe dans le domaine de Fourier a deux limites critiques : Premièrement, la durée maximale des impulsions générées est limitée par la résolution en fréquence la plus fine du générateur d'impulsions ou du filtre, généralement inférieure à ~10 GHz [3]. De plus, la couverture spectrale de l'impulsion de sortie est dictée par la durée de l'impulsion cible et, en tant que telle, pour la synthèse de longues formes d'onde temporelles, une grande partie du spectre d'impulsion d'entrée, c'est-à-dire son énergie, peut devoir être filtrée. Ainsi, l'efficacité énergétique du procédé est fortement réduite pour la synthèse de durées d'impulsion plus longues, une question qui peut être d'une importance critique pour de nombreuses applications, en particulier celles qui exploitent les effets non linéaires [4].

La mise en œuvre photonique de l'étape de filtrage spectral est un autre sujet de recherche principal. Les processeurs de signaux photoniques rapportés précédemment sont généralement conçus pour exécuter une fonction spécifique avec une programmabilité nulle ou très limitée. Pour la génération et le traitement de signaux à usage général, cependant, un processeur de signaux photoniques devrait être capable d'exécuter de multiples fonctions avec une reconfigurabilité élevée. Le concept de du générateur d'impulsions optiques reconfigurables le plus largement utilisé est basé sur un traitement optique en espace libre [1,2]. Dans cette approche, les composantes spectrales d'une impulsion optique incidente sont d'abord décomposées angulairement (par exemple, par des réseaux de diffraction optique en vrac), focalisées, puis modulées linéairement par des masques d'amplitude spatiale et/ou de phase. En utilisant des modulateurs de lumière spatiale programmables (SLMs, pour 'spatial light modulators') ou des modulateurs acoustico-optiques (AOMs, pour 'acoustic-optic modulators'), des générateurs d'impulsions optiques reconfigurables ont été démontrés avec succès avec des résolutions bien dans la gamme des femtosecondes [1,2]. Les contraintes centrales de cette approche comprennent la nécessité d'un couplage efficace entre les fibres optiques et les optiques en espace libre, et l'exigence de multiples points de modulation séparés spatialement, ce qui se traduit par une augmentation des pertes et une configuration encombrante. En outre, l'approche est limitée par le taux de mise à jour restreint des SLM, généralement inférieur à la gamme de kHz pour les SLM à cristaux liquides et de quelques dizaines de kHz pour les modulateurs acoustico-optiques (AOM) [5].

B. Contributions originales

L'objectif central de cette thèse est de développer des méthodes d'optique linéaire pour la mise en forme *reconfigurable* et de haute vitesse de l'intensité temporelle d'impulsions optiques (OPS, pour 'optical pulse shaping'), de préférence implémentées dans les technologies de fibres optiques, qui peuvent surmonter les limites centrales des approches les plus conventionnelles, telles que définies ci-dessus. Un autre objectif connexe est d'explorer des applications novatrices qui exploitent les fonctions améliorées offertes par les nouvelles plates-formes OPS. Les différentes approches explorées dans la thèse sont basées sur la combinaison de deux concepts : (i) la projection optique des fréquences dans le temps (FTM, pour 'frequency-to-time mapping') induite par dispersion. (ii) la modulation d'amplitude spectrale et/ou de phase d'ondes lumineuses à large bande cohérentes ou incohérentes. Le FTM induit par dispersion est l'analogue dans le domaine temporel de l'effet de diffraction de Fraunhofer dans le domaine spatial dans le champ lointain, dans lequel les

composantes de fréquence du signal d'entrée sont distribuées linéairement le long du domaine temporel. Les contributions spécifiques de cette thèse à l'objectif global défini sont les suivantes :

- Une nouvelle méthode d'optique linéaire pour OPS reconfigurable basée sur le FTM dispersif est proposée qui nous permet de surmonter les limitations critiques mentionnées de la technique du domaine de Fourier direct [4]. Les contraintes liées à la durée d'impulsion minimale des méthodes FTM conventionnelles imposées par la condition temporelle de champ lointain sont grandement assouplies par l'émulation d'un processus à lentille temporelle simultanément avec le filtrage de l'intensité spectrale cible, en utilisant un seul dispositif de mise en forme spectrale optique standard. Il est démontré que cette méthode offre une flexibilité considérablement accrue pour obtenir une durée d'impulsion souhaitée, indépendamment de la résolution en fréquence de l'étage de mise en forme spectrale linéaire, ainsi qu'une optimisation de l'énergie de la forme d'onde pour n'importe quelle durée d'impulsion cible. Ce travail est centré sur la synthèse et le contrôle des formes d'ondes optiques paraboliques (quadratique), qui sont ici synthétisées expérimentalement sur une plage de durée temporelle sans précédent, de ~25ps à ~400ps, tout en ayant une puissance optique de sortie jusqu'à ~4 dBm sans utiliser aucune amplification. Des impulsions paraboliques de haute fidélité sont générées à partir du générateur d'impulsions optiques proposé, et utilisées pour la création d'une plate-forme programmable de traitement de signaux à base de lentilles temporelles induites par XPM (XPM, pour ‘cross-phase modulation’). Le facteur de pépiement optiquement programmable est une caractéristique unique de la lentille temporelle à base de XPM, rendue possible par la polyvalence de la technologie de mise en forme d'impulsions paraboliques développée, ce qui évite également d’avoir recours aux lentilles temporelles à base du mélange a quatre ondes (FWM, pour four wave mixing) qui nécessite des conditions d’adaptation de phase très strictes.
- De plus, le concept FTM dispersif permet une configuration toute fibre simple pour un générateur d'impulsions optiques reconfigurable où le filtrage spectral est effectué dans le domaine temporel, ce qu'on appelle les systèmes de mise en forme spectrale dans le domaine temporel (TDSS, pour ‘time-domain spectral shaping’). La conception du TDSS est une solution prometteuse à certaines des limites les plus critiques des approches dans le domaine spatial, telles que définies ci-dessus, permettant des taux de mise à jour rapide de la forme des impulsions dans la gamme des sous-GHz, et un solide potentiel d'intégration. De plus, le système OPS dans le domaine temporel permet la synthèse de formes d'impulsions optiques

picosecondes entièrement arbitraires (y compris asymétriques). Ceci est obtenu grâce à l'utilisation *d'un filtrage multi-niveaux à phase seule*, qui est programmé directement dans le domaine temporel à l'aide d'un seul modulateur de phase à grande vitesse, piloté par un générateur électronique de formes d'ondes arbitraires (E-AWG, pour ‘electronic arbitrary waveform generator’). Le système démontré offre la possibilité de synthétiser des profils d'intensité temporelle de haute qualité, entièrement arbitraire (y compris asymétrique), avec des résolutions en régime picoseconde et plus. Dans les expériences de preuve de concept rapportées, je montre la synthèse de formes d'ondes d'intensité triangulaires asymétriques de haute qualité, de séquences de codes d'impulsions avec une modulation on-off (OOK, pour ‘on-off keying’) de 150 Gbit/s et une modulation d'amplitude d'impulsions de 300 Gbit/s à 4 niveaux (PAM-4) (PAM, pour ‘pulse amplitude modulation’), avec une résolution temporelle de ~ 2 ps sur une fenêtre temporelle allant jusqu'à ~ 60 ps (correspondant à un TBP (TBP, pour ‘time-bandwidth product’) d'environ 30).

- Le chapitre E traite de l'analyse et de l'application novatrice d'un système de mise en forme temporelle de la lumière incohérente dans lequel la forme temporelle de l'onde de sortie est déterminée par la convolution entre la forme spectrale dans le temps d'une source de lumière incohérente à large bande et un modèle de modulation d'intensité temporelle, c'est-à-dire l'exploitation du concept de convolution temporelle induite par dispersion (TSC, pour ‘time-spectrum convolution’). Comme contribution principale, cette partie du travail explore le potentiel de cette méthode pour traiter les spectres incohérents des ondes lumineuses (plutôt que les signaux temporels), en particulier pour l'identification en temps réel reconfigurable d'un modèle de spectre optique prescrit. Ceci est obtenu grâce à une conception appropriée du signal de modulation temporelle qui est programmé dans un E-AWG, évitant entièrement la nécessité d'un post-traitement numérique supplémentaire. Dans les expériences de validation de concept, j'ai démontré expérimentalement la reconnaissance spectrale à un taux d'identification de 650 kHz, sur une bande passante de 1,5-THz avec une résolution en fréquence d'environ 12 GHz dans le régime de rayonnement proche infrarouge (NIR, pour ‘near infrared radiation’).

C. Génération d'impulsions paraboliques de haute qualité et leurs applications

C.1. Génération d'impulsions paraboliques de haute qualité avec une durée et une énergie optimisée par l'utilisation d'une projection fréquence-temps dispersive

Une impulsion optique avec un profil d'intensité parabolique, où l'intensité dans le domaine temporel est proportionnelle au carré de temps, et un pépiement de fréquence linéaire est bien connu pour sa capacité à résister à l'effet nuisible du brise-ondes optiques dans un régime de dispersion normal [6]. Ainsi, les impulsions paraboliques ont attiré beaucoup d'attention au fil des ans pour un large éventail d'applications, y compris l'amplification d'impulsions de puissance élevée et la génération d'impulsions ultra-courtes [7], le développement de sources de continuum hautement cohérentes [8], la synthèse d'impulsions personnalisée [9] et la compression spectrale [10]. Les techniques de mise en forme d'impulsions linéaires sont basées sur la méthode directe du domaine de Fourier, par exemple, en utilisant des SSFBG (SSFBG, pour 'super-structured fiber Bragg grating'), des dispositifs acousto-optiques, et des réseaux de guides d'ondes (AWGs, pour 'arrayed waveguide gratings') [2, 11]. Dans cette technique, le spectre d'une impulsion optique courte est refaçonné en fonction de la transformée de Fourier de la forme d'onde temporelle cible. Cependant, la synthèse directe dans le domaine de Fourier des impulsions paraboliques a deux limites critiques. Premièrement, la durée maximale des impulsions générées est limitée par la résolution spectrale la plus fine du générateur d'impulsions. Les méthodes typiques de mise en forme d'impulsions offrent des résolutions de fréquence supérieures à 10 GHz [11], ce qui a limité la génération linéaire expérimentale d'impulsions paraboliques à des durées inférieures à 100ps. Des durées d'impulsion plus longues sont cependant nécessaires pour une série d'applications importantes, plus particulièrement pour des lentilles temporelles appliquées à de longues séquences d'impulsions optiques [12]. De plus, dans les méthodes de synthèse directe dans le domaine de Fourier, la largeur spectrale de l'impulsion parabolique de sortie est dictée par la durée de l'impulsion cible et, par conséquent, une grande partie du spectre d'impulsion d'entrée, c'est-à-dire l'énergie, peut devoir être filtrée. Encore une fois, l'efficacité énergétique est réduite pour des durées d'impulsion plus longues, un problème qui peut être d'une importance vitale pour un grand nombre d'applications, par exemple, pour des applications impliquant des effets optiques non linéaires.

Nous proposons et démontrons une nouvelle méthode d'optique linéaire pour la génération d'impulsions paraboliques capable de surmonter les limites critiques des approches précédentes. La

méthode proposée offre une flexibilité considérablement accrue pour obtenir une durée d'impulsion parabolique souhaitée, indépendamment de la résolution en fréquence de l'étage de mise en forme spectrale linéaire. Cette méthode est basée sur la projection fréquence-temps induite par dispersion (FTM), y compris la possibilité d'incorporer une lentille temporelle virtuelle afin d'assouplir davantage les contraintes imposées par la condition de champ lointain [13].

La projection linéaire de la fréquence dans le domaine du champ-lointain (FF-FTM, pour 'far-field FTM'), qui est l'analogue dans le domaine temporel de la diffraction de Fraunhofer dans le domaine spatial en champ-lointain, implique essentiellement une distribution linéaire des composantes de fréquence du signal d'entrée le long du domaine temporel, qui est induite par la variation de vitesse du groupe linéaire en fonction de la fréquence optique qui est caractéristique d'un milieu dispersif de second ordre prédominant. Après un certain degré de propagation dans ce milieu dispersif, on s'attend à ce que le profil d'intensité temporelle de sortie soit étroitement lié à la forme du spectre d'impulsions d'entrée. En utilisant ce phénomène, les impulsions paraboliques peuvent être simplement générées en façonnant le spectre d'impulsions d'entrée pour qu'il soit parabolique, suivi d'une propagation à travers un milieu dispersif. Puisque la largeur d'impulsion générée est proportionnelle à la largeur spectrale et à la quantité de dispersion, la méthode FTM proposée permet d'utiliser la majeure partie du spectre d'énergie d'impulsion d'entrée, indépendamment de la durée cible ou de la largeur de bande de la source d'impulsion d'entrée, en optimisant uniquement la quantité de dispersion. Toutefois, la nécessité de satisfaire à une condition équivalente de champ-lointain restreint la durée minimale des impulsions qui peuvent être générées avec une qualité suffisamment élevée en utilisant le système proposé. La durée d'impulsion réaliste devrait généralement être 25 fois plus longue que la durée d'impulsion d'entrée [4].

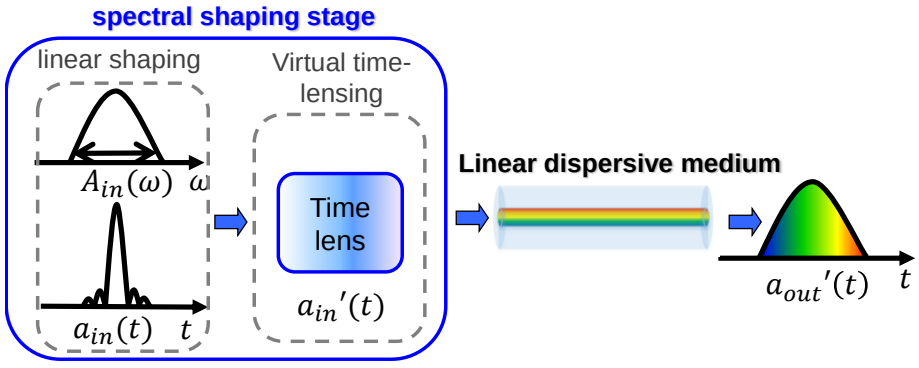

Figure 1 **Schéma de génération d'impulsions paraboliques proposées sur la base du NF-FTM.**

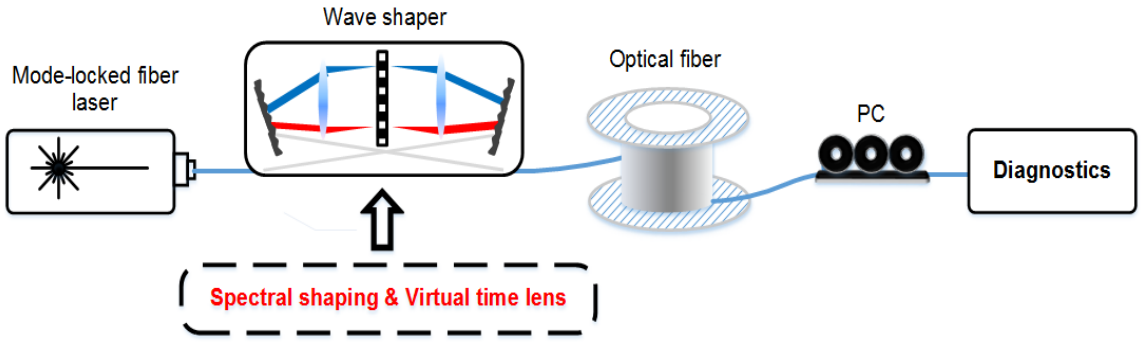

Figure 2 **Installation expérimentale utilisée pour la génération d'impulsions paraboliques. Un contrôleur de polarisation (PC) a été utilisé pour ajuster l'état de polarisation, selon les besoins pour le fonctionnement du diagnostic temporel (oscilloscope d'échantillonnage optique non linéaire).**

Un moyen efficace de surmonter la contrainte décrite de la méthode FF-FTM consiste à utiliser un processus de lentille temporelle, c'est-à-dire la contrepartie temporelle de la production de la transformée de Fourier désirée dans le plan focal d'une lentille spatiale. La figure 1 montre un schéma de la méthode proposée. Cette approche est connue sous le nom de projection fréquence-temps en champ proche (NF-FTM, pour 'near-field FTM'). La conception spécifique de la génération d'impulsions paraboliques basée sur FF-FTM et NF-FTM a été introduit et décrit analytiquement dans [4]. Figure 2 montre le montage expérimental pour la génération d'impulsions paraboliques avec des durées allant de ~25 ps à ~400 ps. Les impulsions optiques initiales ont été générées à partir d'un laser à fibre à verrouillage de mode actif produisant des impulsions de type gaussien de ~2 ps (largeur à mi-hauteur (FWHM, pour 'Full Width Half Maximum')) à une fréquence de répétition de ~10 GHz. La puissance d'impulsion d'entrée était d'environ 10 dBm et la longueur d'onde centrale était de 1550,2 nm. La source d'entrée a été transformée spectralement en spectres complexes désirés en utilisant un générateur d'impulsions optiques en espace libre (Finisar WaveShaper 4000S, résolution >10 GHz). Le milieu dispersif a été créé par une simple combinaison de fibres optiques monomodes facilement disponibles.

Des impulsions paraboliques d'une durée de 400 ps ont été générées en utilisant l'approche FF-FTM (Fig. 3) et des impulsions d'une durée allant de ~25 ps (Fig. 4) à ~100 ps (Fig. 4) ont été générées en utilisant respectivement la technique NF-FTM. À des fins de comparaison, des impulsions paraboliques d'une durée de 25 ps ont été générées en utilisant à la fois la méthode NF-FTM et la mise en forme spectrale directe. Figure 5(a) montre le spectre de sortie pour l'approche de mise en forme spectrale directe, qui montre clairement qu'une grande partie du spectre d'énergie

d'entrée devait être filtrée à partir de l'étape de mise en forme spectrale. D'autre part, en utilisant le NF-FTM, nous avons pu maintenir la plus grande partie du spectre d'énergie d'entrée disponible, comme le montre la Fig. 5(b). Les formes d'onde temporelles de sortie mesurées sont illustrées dans les Fig. 5(c)-5(f). Les impulsions générées étaient toutes les deux très proches de l'ajustement idéal. La puissance de sortie mesurée de l'impulsion parabolique générée par NF-FTM était d'environ 4,2 dBm, soit environ 6 dB de plus que celle de l'impulsion parabolique générée par l'approche de mise en forme spectrale directe.

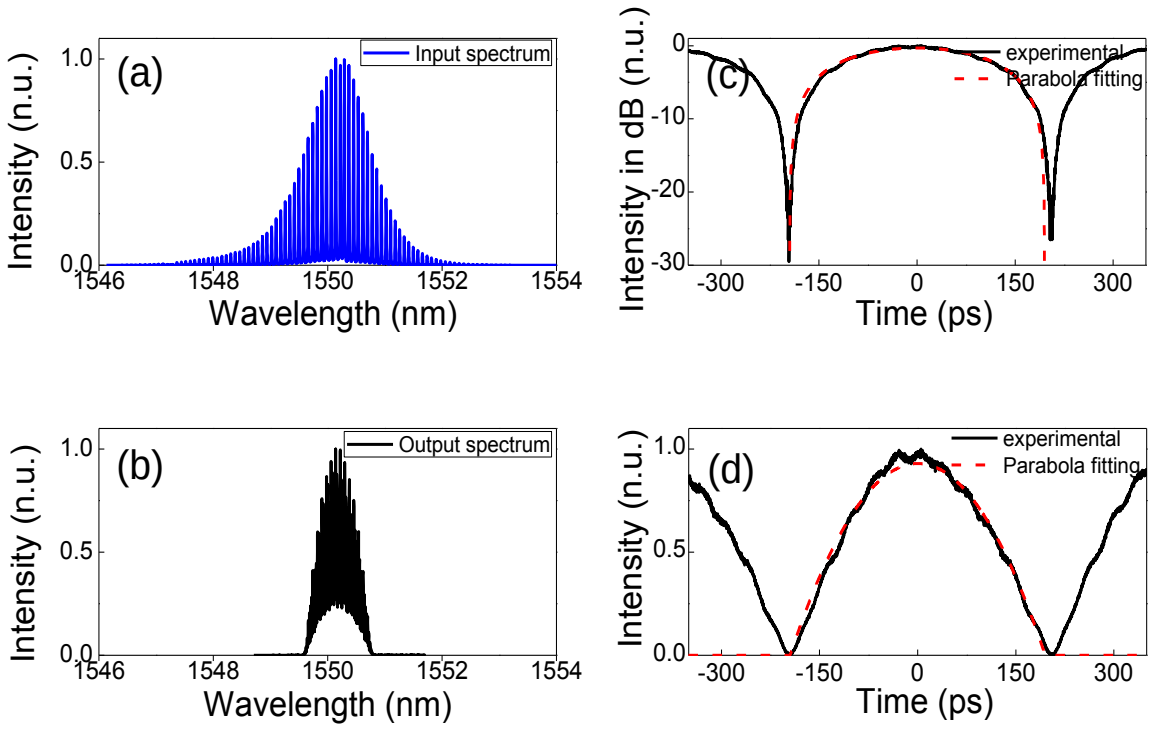

Figure 3 **Spectre d'impulsions d'entrée (a) et spectre de sortie de l'impulsion parabolique de 400 ps de durée après la mise en forme de l'impulsion (b), et profils d'intensité temporelle générés, tracés sur une échelle logarithmique (c) et une échelle linéaire (d).**

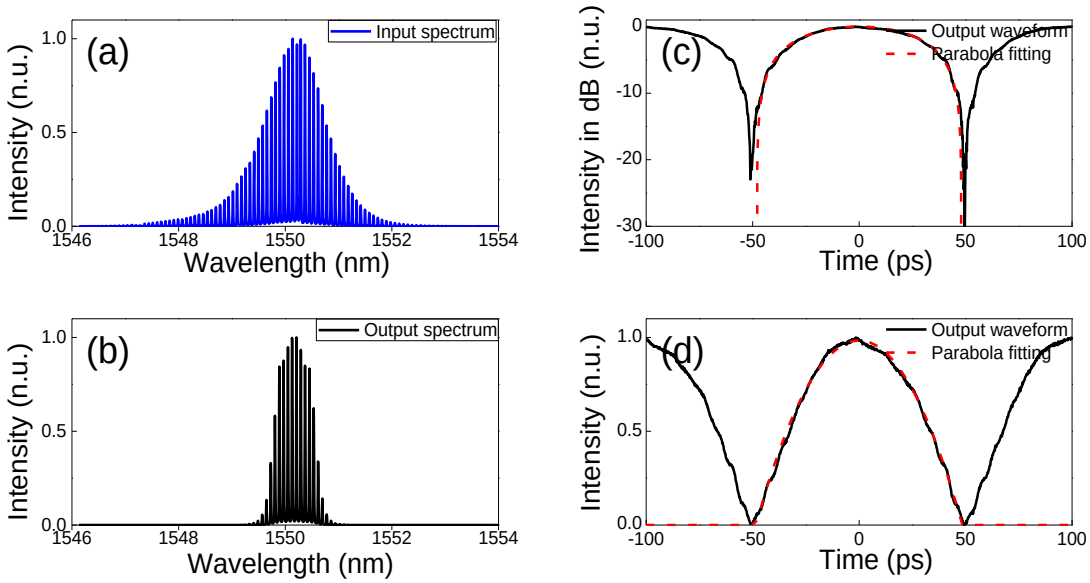

Figure 4 **Spectre d'impulsions d'entrée (a) et spectre de sortie de l'impulsion parabolique d'une durée de 100-ps après le générateur d'impulsions (b), et profils d'intensité temporelle générés sur une échelle logarithmique (c) et une échelle linéaire (d).**

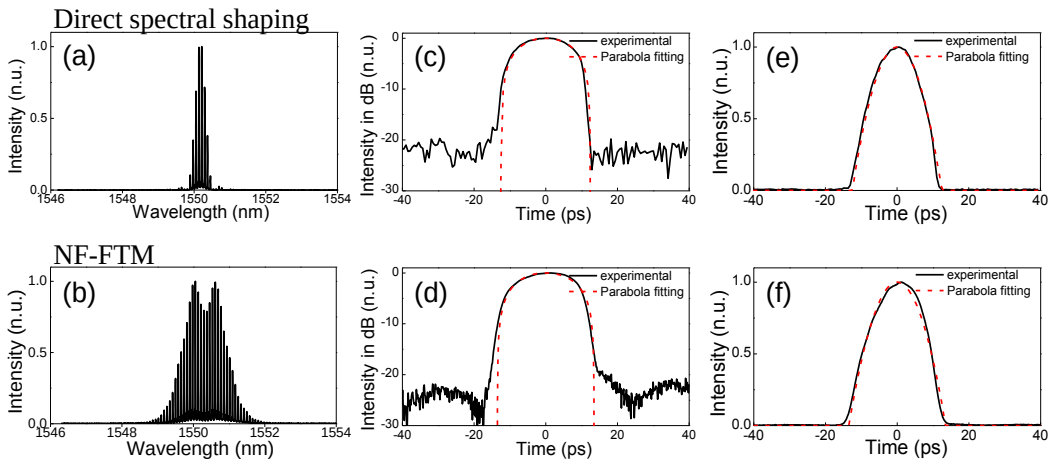

Figure 5 **Spectre de sortie des impulsions paraboliques générées en utilisant une approche de mise en forme spectrale directe (a) et NF-FTM (b). Les profils d'intensité temporelle générés correspondants sont tracés sur une échelle logarithmique (c), (d) et une échelle linéaire (e), (f).**

C.2. Traitement de signal reconfigurable entièrement optique, basé sur une lentille temporelle à modulation de phase croisée.

Une lentille temporelle (TL, pour ‘time-lens’), qui confère une modulation de phase quadratique temporelle sur une forme d'onde entrante, représente la contrepartie temporelle d'une lentille spatiale mince, et c'est un élément principal pour exécuter d'importantes fonctionnalités de traitement de signaux optiques à grande vitesse, y compris le grossissement temporel des formes d'onde optique rapide [14], la compensation des dégradations linéaire et non linéaire dans les liaisons de télécommunication à fibre optique [15], et la projection temps-fréquence (T à F) des formes d'onde optique rapide (par exemple, la division temporelle optique à multiplexage par répartition en longueur d'onde) [16].

Une façon simple de créer une TL utilise un modulateur de phase électro-optique commandé par une forme d'onde de modulation sinusoïdale. Cependant, la quantité de modulation de phase – et la fréquence correspondante – qui peut être obtenue par des moyens électro-optiques est relativement limitée, ce qui affecte la performance globale (par exemple, la résolution temporelle) de cette approche [17]. Alternativement, l'utilisation de phénomènes optiques non linéaires a été largement étudiée pour créer des TLs, notamment le mélange à quatre ondes (FWM, pour ‘four-wave mixing’) avec une longue impulsion de pompe optique modulée linéairement en fréquence (c.à.d. à pépiement) [17]. Cependant, le FWM exige un contrôle précis de la dispersion dans le milieu non linéaire et des conditions rigoureuses d'adaptation de phase devraient également être assurées sur la bande de fréquences d'intérêt. Peut-être plus important encore, le paramètre clé d'une TL, c'est-à-dire le pépiement de fréquence, ne peut pas être facilement accordé dans un schéma FWM car cela nécessiterait de contrôler le chirp de fréquence de l'impulsion de pompe. En revanche, une TL peut également être produite par XPM avec une impulsion de pompe parabolique [17]. Cette solution offre intrinsèquement la possibilité d'accorder le pépiement de fréquence des lentilles temporelles par des moyens tout optique. Dans ce schéma, le pépiement de fréquence de la lentille temporelle est directement proportionnel à la puissance de crête de la pompe parabolique.

L'objectif de ce travail est de mettre en évidence la capacité de reconfiguration entièrement optique d'une lentille temporelle à base de XPM et de montrer comment cette capacité peut être utilisée pour créer des plates-formes de traitement de signaux basées sur la lentille temporelle optiquement programmables. Pour ce faire, nous proposons et démontrons une conception d'une lentille temporelle à base de XPM (LT XPM) –avec une ligne dispersive concaténée– pour la projection reconfigurable T- à -F et l'agrandissement temporel des formes d'ondes optiques rapides,

où l'on peut régler le rapport de conversion T- à -F et le facteur d'agrandissement temporel *en changeant simplement la puissance de crête de l'impulsion parabolique de pompe*. La même plate-forme pourrait également être ajustée pour produire une transformée de Fourier en temps réel de la forme d'onde optique d'entrée.

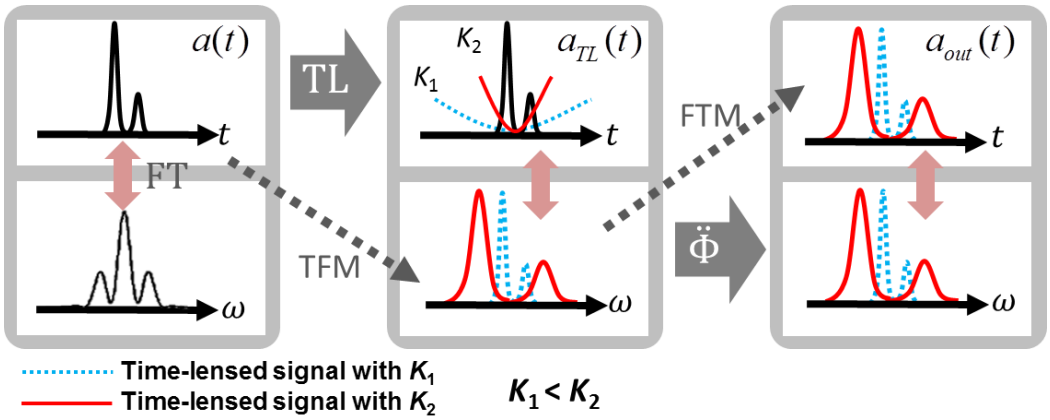

Figure 6 **Illustration du schéma de traitement de signal reconfigurable entièrement optique proposé, basé sur un processus XPM-TL. Les paramètres t et ω représentent respectivement le temps et la fréquence radiale, tandis que $\ddot{\Phi}$ représente la dispersion du second ordre (vitesse de groupe). TFM et FTM signifient respectivement le mappage T- à -F et F- à -T.**

La figure 6 illustre le concept du schéma de traitement du signal reconfigurable entièrement optique proposé. La lentille temporelle sur le signal entrant (sonde) $a(t)$ (enveloppe temporelle complexe modulée sur une porteuse optique) est réalisé par XPM dans une fibre hautement non linéaire (HNLF, pour 'highly-nonlinear fiber') avec une impulsion de pompe optique parabolique. La forme d'onde dans le domaine temporel du signal à l'entrée de la TL peut être projeter dans le domaine fréquentiel à la sortie de la TL si le taux de pépiement fréquentiel K du processus TL est suffisamment fort [18]. En particulier, la transformée de Fourier du signal après passage dans la lentille temporelle, $A_m(\omega)$, peut-être approchée comme suit

$$A_m(\omega) \propto \exp(-j\omega^2/2K)[a(\tau)]_{\tau=\omega/K} \quad (1)$$

Cette dernière équation indique que le profil d'intensité spectrale du signal de la sonde à la sortie de la TL est une réplique à l'échelle de la forme d'onde temporelle d'entrée, avec un rapport de conversion T-à -F qui est directement proportionnel à *K*, le taux de pépiement de fréquence de la TL. Par la suite, on peut obtenir un grossissement temporel non déformé du signal original $a(t)$ en

propageant le signal de la sonde à travers une ligne dispersive du second ordre, avec un coefficient de dispersion constant $\ddot{\Phi}$ (pente du retard de groupe en fonction de ω) [18]. La forme d'onde temporelle résultante (enveloppe complexe) à la sortie de la ligne dispersive peut être exprimée comme suit

$$a_{out}(t) \propto \exp(-jt^2/2M)[a(t/M)] \quad (2)$$

Où le facteur d'agrandissement temporel est $M = 1 + K\ddot{\Phi}$. La caractéristique clé du schéma que nous proposons est que le rapport de conversion T-à-F et le facteur d'agrandissement temporel sont programmables en contrôlant *K*, ce qui peut être facilement réglé en changeant la puissance de crête de l'impulsion de la pompe parabolique seulement.

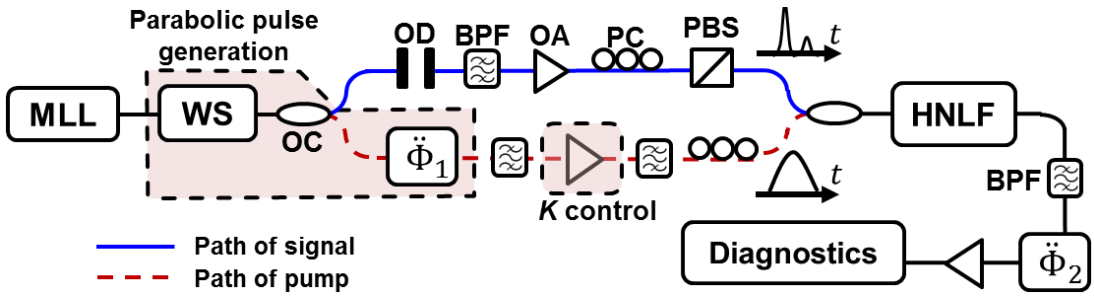

Figure 7 Installation expérimentale du système de traitement du signal entièrement optique reconfigurable basé sur XPM-TL, y compris la partie génération de la pompe parabolique. Les acronymes sont définis dans le texte.

Le montage expérimental utilisé pour la preuve de concept est illustré à la Fig. 7. Les signaux de la pompe et de la sonde (entrée) sont générés à partir d'une source laser à fibre optique à verrouillage de mode (MLL, pour 'mode-locked laser'). Le MLL d'entrée est façonné spectralement à l'aide d'un façonneur d'ondes optiques linéaires avec une résolution en fréquence d'environ 10 GHz pour la génération des formes d'ondes d'impulsion de la pompe et de la sonde. Le signal de la sonde à traiter est constitué de deux impulsions optiques gaussiennes consécutives d'intensité différente, séparées par ~21 ps. Chaque impulsion individuelle a une largeur temporelle FWHM de ~10 ps. La puissance de crête de la pompe –et l'amplitude du chirp induit par XPM– est modifiée en contrôlant le gain d'un amplificateur à fibre dopée à l'erbium. Le signal de la sonde est combiné avec le signal parabolique amplifié de la pompe parabolique dans un coupleur optique (OC, pour optical coupler) et envoyé dans une section HNLF d'environ 1 km de long. Le coefficient non linéaire du HNLF est ~11.3 $W^{-1}{\cdot}km^{-1}$.

Les figures 8(a) et (b) montrent les spectres mesurés du signal de la sonde à la sortie TL pour différentes valeurs d'amplification de la pompe (puissance moyenne de la pompe donnée dans les graphiques) pour les cas de (a) impulsions paraboliques claires et (b) sombres de la pompe parabolique. Dans tous les cas, les spectres mesurés ressemblent étroitement au profil d'intensité temporelle du signal à double impulsion sous test, illustré dans Fig. 8(c), démontrant le processus de projection T- à-F prévu avec un rapport de conversion T-à-F ajustable. La figure 9 montre les résultats expérimentaux sur l'agrandissement temporel direct et inverse de la forme d'onde d'entrée après propagation à travers la ligne dispersive. Là encore, les formes d'onde temporelle de sortie mesurées sont des répliques amplifiées dans le temps du signal dans le domaine temporel de la sonde d'entrée avec un facteur d'agrandissement temporel *M* qui est accordé sur une plage d'environ deux fois plus grande en changeant le gain de l'amplificateur optique de la pompe.

Comme prévu, la transformation optique de Fourier dans le domaine temporel du signal de la sonde est également obtenue avec succès à la sortie du système lorsque l'étage XPM est contourné en appliquant un gain nul dans la pompe EDFA (EDFA, pour ‘Erbium-doped fiber amplifier’) comme le montre la Fig. 10.

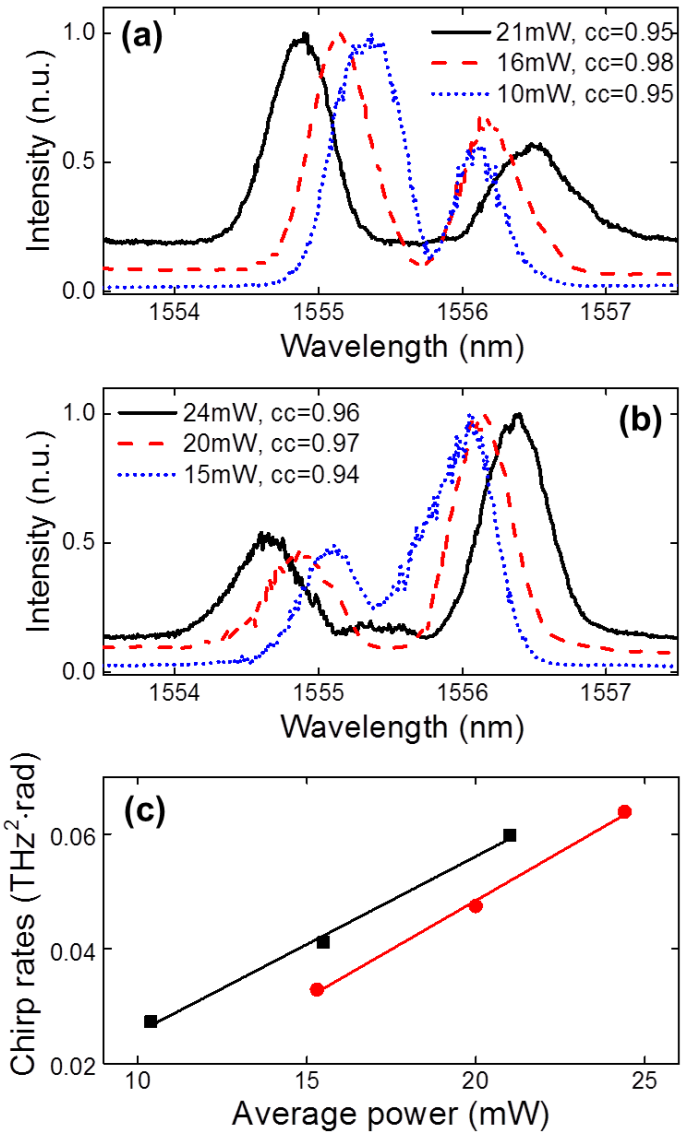

Figure 8 **Démonstration de la conversion T-F avec différents rapports de conversion en changeant la puissance moyenne de la pompe P_{avr} pour les cas de (a) taux de pépiement de fréquence positifs et (b) négatifs (pompes paraboliques claires et sombres, respectivement). Le graphique (c) montre un graphique de relation des taux de pépiement estimés (à partir des mesures) en fonction du P_{avr} mesuré pour les pompes paraboliques claires (points carrés noirs) et sombres (points cercles rouges). Les coefficients de corrélation croisée (cc) sont estimés comme le pic de la fonction de corrélation normalisée entre le signal de la sonde et les spectres de sortie (mappés dans le temps).** $cc(\tau) = \int_{-\infty}^{\infty} a(t)b(t+\tau)dt \,/\sqrt{E_a E_b}$

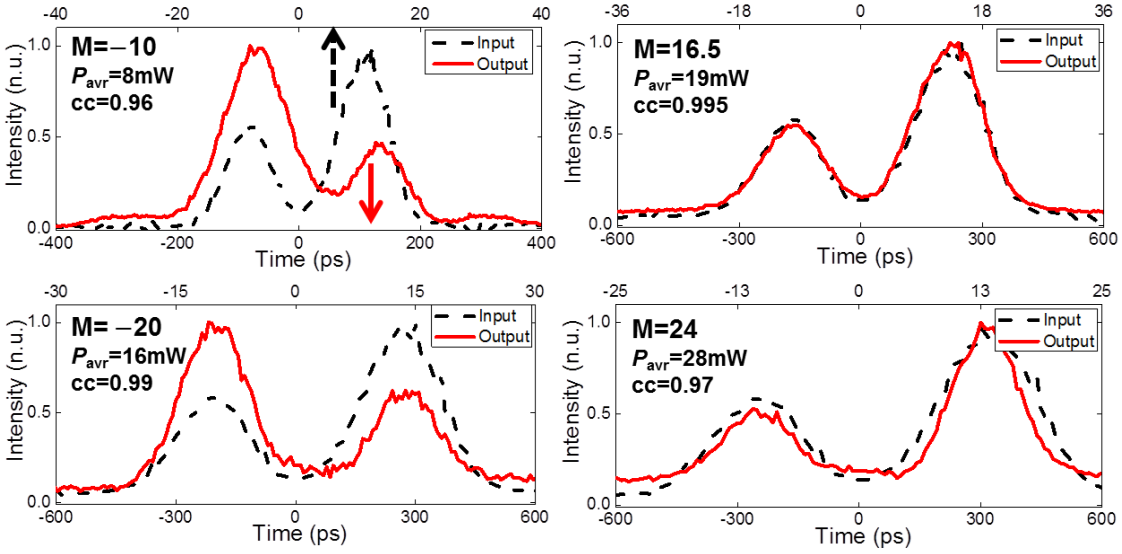

Figure 9 **Profils d'intensité temporelle mesurés de la sonde d'entrée (lignes pointillées noires, mises à l'échelle temporelle par le facteur d'agrandissement *M*, l'échelle temporelle originale étant indiquée dans l'axe horizontal supérieur) et forme d'onde de sortie (lignes pleines rouges) pour l'agrandissement temporel direct et inverse avec différents facteurs d'agrandissement.**

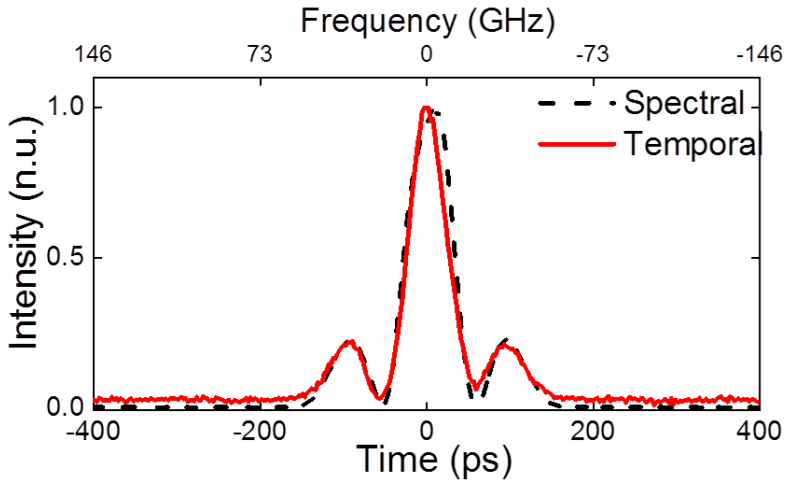

Figure 10 **Profil d'intensité temporelle mesuré (ligne solide rouge, axe inférieur) de la forme d'onde de sortie avec une puissance de pompe nulle pour la transformation de Fourier optique dans le domaine temporel, et le spectre du signal de la sonde d'entrée d'origine (ligne pointillée noire, axe supérieur).**

D. Génération reconfigurable en fibre de formes d'ondes arbitraires (asymétriques) d'intensité temporelle picoseconde par mise en forme d'impulsions optiques dans le domaine temporel

Alternativement à l'approche spatiale, les générateurs d'impulsions optiques dans le domaine temporel, où la fonction de filtrage est programmée directement dans le domaine temporel à l'aide d'un modulateur électro-optique à grande vitesse (EO-M, pour 'electro-optic modulator'), ont attiré beaucoup d'attention en raison de leur configuration toute fibre simple, de leur capacité à atteindre des taux de mise à jour rapide de la forme des impulsions, dans la gamme des sous-GHz, et du solide potentiel d'intégration [19]. Cependant, au meilleur de nos connaissances, tous les schémas précédemment démontrés pour la mise en forme d'impulsions dans le domaine temporel se limitaient à synthétiser des formes d'onde d'intensité purement symétriques dans le temps grâce à l'utilisation d'un simple filtrage de phase binaire (à deux niveaux). Il s'agit d'une limitation très restrictive, en fait, des profils d'intensité temporelle asymétrique sont nécessaires pour de nombreuses applications importantes, y compris (i) le codage arbitraire d'amplitude d'impulsions optiques à grande vitesse, (ii) la conversion non linéaire en longueur d'onde, et (iii) le multiplexage à répartition dans le temps par insertion–extraction avec des performances améliorées en utilisant des impulsions de pompe triangulaires asymétriques [5, 20, 21].

Dans ce travail, on fait la démonstration expérimentale d'un générateur d'impulsions picosecondes programmable à fibre optique en utilisant un filtrage linéaire *à plusieurs niveaux* de phase seulement dans le domaine temporel, ce qui permet la synthèse de profils d'intensité temporelle de haute qualité, entièrement arbitraire (y compris asymétrique). La technique proposée utilise un modulateur de phase EO (EO-PM, pour 'EO phase modulator') entraîné par un AWG à grande vitesse entre deux lignes dispersives à fibres optiques conjuguées, qui sont ici mises en œuvre en utilisant un seul réseau de Bragg à fibre à pas variable linéairement (LC-FBG, pour 'linearly-chirped fiber Bragg grating') fonctionnant consécutivement à partir de ses deux extrémités. Nous présentons ici la synthèse de formes d'impulsions triangulaires asymétriques et de séquences de codes d'impulsions et de modulation d'amplitude d'impulsions (PAM) à grande vitesse (~150 Gbaud), avec une résolution de ~2 ps sur une fenêtre temporelle maximale de ~60 ps, ce qui correspond à une résolution de fréquence estimée à ~16 GHz.

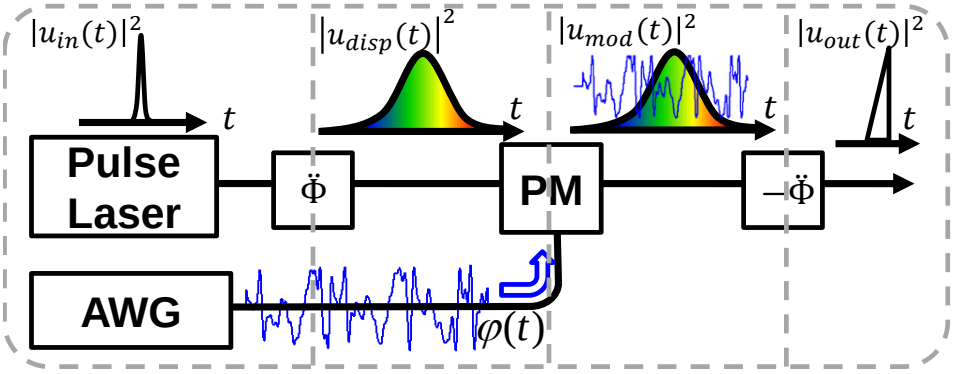

Figure 11 **Schéma du système de mise en forme programmable d'impulsions optiques à base de fibres optiques. PM : modulation de phase.**

Le schéma du système de mise en forme des impulsions dans le domaine temporel est illustré à la Fig. 11. Pour mettre en œuvre le filtrage spectral calculé du profil de phase de l'impulsion, les composantes de fréquence de l'impulsion d'entrée sont d'abord distribuées linéairement le long du domaine temporel par propagation linéaire à travers un milieu dispersif de second ordre. Un réseau de Bragg à fibre linéairement variable (LC-FBG) a été utilisé comme milieu dispersif dans notre expérience. L'impulsion étirée dans le temps est ensuite modulée en phase à l'aide d'un EO-PM piloté par un signal de modulation dans le domaine temporel qui fait la projection de la fonction de transfert spectral de phase désirée. La fonction de filtrage de phase spectrale nécessaire est obtenue par un algorithme combiné de Gerchberg-Saxton (GSA, pour 'Gerchberg-Saxton algorithm') et un algorithme génétique (GA, pour 'genetic algorithm') [5]. En comprimant ensuite l'impulsion étirée modulée en phase avec un compensateur de dispersion fournissant la dispersion conjuguée exacte du premier élément dispersif, le profil d'intensité temporelle cible peut être obtenu directement à la sortie du système.

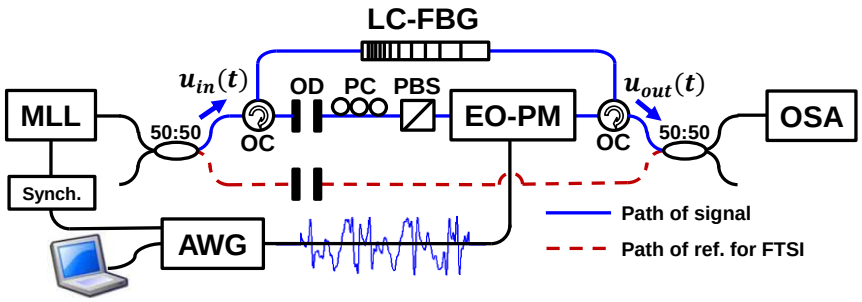

Figure 12 **Configuration expérimentale du système de mise en forme programmable, et à base de fibres optiques, d'impulsions optiques, y compris une configuration interférométrique pour la caractérisation des impulsions de sortie basée sur FTSI. OC : circulateur optique. Les acronymes sont dans le texte.**

Le montage expérimental est illustré à la Fig. 12. Les impulsions optiques initiales ont été générées à partir d'un laser à fibre à verrouillage de mode passif (MLL) produisant des impulsions gaussiennes quasi-limitées par transformée de Fourier avec une largeur de ~2 ps (FWHM) et une puissance moyenne de ~3 dBm à un taux de répétition de ~16 MHz, centrées spectralement autour de ~1554,5 nm. Les impulsions d'entrée ont été étirées dans le temps par réflexion sur le LC-FBG. Les impulsions dispersées ont été modulées par un EO-PM de 40 GHz piloté par le signal de modulation temporel optimisé $\phi(t)$, obtenu à partir des algorithmes numériques décrits, qui a été généré par un AWG à grande vitesse. Les impulsions étirées et modulées en phase ont été exactement comprimées en retour par réflexion sur le même LC-FBG mais dans la direction opposée.

La figure 13 présente les résultats de deux exemples de génération de formes d'ondes triangulaires temporelles asymétriques avec des pentes de montée et de descente différentes et personnalisées, pour une durée d'impulsion totale d'environ 30 ps (largeur à 1 % de l'intensité maximale). Les figures 14 et 15 montrent les profils d'intensité de sortie mesurés des codes d'impulsions aléatoires OOK de 150 GHz à 8 bits et des séquences PAM de 150 GHz à 8 bits avec 5 niveaux d'intensité d'impulsions différents et équidistants (y compris le niveau zéro). Les profils d'intensité temporelle de sortie mesurés sont de nouveau en excellente concordance avec les formes cibles calculées numériquement et idéales. La largeur FWHM des impulsions individuelles (résolution temporelle) était de ~2 ps, l'espacement entre les impulsions dans les codes d'impulsions était de ~6,7 ps (débit binaire correspondant ~150 GHz), et la fenêtre temporelle globale de chaque séquence synthétisée était de ~60 ps.

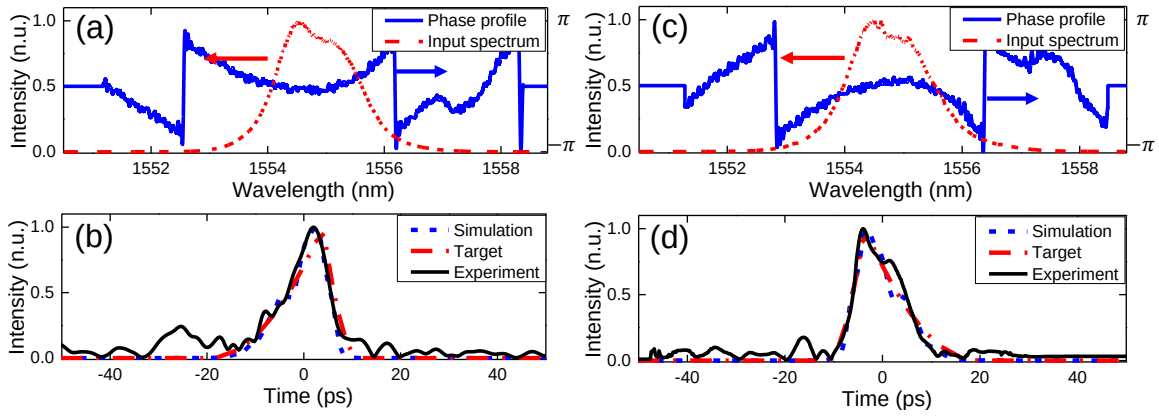

Figure 13 **Spectre d'impulsions d'entrée et profil de phase spectrale calculé ((a), (c)), et profils d'intensité temporelle de sortie mesurée (vs. simulée et cible) ((b), (d)) des formes d'ondes triangulaires asymétriques synthétisées avec des pentes personnalisées. n.u. (for normalized units) représente les unités normalisées par rapport au pic de forme d'onde.**

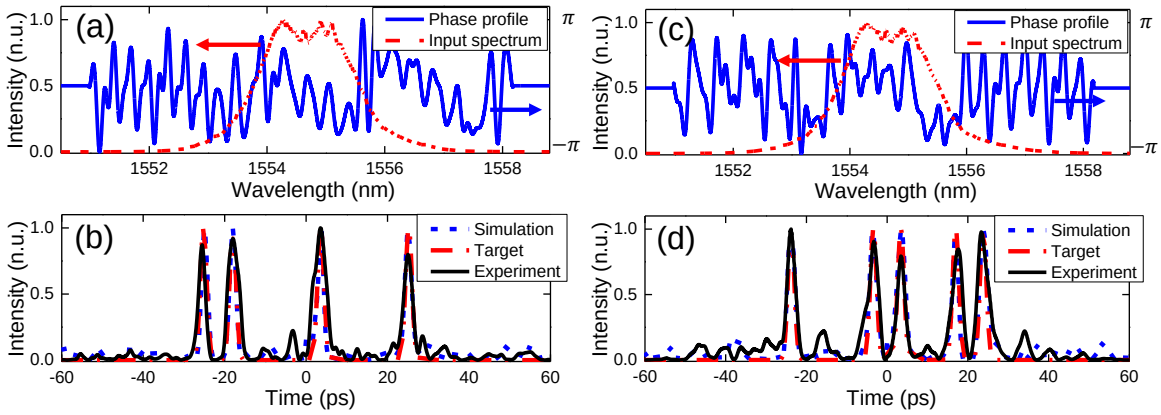

Figure 14 **Spectre d'impulsions d'entrée et profil de filtrage de phase spectrale calculé ((a),(c)), et profils d'intensité temporelle de sortie mesurés (vs. simulés et cibles) ((b),(d))) des codes d'impulsions aléatoires OOK 8 bits synthétisés.**

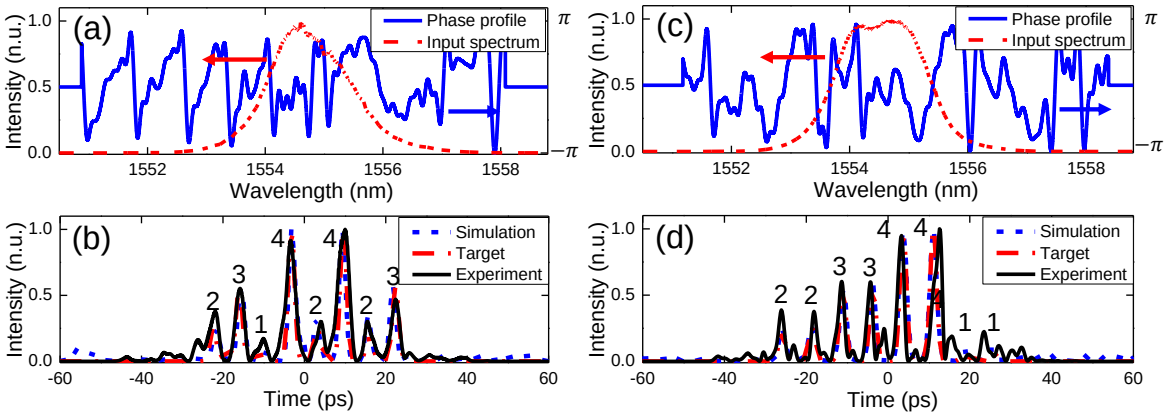

Figure 15 **Spectre d'entrée et profil de phase spectrale calculé ((a), (b)), et profils d'intensité temporelle de sortie mesurés (vs. simulés et cibles) ((b), (d)) des PAM 8 bits synthétisés avec 5 niveaux d'intensité d'impulsion différents.**

E. Reconnaissance à grande vitesse en fibre optique de structures de spectre d'énergie à large bande de lumière incohérente

Le processus d'identification implique généralement la détection d'une multitude de spectres d'énergie entrants à partir du matériau, du dispositif, ou du système sondés en utilisant des spectromètres conventionnels, et le post-traitement numérique ultérieur des spectres détectés en utilisant le traitement numérique du signal (DSP, pour ‘digital signal processing’) pour identifier et extraire le(s) motif(s) désiré(s). L'utilisation de l'analyse conventionnelle du spectre optique (OSA, pour ‘optical spectrum analysis’), impliquant la dispersion spatiale du spectre optique entrant, est par nature lente, avec des taux typiques de mis à jour dans la gamme des kHz. En tant que tel, cette technique n'est pas adaptée à de nombreuses applications, en particulier celles qui visent l'analyse d'un échantillon ou d'une cible dont les spécifications changent rapidement, comme la surveillance ou la détection de phénomènes chimiques ou physiques dynamiques [22-24]. Il est intéressant de noter que la nature déterministe du ou des motifs spectraux cibles peut être exploitée pour obtenir le processus d'identification souhaité à la volée, grâce à une corrélation optique directe entre la lumière réfléchie/transmise par l'échantillon et le motif cible. Ce principe a été exploité dans un système de corrélation optique en temps réel basé sur le filtrage spectral dans le domaine temporel des spectres lumineux cohérents [25]. Cependant, ce système précédent ne peut être appliqué que pour la reconnaissance de spectres d'ondes lumineuses *cohérents*, tout en exigeant une synchronisation précise entre les spectres à identifier, projetés dans le temps, et le motif d'intensité temporelle cible.

Dans ce travail, nous proposons et démontrons expérimentalement un système de fibres optiques pour la reconnaissance à la volée et à grande vitesse d'une structure spectrale d'énergie lumineuse incohérente prescrite, en évitant le post-traitement numérique. Le schéma est basé sur le concept de convolution temps-spectre (TSC) dans un réseau de fibres dispersive [26]. Le système calcule directement une corrélation en temps réel des spectres entrants avec le motif cible qui est programmé dans un modulateur temporel, sans avoir besoin de synchronisation entre les spectres lumineux entrants et le motif de modulation.

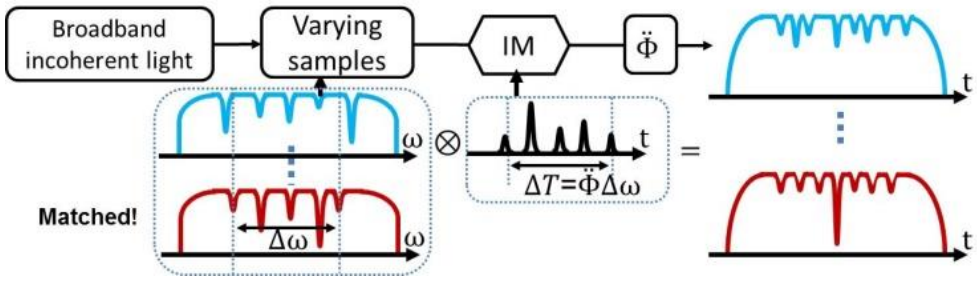

Figure 16 **Illustration du système proposé de reconnaissance du spectre d'énergie en temps réel. Les paramètres t et ω représentent respectivement le temps et la fréquence radiale, tandis que ⊗ représente la convolution. Les acronymes sont définis dans le texte.**

Le schéma du système de reconnaissance spectrale en temps réel proposé est illustré à la Fig. 16. Une source de lumière incohérente à large bande est filtrée spectralement de façon linéaire pour émuler le spectre d'absorption d'un échantillon donné. Les spectres d'ondes lumineuses façonnés à identifier sont d'abord modulés dans le temps à l'aide d'un modulateur d'intensité électro-optique (IM, pour 'intensity modulator') piloté par le motif correspondant. Il s'agit de la version temporelle du spectre énergétique cible. Par la suite, le signal optique modulé se propage linéairement à travers un milieu dispersif chromatique du second ordre, caractérisé par un profil de retard de groupe principalement linéaire. La forme d'onde d'intensité temporelle moyenne à la sortie du milieu dispersif est proportionnelle à la convolution temporelle entre la version temporelle du spectre énergétique entrant et la cible de modulation temporelle [26]. Ce schéma calcule la corrélation croisée entre la version temporelle du spectre d'énergie et le modèle de modulation *temporellement inversé* (ou vice versa), mis à jour au taux de répétition du signal de modulation.

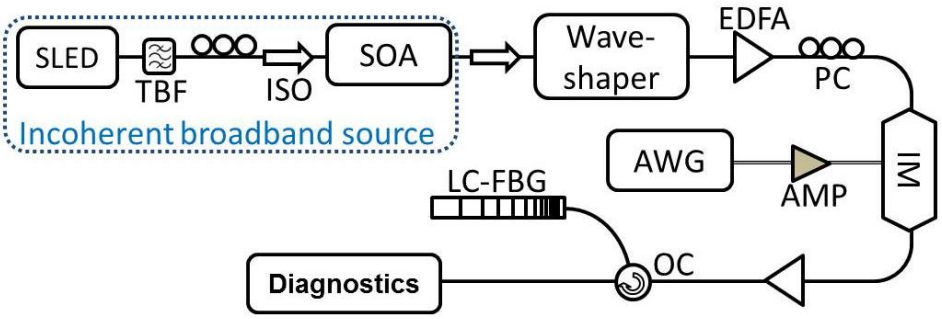

Figure 17 **Installation expérimentale pour la démonstration de la preuve de concept du système de reconnaissance du spectre d'énergie en temps réel proposé. Les acronymes sont définis dans le texte.**

Le montage expérimental est illustré à la Fig. 17. La lumière incohérente à large bande est produite à partir d'une diode super-luminescente (SLED, pour 'super-luminescent diode') suivie d'un filtre passe-bande accordable (TBF, pour 'tunable bandpass filter') et d'un amplificateur optique à semi-conducteur saturé (SOA, pour 'semi-conductor optical amplifier'). Les structures de spectre d'énergie à identifier sont produites par un façonneur d'ondes spectrales (Finisar WaveShaper 4000S) avec une résolution en fréquence de ~10 GHz. La figure 18 montre les spectres mesurés pour trois cas différents, y compris le diagramme spectral d'absorption cible (Fig. 18(b)), le même diagramme d'absorption avec un axe de fréquence rééchelonné, 10% plus large que la cible (Fig. 18(c)), et le motif cible, en conservant l'échelle de fréquence originale (c'est-à-dire la séparation spectrale de crête), mais avec une amplitude différente des pics d'absorption (Fig. 18(d)). Le signal est amplifié optiquement par un amplificateur à fibres dopées à l'Erbium (EDFA), puis modulé dans le temps par le motif cible (Fig. 18(a)) en utilisant un modulateur d'intensité (IM) électro-optique de Mach-Zehnder à 40 GHz commandé par un générateur électroniques de formes d'ondes arbitraires à grande vitesse (AWG) avec une fréquence d'échantillonnage de 20 GSample/s. La lumière modulée est réamplifiée, puis réfléchie par un réseau de Bragg à fibre optique (LC-FBG).

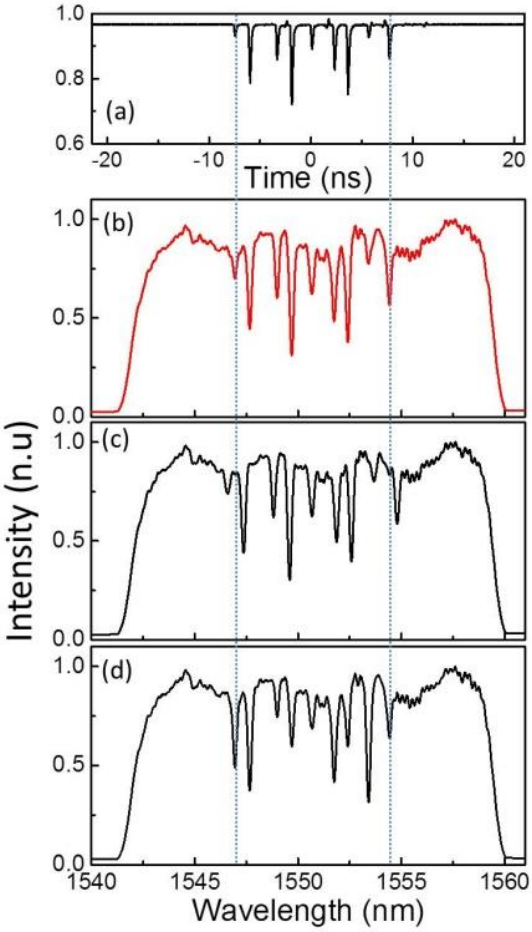

Figure 18 **Motif temporel cible mesuré à partir de l'AWG (a), et motifs spectraux d'absorption émulés pour trois essais différents, y compris le motif spectral cible (b), le même motif mais avec un espacement spectral plus large de 10 % (c), et le motif cible mais avec une amplitude différente des pics d'absorption (d). n.u. représente des unités normalisées.**

La figure 19 montre les formes d'onde temporelles de sortie moyennes mesurées correspondant aux spectres d'absorption de Fig. 18. La figure 19(a) montre le résultat expérimental (ligne rouge) et la simulation numérique correspondante (ligne bleue en pointillés) lorsque la forme du spectre d'absorption correspond au modèle programmé. Comme prévu, le creux le plus élevé pour cette forme d'onde, correspondant au pic d'autocorrélation, est observé au centre de la forme d'onde de fond temporelle. Fig. 20 montre des résultats expérimentaux supplémentaires dans le cas d'un spectre d'absorption cible différent.

Dans l'expérience suivante, différentes configurations spectrales sont émulées en modifiant en conséquence le signal de modulation temporelle de commande (à partir de l'AWG) tandis que le spectre d'énergie entrant est maintenu inchangé à une configuration spectrale binaire de 16 bits. La

forme d'onde temporelle de sortie mesurée expérimentalement (Fig. 21(b), moyenne 32 fois) correspond bien à celle calculée théoriquement (Fig. 21(a)). Comme prévu, le pic d'autocorrélation (puissance de crête la plus élevée) est obtenu lorsque le spectre d'énergie testé correspond au motif pilotant la modulation. Les résultats présentés montrent que la corrélation de sortie peut être mesurée avec un taux de rafraîchissement qui n'est limité que par la durée des modèles de convolution temporelle résultants, soit environ deux fois la durée du motif de modulation temporelle correspondant (p. ex. 2×24 ns dans notre exemple), et la moyenne de 32 nécessaire pour détecter les formes d'onde de sortie. Cela permet une identification spectrale directe à des fréquences inférieures au MHz (1/(32×48 ns)~650 kHz sur une bande passante de 1,5-THz avec une résolution en fréquence de ~12 GHz (démontrée ici) sans qu'il soit nécessaire d'effectuer un post-traitement supplémentaire.

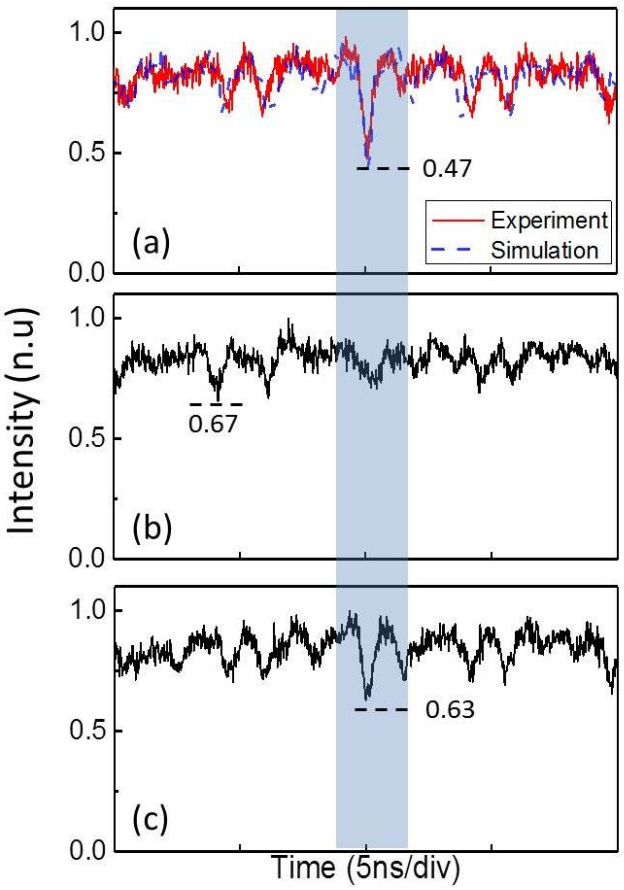

Figure 19 **Formes d'onde temporelle de sortie mesurées (moyenne 32 fois) lorsque le spectre entrant est le motif cible (a), le modèle avec un espacement spectral de 10% plus large (b) et le motif avec différentes grandeurs de pics d'absorption (c).**

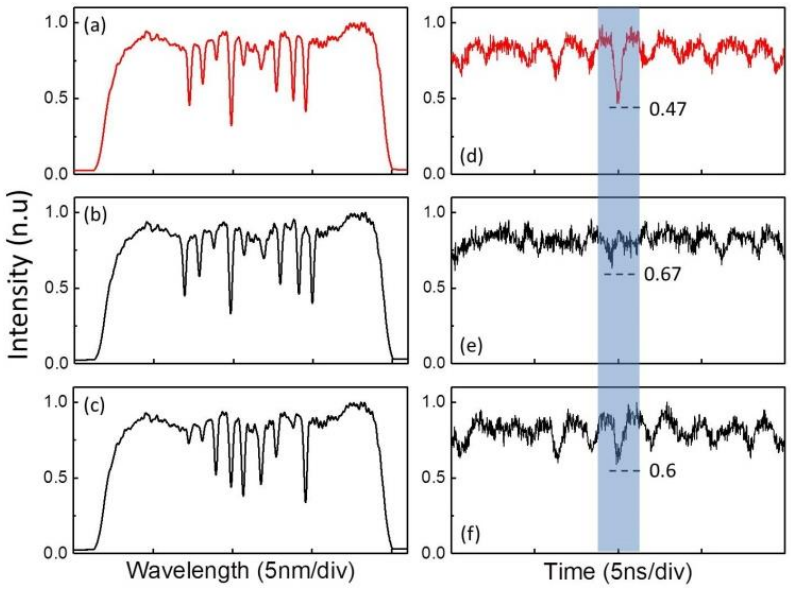

Figure 20 **Motifs spectraux d'absorption émulés et mesurés, et leurs formes d'onde temporelle de sortie correspondantes (moyenne 32 fois), pour trois essais différents, y compris le motif spectral cible ((a), (d)), le même motif mais avec un espacement spectral plus large de 10 % ((b), (e)), et le motif cible mais avec une amplitude différente des pics d'absorption ((c), (f))), respectivement.**

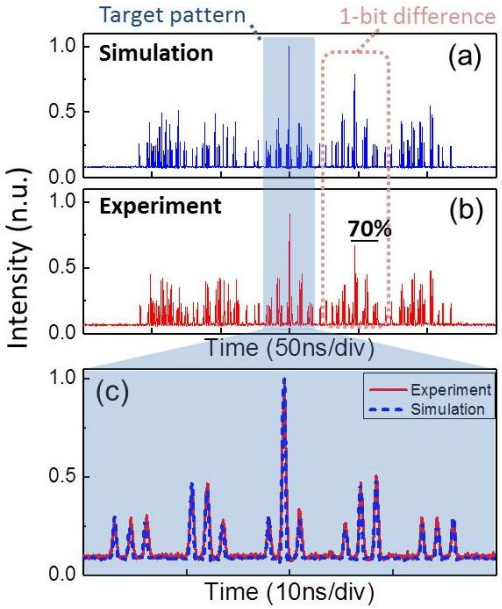

Figure 21 **Démonstration de la reconnaissance du spectre énergétique avec une fréquence de mise à jour rapide. Simulation (a) et mesure expérimentale (b) des motifs temporels moyens de sortie (corrélation croisée), car le motif de modulation temporelle est modifié toutes les 24 ns. Le graphique en (c) montre un gros plan du profil d'intensité temporelle de sortie dans l'expérience (solide rouge) et la simulation (bleu pointillé) autour du pic d'autocorrélation.**

F. Conclusion de la thèse

Diverses techniques de mise en forme d'impulsions optiques linéaires sont présentées comme un outil puissant pour exploiter la bande passante ultra-large des sources photoniques cohérentes/incohérentes. Deux thèmes principaux de la mise en forme des impulsions optiques, une conception d'une fonction de filtrage et sa mise en œuvre, sont abordés dans cette thèse. L'utilisation du milieu dispersif passif simple permet de développer de nouvelles approches linéaires pour les méthodes programmables de mise en forme d'impulsions optiques par fibre optique et leurs applications innovantes pour les traitements tout-optiques de signaux. Généralement, les techniques proposées sont basées sur une projection fréquence-temps induite par dispersion (FTM) combinée à une modulation d'amplitude spectrale et/ou de phase de lumières cohérentes et incohérentes. Les méthodes proposées offrent une flexibilité grandement accrue pour atteindre une durée d'impulsion arbitraire désirée et minimiser les pertes d'énergie du processus de filtrage, indépendamment de la résolution en fréquence du générateur d'impulsions optiques linéaires.

Dans la section C, nous avons proposé et démontré une nouvelle méthode d'optique linéaire pour la génération d'impulsions paraboliques. La méthode est basée sur la projection fréquence-temps induite par dispersion (FTM), ce qui permet de préserver une grande partie des spectres d'énergie disponibles à partir des sources optiques d'entrée, quelle que soit la durée de l'impulsion cible. Ceci contraste avec la méthode conventionnelle de synthèse directe de Fourier où les durées d'impulsion sont essentiellement limitées par les pertes de spectre d'énergie dans l'étage de mise en forme d'impulsion, ou finalement par la résolution spectrale la plus fine de l'appareil de mise en forme d'impulsion. Des lignes directrices de conception basées sur le FTM de champ lointain (FF-FTM) et le FTM de champ proche (NF-FTM) sont suggérées pour la génération d'impulsions optiques paraboliques sur un large éventail de durées cibles. Tout d'abord, la synthèse d'impulsions basée sur FF-FTM combinée à la mise en forme spectrale s'avère capable de surmonter les limites de l'approche de mise en forme spectrale directe. Comme preuve de concept, une impulsion parabolique de 400 ps a été générée avec succès à partir d'une source laser à verrouillage de mode d'entrée à ~2 ps. Au fur et à mesure que la durée de l'impulsion diminue, les distorsions de forme d'onde imposées par l'exigence de satisfaire une condition stricte de champ lointain deviennent plus critiques. Cette restriction a été assouplie par l'utilisation d'une lentille temporelle virtuelle, incorporée dans l'étape de mise en forme spectrale linéaire, mettant en œuvre efficacement une approche NF-FTM. Cette méthode a permis de générer des impulsions paraboliques avec des durées

allant de ~25 ps à ~400 ps, et les impulsions synthétisées expérimentalement étaient des paraboles de haute qualité avec des puissances de sortie allant jusqu'à ~4 dBm sans utiliser d'amplification.

Les impulsions paraboliques générées sont utilisées comme pompe pour la création d'une lentille de haute qualité (TL) par XPM. Cette approche n'exige pas de satisfaire à des conditions rigoureuses d'adaptation de phase et de fournir des capacités additionnelles entièrement optiques et programmables, en exploitant la caractéristique que le facteur de pépiement de l'objectif (c.-à-d. la longueur focale de la lentille temporelle) dépend de la puissance de crête de l'impulsion de la pompe parabolique. Afin de démontrer cette capacité, nous avons conçu et démontré un schéma XPM TL pour la conversion reconfigurable T-à-F et l'agrandissement temporel des formes d'ondes optiques picosecondes ; le schéma peut effectuer la transformée de Fourier optique dans le domaine temporel du signal d'entrée lorsque l'étage XPM est contourné. Toutes les fonctionnalités sont contrôlées optiquement par un simple réglage du gain d'un amplificateur optique.

Dans la section D, nous avons fait la démonstration expérimentale d'un générateur d'impulsions optiques programmable, à faible perte, et à base fibre optique, utilisant un seul EO-PM, mettant en œuvre un filtrage linéaire à phase seule. La fonction de modulation multi-niveaux est calculée à partir d'une combinaison d'algorithmes d'optimisation, à savoir l'algorithme de Gerchberg-Saxton (GSA) et un algorithme génétique (GA), et générée à partir d'un générateur électronique de formes d'ondes arbitraires. La méthode permet la synthèse de profils d'intensité temporelle de haute qualité, entièrement arbitraire, avec une résolution temporelle limitée par la largeur de bande optique de l'impulsion d'entrée uniquement (~2 ps dans les exemples montrés), et une fenêtre temporelle dépendant directement du produit de la dispersion et de la largeur de bande de fréquence de modulation (jusqu'à ~60 ps dans notre schéma rapporté). Comme preuve de concept, nous présentons la synthèse des formes d'ondes triangulaires asymétriques et des séquences de code de modulation d'impulsion et d'amplitude d'impulsion et de modulation d'amplitude d'impulsion (OOK) de ~150 Gbaud, avec une résolution temporelle de ~ 2 ps sur une fenêtre temporelle maximale de ~60 ps, qui fournit un produit de largeur de bande de temps (TBP) d'environ 30, mesuré comme le rapport de la fenêtre temporelle de mise en forme à la résolution temporelle.

Dans la section E, nous avons proposé et démontré expérimentalement un système à fibres optiques pour l'identification en temps réel et à la volée de la structure d'un spectre d'énergie lumineuse incohérent. Le schéma est basé sur la convolution temporelle du spectre induit par dispersion (TSC), qui implique une modulation temporelle des ondes lumineuses incohérentes à large

bande en cours d'analyse avec une version temporelle à l'échelle du motif spectral cible, suivie d'un milieu dispersif approprié. La forme d'onde temporelle moyenne de sortie est une corrélation des spectres entrants avec le motif cible programmé. Ce système calcule directement la corrélation croisée des spectres d'énergie lumineuse entrants avec le motif cible, sans avoir besoin d'une synchronisation temporelle ou d'un post-traitement numérique supplémentaire. Dans les expériences de validation de concept, nous avons démontré la reconnaissance de structures spectrales infrarouges à un taux de mise à jour de 650 kHz, sur une bande passante de 1,5 THz avec une résolution spectrale de ~ 12 GHz.

G. References

[1] A. M. Weiner, "Femtosecond pulse shaping using spatial light modulators," Rev. Sci. Instrum. **71**, 1929-1960 (2000).

[2] A. M. Weiner, "Ultrafast optical pulse shaping: a tutorial review," Opt. Commun. **284**, 3669-3692 (2011).

[3] Finistar, " Finistar 4000S," [Online]. Available: https://www.finisar.com/sites/default/files/downloads/waveshaper_12page_product_brochure_09_16_3.pdf [Accessed 12 03 2018].

[4] J. Huh and J. Azaña, "Generation of high-quality parabolic pulses with optimized duration and energy by use of dispersive frequency-to-time mapping," Opt. Express **23**, 27751-27762 (2015).

[5] S. Thomas, A. Malacarne, F. Fresi, L. Poti, and J. Azaña, "Fiber-based programmable picosecond optical pulse shaper," J. Lightwave Technol. **28**, 1832-1843 (2010).

[6] D. Anderson, M. Desaix, M. Karlson, M. Lisak, and M. L. Quiroga-Teixeiro, "Wave-breaking-free pulses in nonlinear optical fibers," J. Opt. Soc. Am. B **10**, 1185-1190 (1993).

[7] M. E. Fermann, V. I. Kruglov, B. C. Thomsen, J. M. Dudley, and J. D. Harvey, "Self-similar propagation and amplification of parabolic pulses in optical fibers," Phys. Rev. Lett. **84**, 6010-6013 (2000).

[8] D. Krcmarik, R. Slavik, Y. Park, and J. Azana, "Nonlinear pulse compression of picosecond

parabolic-like pulses synthesized with a long period fiber grating filter," Opt. Express **17**, 7074-7087 (2009).

[9] C. Finot and G. Millot, "Synthesis of optical pulses by use of similaritons," Opt. Express **12**, 5104-5109 (2004).

[10] E. R. Andresen, J. M. Dudley, C. Finot, D. Oron, and H. Rigneault, "Transform-limited spectral compression by self-phase modulation of amplitude shaped pulses with negative chirp," Opt. Lett. **36**, 707-709 (2011).

[11] T. Hirooka, M. Nakazawa, and K. Okamoto, "Bright and dark 40 GHz parabolic pulse generation using a picosecond optical pulse train and an arrayed waveguide grating," Opt. Lett. **33**, 1102-1104 (2008).

[12] R. Maram and J. Azaña, "Spectral self-imaging of time-periodic coherent frequency combs by parabolic cross-phase modulation" Opt. Express **21**, 28824-28835 (2013).

[13] A. Dezfooliyan and A. M. Weiner, "Photonic synthesis of high fidelity microwave arbitrary waveforms using near field frequency to time mapping," Opt. Express **21**, 22974–22987 (2013).

[14] V. J. Hernandez, C. V. Bennett, B. D. Moran, A. D. Drobshoff, D. Chang, C. Langrock, M. M. Fejer, and M. Ibsen, "104 MHz rate single-shot recording with subpicosecond resolution using temporal imaging," Opt. Express **21**, 196-203 (2013).

[15] T. T. Ng, F. Parmigiani, M. Ibsen, Z. Zhang, P. Petropoulos, and D. J. Richardson, "Compensation of linear distortions by using XPM with parabolic pulses as a time lens," IEEE Photon. Technol. Lett. **20,** 1097-1099 (2008).

[16] O. Kuzucu, Y. Okawachi, R. Salem, M. A. Foster, A. C. Turner-Foster, M. Lipson, and A. L. Gaeta, "Spectral phase conjugation via temporal imaging," Opt. Express **17**, 20605-20614 (2009).

[17] R. Salem, M. A. Foster, and A. L. Gaeta, "Application of space–time duality to ultrahigh-speed optical signal processing," Adv. Opt. Photonics **5**, 274-317 (2013).

[18] J. Azaña, N. K. Berger, B. Levit, and B. Fischer, "Simplified temporal imaging systems for optical waveforms," IEEE Photon. Technol. Lett. **17**, 94-96 (2005).

[19] R. E. Saperstein and Y. Fainman, "Information processing with longitudinal spectral decomposition of ultrafast pulses," Appl. Opt. **47**, A21-A31 (2008).

[20] F. Parmigiani, P. Petropoulos, M. Ibsen, P. J. Almeida, T. T. Ng, and D. J. Richardson, "Time domain add-drop multiplexing scheme enhanced using a saw-tooth pulse shaper," Opt. Express **17**, 8362 -8369 (2009).

[21] J. P. Heritage and A. M. Weiner, "Advances in spectral optical code division multiple-access communications," IEEE J. Sel. Top. Quantum Electron. **13**, 1351-1369 (2007).

[22] J. Hult, R. S. Watt, and C. F. Kaminski, "High bandwidth absorption spectroscopy with a dispersed supercontinuum source." Opt. Express **15**, 11385-11395 (2007).

[23] A. Sakudo, "Near-infrared spectroscopy for medical applications: Current status and future perspectives," Clin. Chim. Acta **455**, 181-188 (2016).

[24] D. R. Solli, J. Chou, and B. Jalali, "Amplified wavelength-time transformation for real-time spectroscopy," Nat. Photonics **2**, 48-51 (2008).

[25] S. Kim, K. Goda, A. Fard, and B. Jalali, "Optical time-domain analog pattern correlator for high-speed real-time image recognition," Opt. Lett. **36**, 220-222 (2011).

[26] Y. Park and J. Azaña, "Optical signal processors based on a time-spectrum convolution," Opt. Lett. **35**, 796-798 (2010).

TABLE DES MATIÈRES

LISTE DES FIGURES

PUBLICATIONS ASSOCIÉES

Articles de journaux

[1] J. Huh and J. Azaña, "In-fiber high-speed recognition of incoherent-light broadband energy-spectrum patterns," Opt. Lett. **43**, 300-303 (2018).

[2] J. Huh and J. Azaña, "All-optical reconfigurable signal processing based on cross phase modulation time lensing," IEEE Photon. Technol. Lett. **29**, 826-829 (2017).

[3] J. Huh and J. Azaña, "In-fiber reconfigurable generation of arbitrary (asymmetric) picosecond temporal intensity waveforms by time-domain optical pulse shaping," Opt. Lett. **41**, 693-696 (2016).

[4] J. Huh and J. Azaña, "Generation of high-quality parabolic pulses with optimized duration and energy by use of dispersive frequency-to-time mapping," Opt. Express **23**, 27751-27762 (2015).

Articles de conférences internationales

[5] J. Huh and J. Azaña, "On-the-fly real-time optical energy spectrum recognition system based on time-to-spectrum convolution," in *2017 IEEE Photonics Conference* (IPC), Orlando, Florida, USA, paper WD1.4.

[6] J. Huh and J. Azaña, "All-optical reconfigurable time-lens based signal processing," in *2017 Optical Fiber Communication Conference* (OFC), Los Angeles, CA, USA, paper M3J.4.

[7] J. Huh and J. Azaña, "Programmable fiber-based arbitrary optical pulse-intensity shaper based on time-domain phase-only linear filtering," in *2016 Optical Fiber Communication Conference* (OFC), Anaheim, CA, USA, paper Th2A.9.

[8] J. Huh, D. Duchesne, and J. Azaña, "Generation of parabolic pulses with optimized duration & energy by use of dispersive frequency-to-time mapping", in *2015 Conference of Laser and Electro-Optics* (CLEO), San Jose, CA, USA, Paper SM2P. 6.

Autres publications qui ne sont pas directement en rapport avec la thèse

[9] M. R. Fernández-Ruiz, J. Huh, and J. Azaña, "Time-domain Vander–Lugt filters for in-fiber complex (amplitude and phase) optical pulse shaping," Opt. Lett. **41**, 2121-2124 (2016).

[10] M. R. Fernández-Ruiz, J. Huh and J. Azaña, "Fiber-optics reconfigurable arbitrary (complex) picosecond pulse shaping/coding by time-domain amplitude-only spectrum modulation," in *2016 Optical Fiber Communication Conference* (OFC), Anaheim, CA, USA, paper Th3H.2.

[11] L. Lei, J. Huh, Luis Romero Cortés, R. Maram, B. Wetzel, D. Duchesne, R. Morandotti, and J. Azaña, "Observation of spectral self-imaging by nonlinear parabolic cross-phase modulation," Opt. Lett. **40**, 5403-5406 (2015).

CHAPTER 1

Introduction

Optical pulse shaping is described as a technique that enables enhancing the capabilities of ultrafast pulse laser generation methods. Applications of optical pulse shaping particularly relevant to this Thesis are briefly discussed. Various methods are outlined for designing a filtering function that reshapes an input broadband optical source into a desired waveforms, and technical implementations of these methods are also reviewed, with a focus on programmable filtering technologies. The goals of the Thesis are established with the aim of overcoming some of the key limitations of previous reconfigurable optical pulse shaping techniques. The original contributions by the author are briefly presented and the structure of the Thesis is outlined.

1.1 **Pulsed lasers and optical pulse shaping**

The invention of the laser in Hughes research labs in Malibu began a new age of technologies [1]. In sharp contrast to the primitive prediction of a laser being "a solution looking for a problem", the lasers have become ubiquitous in modern society as they play a significant role in our everyday lives, for civil and defense applications alike, scientific research, etc. Lasers can be classified by the operating mode in continuous wave (CW) or pulsed lasers, depending on whether the output optical power is delivered in a continuous fashion over time or it is delivered only at regular but short time periods. Each of these kinds of lasers is dedicated to a different set of applications. To give a quick reference on the state of the art, in 2015, Lockheed Martin produced a mobile CW laser weapon with a single beam power of 30 kW that is sufficiently powerful to destroy a truck, and they successfully doubled the output power to 58 kW in 2017 [2]. On the other hand, the generation of pulsed light with the shortest possible duration keeps attracting great interest from both fundamental and applied standpoints. Generally, electromagnetic pulses with intensity full width at half maximum (FWHM) duration of the order of a picosecond (10^{-12} second) or less are considered as ultrashort (or ultrafast) pulses. A unique characteristic of an ultrafast pulse laser is its intrinsic fast temporal feature (i.e., broad frequency bandwidth) as this enables very high temporal/spatial resolution for observation and excitation of rapid microscopic (physical) processes in solid-state, chemical, and biological materials [3-6]. Electron and phonon dynamics in semiconductors were among the earliest physical phenomena to be studied using the femtosecond laser [7]. The broad frequency bandwidth intrinsic to an optical pulse can be also exploited for ultra-high-speed communication and information processing applications [8-10]. Additionally, focused pulse lasers can produce extremely high peak intensities in a short time duration, giving access to powerful nonlinear optics phenomena, which can be used for telecommunication, material processing and biomedical applications, among many others [3-12]. Applications of ultrafast pulse lasers are described in greater detail in the literature [3-7,9-12].

A pulsed laser typically generates a train of individual short optical pulses repeating periodically at a fixed rate. Through Fourier analysis[1], such a pulse train can be mathematically described as a

[1] More details are provided in Section 1.3.

coherent superposition of quasi-monochromatic waves whose frequencies are equally spaced in the optical spectrum with an approximately constant (or linear) phase difference, as illustrated in Fig. 1.1. A light wave is temporally coherent when the phase relationship is deterministic among the constituents frequency components, allowing for observation of interference fringes along the time axis, which can lead to the formation of energy peaks when the associated frequency components interfere constructively. For a shorter pulse duration, the constituent waves exhibit a wider spectral range, and vice versa. Commonly, ultrafast pulses are generated from mode-locking lasers. The advances in the technique allow for mode-locked lasers to be capable of emitting short pulses over a relatively wide range of durations, from tens of picoseconds down to below a few femtoseconds, while being readily available over a broad range of wavelengths, including wavelengths along the typical optical telecommunication bandwidth[2] (wavelengths around 1550 nm) [6,9,10,12].

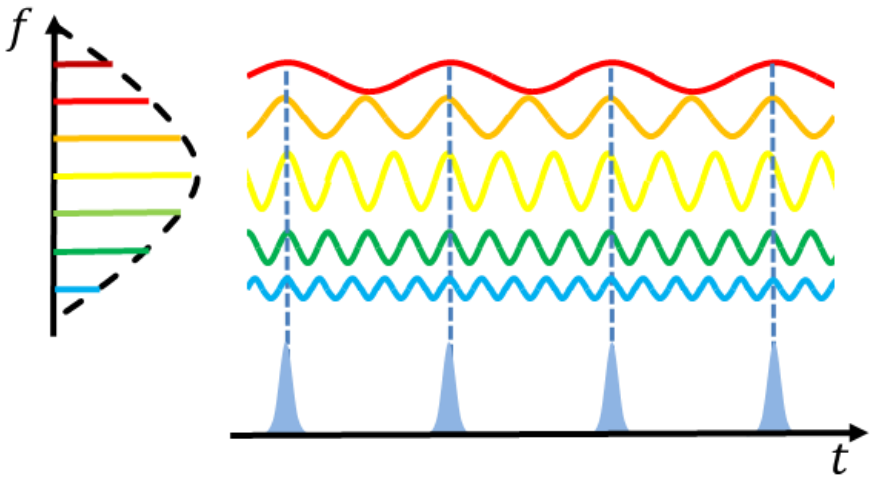

Figure 1.1 **Fourier analysis of an optical short pulse.**

[2] Typical fiber-optic telecommunication bandwidth refers to the wavelength range from 1260 nm to 1625 nm, which is divided into the O-, E-, S-, C- and L-bands.

For many practical applications, the specifications of the ultrafast light source (e.g., pulse duration, shape or energy) will need to be controlled in and efficient and well-defined manner [3-9]. This need has led to the development of optical pulse shaping (OPS) techniques, a key enabling technology in ultrafast optics and science [6,8,12-20]. Generally, OPS involves synthesizing the amplitude and/or phase variation of an optical broadband source both in the time and frequency domains. This enables the precise synthesis of the temporal shape of optical pulses, allowing for generation of ultrafast customized waveforms according to user specifications, with typical durations from the picosecond down to the femtosecond regime. The focus of this Thesis is on linear OPS methods, which enable synthesizing a desired output intensity waveform with an spectral bandwidth that is comparable to that of the input pulse source.

In the late 1960's, OPS was primarily employed for compensation of spectral phase distortions induced by stretcher/compressor pairs in chirped pulse amplification (or compression) schemes, typically consisting of bulk diffraction gratings, prisms, and lenses [18-20]. Since then, a large number of approaches for OPS have been demonstrated for a very wide range of applications. The focus of this Thesis is on fiber-optics OPS techniques for the synthesis of ultrafast optical arbitrary intensity waveforms with temporal resolution in the picosecond regime or higher, over the temporal window up to the sub-nanosecond; such techniques are particularly interesting for applications in high-speed optical communication systems, nonlinear fiber optics studies, and ultrafast spectroscopy. Other important OPS applications, including biomedical applications, ultrabroadband radio-frequency photonics, and even the control of quantum dynamics, are well described in some excellent review papers [6,12,15-17].

Simultaneously, incoherent light sources have attracted an increased attention as alternative broadband optical sources for OPS [21-25]. Incoherent light waves generated by amplified spontaneous emission (ASE) from super-luminescent diodes (SLDs), light-emitting diodes (LEDs), and erbium-doped fiber amplifiers (EDFAs), are inherently broadband since the transitions from an excited energy state to a lower energy state (e.g., ground state), required for photon emission, is an entirely random process in a quantum mechanical system (e.g., an atom, molecule, etc.). This leads to no (or very low) phase correlation among the associated optical-frequency components that constitute the incoherent light wave. In the late 1990's, V. Binjrajka et al. experimentally demonstrated that spectral phase shaping can strongly affect the coherent function of a broadband

incoherent light [21]; no further discussions of explanations of this observation were provided at the time. In a more recent work, C. Dorrer developed the temporal domain equivalent of the van Cittert–Zernike theorem [23], where partial temporal coherence can be achieved after temporal gating of an incoherent light wave followed by propagation through a chromatic dispersive medium. Dorrer's theoretical work and experimental demonstration show that the temporal degree of coherence is closely related to the magnitude of the Fourier transform of the temporal gate, also referred to as partially coherent frequency-to-time mapping [23]. This mechanism has been later used for generation of well-defined temporal intensity profiles (ensemble averaged), with frequency content in the microwave range, by the spectral shaping of an incoherent broadband light into a target intensity waveform followed by temporal gating and propagation in a dispersive medium [24]. This mechanism is further discussed in Section 1.2.2. These earlier studies are the foundation of the time-spectrum convolution (TSC) technique, the key concept in **Chapter 4**, as proposed by Y. Park et al. [25].

1.2 Relevant applications of optical intensity pulse shaping

Optical pulse shaping has a deep impact on a wide branch of disciplines. Among those, high-speed telecommunication applications that are directly relevant to my Thesis work are reviewed in this section. A brief review of topics and concepts concerning optical communication systems of specific interest to my doctoral work is first presented.

1.2.1 Coherent optical pulse shaping

The exponentially increasing data traffic in modern society is supported by gigantic transmission capacities in optical fibers ultimately enabled by various multiplexing technologies and advanced modulation formats in the optical domain [8,37-43]. Optical time division multiplexing (OTDM) is a scalable technique that allows high-speed data transmission beyond the bandwidth limitation of opto-electronics through time-interleaving of low-speed date tributaries consisting

of low-duty cycle[3] optical pulses at the same wavelengths [38]. In contrast, in wavelength division multiplexing (WDM) systems, each of the electronic data tributaries can be also allocated to a single narrow-band optical channel with its own different central wavelength (subcarrier frequency) [39]. The bandwidth efficiency can be further increased by using orthogonality[4] between the narrow-band channels (sinc shape), so that the subcarriers can be closely packed in the frequency domain, namely optical orthogonal frequency-division multiplexing (OFDM) [40]. All multiplexing techniques are fundamentally compatible with advanced modulation formats, which can offer higher spectral efficiency[5] ($\geq$ 2 bit/s/Hz) than the basic on-off keying (OOK) modulation [37-43]. Popular advanced modulation formats are the multi-level quadrature-amplitude modulation (QAM) and pulse amplitude modulation (PAM).

The quadrature-amplitude modulation (QAM) format involves a combination of phase modulation and amplitude modulation; this has been widely considered for future optical communication systems since it can provide a very high spectral efficiency, though at the expense of a reduced receiver sensitivity[6] [38]. For instance, recent reports have shown transmission of 10.2 Tbit/s of OTDM data based on the QAM-16 format [8]. On the other hand, pulse amplitude modulation (PAM) has its unique advantages since it allows for a simple direct detection of the pulse intensity rather than the complicate coherent detection[7] that is needed with a QAM scheme. In particular, PAM-4 is very attractive for short-reach applications due to its simpler implementation and higher sensitivity at the receiver compared to other higher order modulation formats [41,42].

---

[3] The percentage of the ratio of a pulse duration to the pulse period.

[4] Typically, the orthogonality can be achieved by allocating subcarriers in a manner that all the other sinc-shaped optical channels have a zero point at the peak of one channel.

[5] The spectral efficiency can be calculated by the net bit rate divided by the signal bandwidth. For instance, the spectral efficiency of a telecommunication link that transmits a 1 Mbit/s data over 1 MHz bandwidth is 1 bit/s/Hz.

[6] The receiver sensitivity is generally defined as the minimum power of an input signal to produce a specified output signal-to-noise ratio.

[7] In coherent detection, the phase state is detected from the beating signal between the reference laser and incoming data.

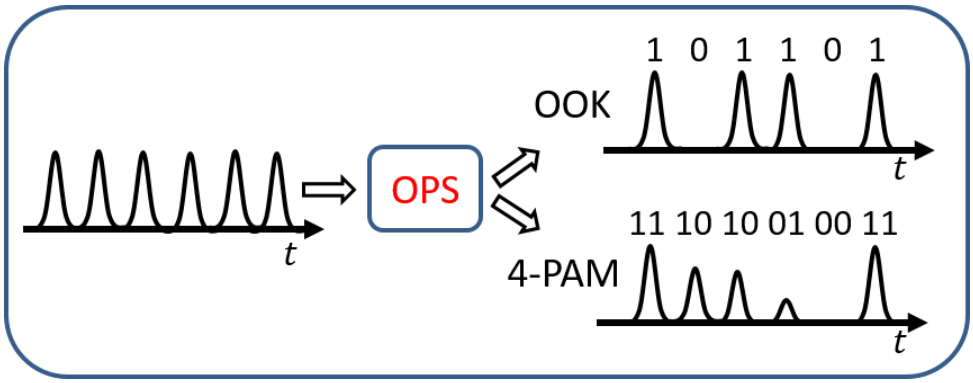

Figure 1.2 **Illustration of the basic OOK format and PAM-4 for telecommunication applications.**

In a conventional optical telecommunication link, the modulated/multiplexed lightwave signals (analog data streams) are sent to a final destination through intermediate network nodes for data redistribution; these nodes are heavily reliant on electronic signal processing (e.g., routing and switching) in today telecommunication networks [47]. In fact, the limited bandwidth of electronics may significantly slow down the optical transmission capacities offered by the aforementioned technologies, namely, what is usually referred to as the electronic bandwidth bottleneck. Moreover, this conventional scheme demands multiple conversions between the optical domain to the electronic domain. In D-WDM[8] and OFDM networks, where the available transmission capacities are divided into a large number of sub-channels, the required opto-electronics for the conversions (e.g., laser sources, electro-optic modulators, and photodetectors) are multiplied by the number of sub-channels and network nodes. All-optical signal processing has been envisioned as a potential solution for both the conversion issues and the bandwidth bottleneck in optical communication systems [43].

Many high-speed optical signal processors utilize the femtosecond response time of nonlinear light-matter interactions, such as the nonlinear Kerr effect [43-46]. The Kerr effect - based nonlinear interactions are dependent on the particular temporal intensity profile of the ultrafast

[8] Dense wavelength division multiplexing (D-WDM) in modern network systems uses narrow channel spacing (50 GHz or 25 GHz).

lasers involved in the process [3-7,12-17,26]. The intensity dependence of the refractive index in a dielectric medium results in a phase perturbation (i.e., nonlinear-phase shift) on the control pulse itself (pump) and copropagating signal (probe), processes that are known as self-phase modulation (SPM) and cross-phase modulation (XPM), respectively [27]. However, the third-order susceptibility ($\chi^{(3)}$) of a medium, responsible for the magnitude of the Kerr effect, is extremely small in most materials [47]. Thus, high-intensity electric fields are needed for modification of the optical properties of the medium. This requirement directly affects the energy efficiency of data processing sub-systems based on all-optical mechanisms, particularly as compared to their electronic counterparts [47]. The energy efficiency/consumption problem has been increasingly recognized as a key shortcoming of nonlinear optical signal processing sub-systems in telecommunication applications [47]. Nonetheless, the steady-increasing transmission capacities in optical fibers and recent advances in enabling technologies, including the discovery of new highly nonlinear materials and innovative designs for optical waveguides, has attracted renewed interest towards the potential of nonlinear signal processing as a future solution in optical telecommunications [43,48-52]. In particular, the strong optical field confinement and additional versatility enabled by current nanophotonics waveguide designs can result in gigantic nonlinearities, including the third-order susceptibility [51, 52].

Optical pulse shaping (OPS) is an enabling technology for implementation of many important functionalities in high-speed optical telecommunications [3,8,6,12,14,17,37-47], particularly for all-optical signal processing applications. A brief review of relevant optical pulse waveforms and their telecommunication applications follows.

As a first relevant example, an optical pulse with a parabolic intensity profile, where the intensity in temporal domain is proportional to square of time, self-induces a linear frequency chirp[9] as it propagates through a nonlinear Kerr medium, i.e., subject to SPM. As a result, this kind of pulse is well known for its capability to resist the deleterious effect of optical wave-breaking[10] in the

[9] A chirp is referred to as frequency variation with respect to time, defined by the first-order derivative of a temporal phase profile as a function of time.

[10] The interplay between SPM and group-velocity dispersion (GVD) in a medium can lead to complete distortion of the original temporal shape of an incident pulse. This phenomenon is referred to as optical wave breaking.

normal dispersion regime[11] [28]. As such, parabolic pulses have attracted a great deal of attention over the years for a wide range of applications, including high power pulse amplification and ultrashort pulse generation [29,30], highly coherent continuum sources development [31,32], customized pulse synthesis [33], and spectral compression [34,35]. Another interesting feature of a parabolic pulse is that a pulse with such a temporal intensity shape can be readily used as a pump for creation of a high-quality time-lens though XPM. A time-lens is a device that imparts a temporal quadratic phase modulation on an incoming temporal waveform; this device can be interpreted as temporal equivalent of a spatial thin-lens so that it is of fundamental importance for realization of many important signal-processing functionalities on time-domaim waveforms when utilized in combination with a group-velocity dispersive medium (itself the temporal equivalent of free-space diffraction). For instance, systems based on a time-lens and dispersive lines can be designed to perform temporal/spectral imaging or the temporal Fourier transform of an incoming waveform [36]. Figure 1.3 shows an example of temporal Fourier transformation of an input fast waveform when the parabolic pump pulse-induced XPM-based time-lens compensates the chirp, K, from the dispersive medium, $K = 1/\ddot{\Phi}$. It is worth noting that this specific scheme requires a linear dispersive medium offering a sufficiently high linear group delay over the input spectral bandwidth so that to induce frequency-to-time mapping on the incoming waveform; this latest mechanism is thoroughly discussed in Section 1.3.3. The XPM-induced time-lens does not require to satisfy stringent phase-matching conditions[12], contrary to other alternative methods for time lensing based on four-wave mixing[13] (FWM) [38]. Moreover, this approach can provide additional all-optical reconfigurable capabilities, exploiting the feature that the lens chirp factor (i.e., focal length of the time-lens) is directly dependent on the peak power of the parabolic pump pulse. These capabilities have been studied and exploited in my Thesis work, as detailed below.

[11] In a dispersive medium, a lower frequency wave travels faster than a higher frequency wave if the frequencies are within the normal dispersion regime.

[12] Phase-matching condition requires a proper phase relationship among the interacting waves for constructive contribution to the mixing, which should be maintained along the entire propagation direction.

[13] Four-wave mixing is a nonlinear effect inducing interactions among associated waves or producing one or two new waves.

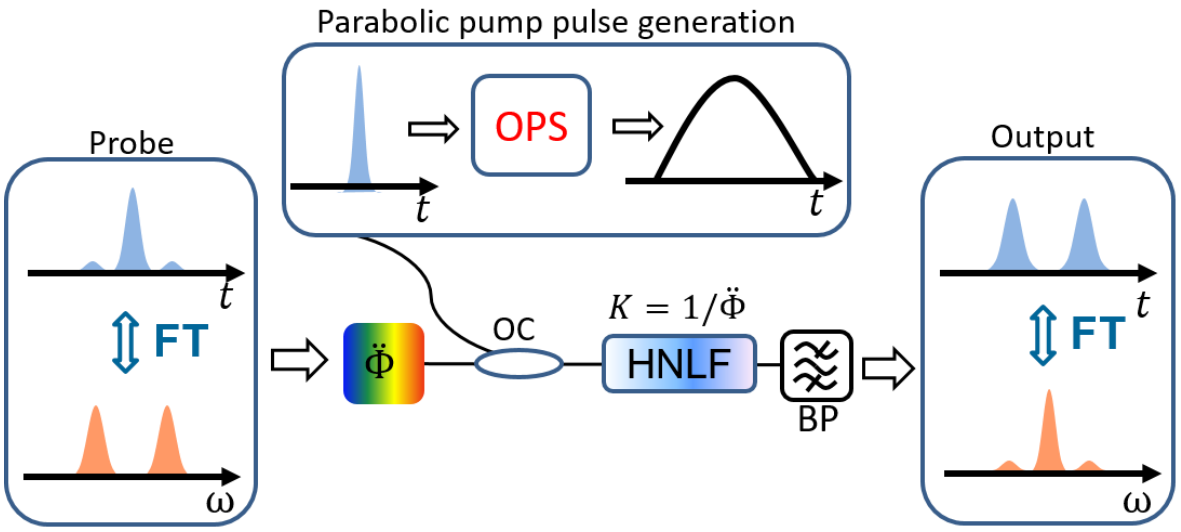

Figure 1.3 **Schematic of a temporal Fourier transformation using XPM induced by an optical parabolic pump pulse. HNLF and FT stands for a highly nonlinear fiber and Fourier transformation, respectively. Acronyms are defined in the text.**

A temporal intensity waveform that has been extensively used for telecommunication applications is a flat-top shaped pulse. This waveform defines a very precise ('sharp') temporal gate, as desired for various important applications, including ultrafast optical switching and frequency conversion [53,54]. Figure 1.4 illustrates an example of ultrafast optical switching for demultiplexing a 640-Gbit/s OTDM data signal, consisting of 64 channels of 10 Gbit/s tributaries, using a XPM-induced nonlinear optical loop mirror (NOLM) [54]. The required switching time for demultiplexing (< 2 ps) is well beyond the capability of electrical switches. In the scheme, the input 64-channel OTDM signal with the central wavelength of λ_1 is split into two data streams that propagate in opposite directions in the NOLM. The NOLM is designed to have a zero transfer function at the output port using destructive interference between the split streams without the existence of XPM-induced phase shifts from the flat-top pump pulses [54]. In the presence of pump pulses at the rate of a single channel (10 GHz), nonlinear phase shifts are imprinted between the co-directional OTDM signals corresponding to the target channel. Thus, the target channel can be then efficiently demultiplexed at the output of the NOLM, as illustrated in the figure. The use of a flat-top pump pulse provides an improved accuracy in defining the temporal gating process and this translates into important performance advantages, such as an improved tolerance to the presence of timing jitter in

the incoming data pulses and the associated enhancements in regards to detection sensitivity. For instance, in a scheme similar to that illustrated in Fig. 1.4 (as described above), L.K. Oxenløwe et al. reported that the timing-jitter tolerance improves by around 30% of the bit time slot as compared to the use of Gaussian-like pump pulse; this translates into an improved sensitivity at the receiver by at least 13 dB [54].

Another important intensity waveform that has been widely exploited for signal-processing operations based on nonlinear SPM and XPM is an asymmetric triangle (also known as "saw-tooth") optical pulse. This particular shape offers constant frequency shifts over an enlarged temporal aperture, compared to other pulse shapes, enabling to perform effective wavelength conversion of data signals, a functionality that is of great interest for many important applications, including all-optical ultrafast optical switching and channel add-drop in optical time-division multiplexing systems with enhanced timing-jitter tolerance [44-46]. As an example, Figure 1.5 illustrates the XPM-induced wavelength conversion for an all-optical channel drop using an asymmetric triangle optical pulse [44]. The raising slopes of the 10-GHz saw-tooth pulse train shift a portion of the copropagating pulse

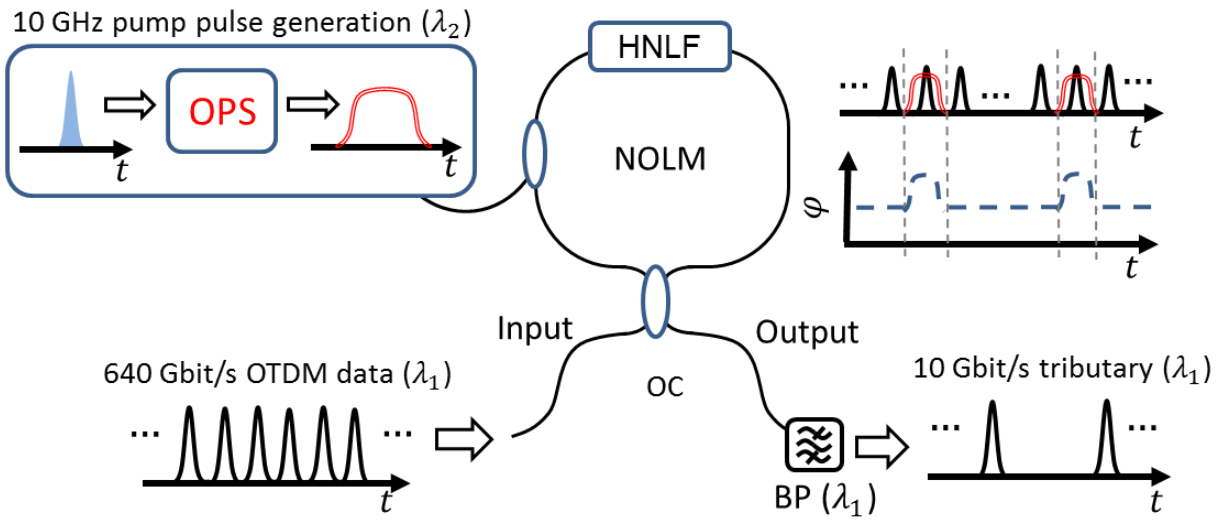

Figure 1.4 **Schematic of a XPM nonlinear optical loop mirror (NOLM) based optical gating for extracting a single 10 Gbit/s channel from 640-Gbit/s OTDM data using a flat-top optical pump pulse. a Acronyms are defined in the text.**

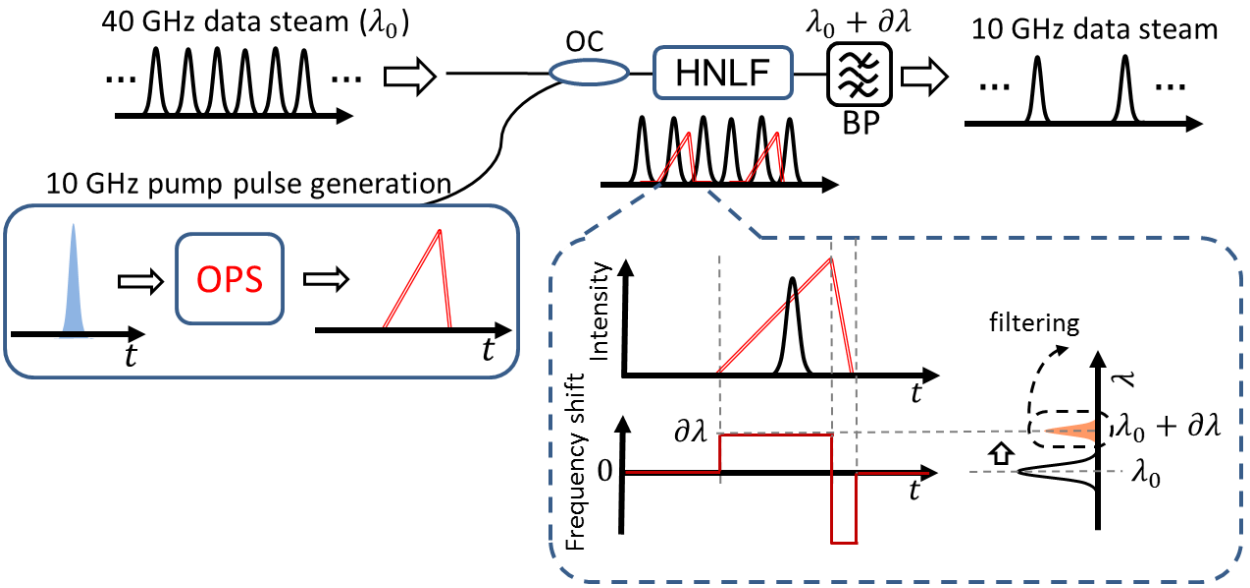

Figure 1.5 **Schematic of an all optical channel drop from a 40 GHz data stream to 10 GH using a saw-tooth optical pump pulse for XPM-induced wavelength (frequency) shift. Acronyms are defined in the text.**

energy to a lower frequency (i.e., longer wavelength λ), for the portion of the incoming signal that is within the corresponding time slot. A single 10-GHz channel is then efficiently selected from the 40-GHz data stream with central wavelength λ_0 by simply placing a bandpass filter (BP) at the shifted wavelength ($\lambda_0 + \partial\lambda$).

1.2.2 Incoherent optical pulse shaping

The practical use of optical pulse shaping (OPS) is not limited to coherent light [23-25,55-58]. The deterministic phase relationship among the associated spectral components of coherent light (e.g., broadband optical pulse) allows for a precise synthesis of an arbitrary waveform by manipulating the amplitude and/or phase of the frequency components. On the other hand, the random phase relationship of incoherent light (e.g., broadband ASE) produces a continuous-like output power over the time of interest. Thus, different approaches have been proposed for the generation of well-defined

temporal intensity profiles [23-25]. Incoherent light based time-domain optical signal processing has demonstrated its interest for a range of telecommunication and microwave photonic applications [55-58].

For instance, fundamental signal processing functionalities, such as all-optical correlation and convolution of an incoming signal with a predefined temporal pattern, have been demonstrated using an incoherent optical broadband source, first reshaped into a suitably designed spectral shape (or pattern) [25,58]. This work is based on the concept of time-spectrum convolution (TSC), which involves a spectral amplitude filtering of an incoherent optical broadband source, followed by intensity modulation with an incoming temporal waveform (the signal under analysis) and subsequent linear propagation in a dispersive medium, as depicted in Fig. 1.6. The operation principle of TSC and mathematical derivations are presented in Appendix A. In this scheme, the output temporal waveform is re-shaped, in average, according to the real-time convolution between the modulation temporal pattern (e.g., binary codes in the shown example) and the time-mapped spectral shape of the incoherent light source [25]. The implementation of this convolution operation directly along the time domain can be exploited for many important applications, such as to be able to find a prescribed matching pattern along an incoming temporal waveform (the modulation waveform) in real time and entirely avoiding the need for digital signal processing (DSP). This is of specific interest for applications in fast optical packet switching (e.g., for all-optical self-routing) and optical code division multiple access (O-CDMA) systems, among others [25,58].

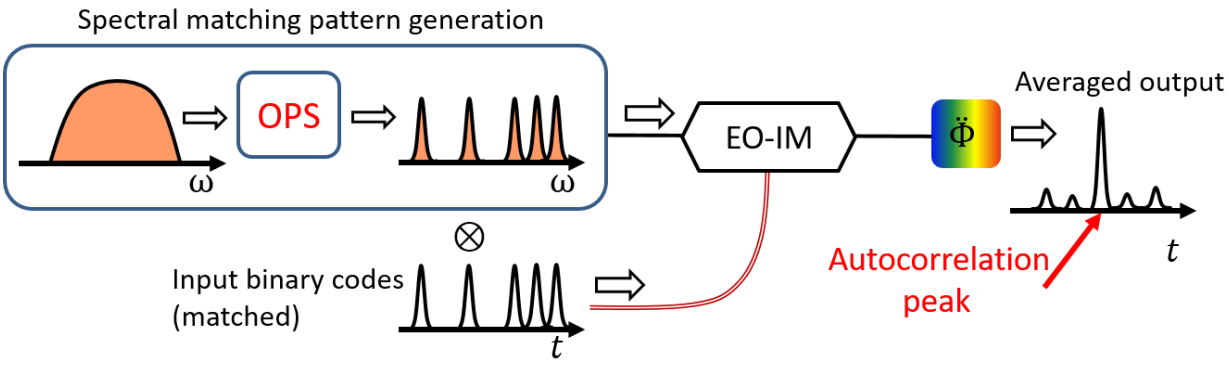

Figure 1.6 **Schematic of an all-optical correlator based on incoherent light shaping for temporal binary-code recognition. EO-IM stands for an electro-optics intensity modulator. Acronyms are defined in the text.**

1.3 Coherent optical pulse shaping based on linear photonics signal processing

Pulse shaping methods discussed here are mainly based on linear photonics signal processing since they provide simpler configurations, higher energy efficiency and superior noise performance, as compared with their nonlinear pulse-shaping counterparts.

1.3.1 Direct Fourier-domain synthesis

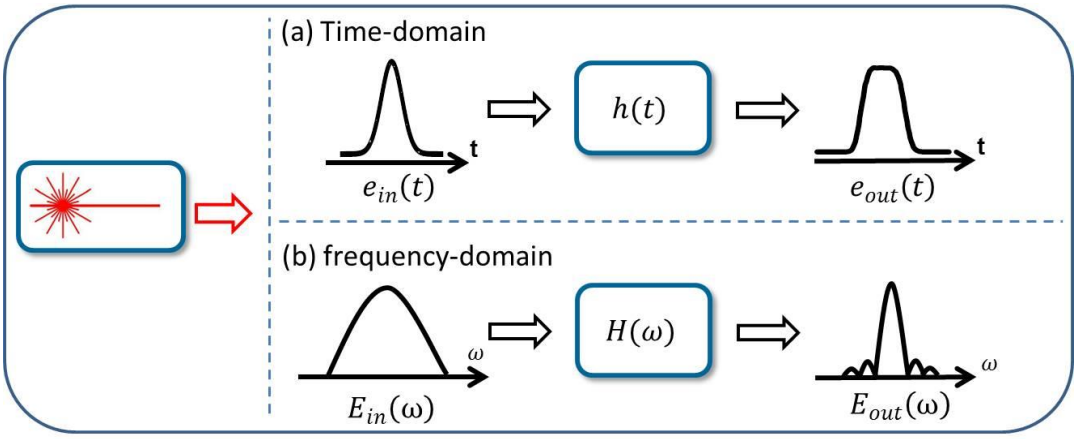

Figure 1.7 **Linear filtering in time-domain (a) and frequency-domain (b). Acronyms are defined in the text.**

Linear time-invariance (LTI) is a well-known concept that is generally useful in the analysis of the system response to a given arbitrary signal or waveform [59]. A linear system is one that has the property of superposition; specifically, the output of a linear system to an input consisting of the weighted sum of several signals is the weighted superposition of the system response to each of the individual signals. Many linear systems possess also the property of time-invariance, which enables to simplify further the analysis of the system response to an arbitrary signal. In a time-invariant

system, a time shift of the input signal causes the same time shift in the output signal with no further distortions.

An LTI system, generally known as a linear filter, can be characterized in the time domain by the system response to a temporal impulse, i.e., the impulse response $h(t)$ [12,59], as illustrated in Fig. 1.7. In response to an arbitrary input waveform $e_{in}(t)$, the output of the system $e_{out}(t)$ is given by the convolution of $e_{in}(t)$ and $h(t)$, expressed as

$$e_{out}(t) = e_{in}(t) * h(t) = \int_{-\infty}^{\infty} e_{in}(\tau)\mathrm{h}(t-\tau)\, d\tau \tag{1.1}$$

where $*$ denotes convolution. Assuming that the input pulse is sufficiently short for the time scale of interest, then, the target output can be generated by designing a filter with an appropriate impulse response that is directly proportional to the desired output waveform.

The Fourier analysis can provide insights for the design and understanding of the process. In the spectral domain, the output $E_{out}(\omega)$ is simply the product of the input signal Fourier transform $E_{in}(\omega)$ and the frequency response of the filter $H(\omega)$ [12,59], as follows

$$E_{out}(\omega) = E_{in}(\omega)H(\omega) \tag{1.2}$$

where ω is the angular frequency variable. $E_{out}(\omega)$, $E_{in}(\omega)$, and $H(\omega)$ are the Fourier transforms of $e_{out}(t)$, $e_{in}(t)$, and $h(t)$, respectively. The mathematical relationship between $H(\omega)$ and $h(t)$ can be described as

$$H(\omega) = \int_{-\infty}^{\infty} h(t)\exp[-j\omega t]dt = F[h(t)]$$

$$h(\mathrm{t}) = \frac{1}{2\pi}\int_{-\infty}^{\infty} H(\omega)\exp[j\omega t]dt = F^{-1}[H(\omega)], \tag{1.3}$$

where $F[\ \ ]$ and $F^{-1}[\ \ ]$ stand for Fourier transform and inverse Fourier transform, respectively. Owing to the Fourier transform relationships, a desired output waveform can be synthesized by designing a filter that provides a frequency response such that it re-shapes the input spectrum of the optical short pulse into the target spectral amplitude and phase, which can be easily obtained from Fourier transforming the target output waveform. This technique is usually referred to as ***direct***

Fourier-domain synthesis, and it has been widely used in optical pulse shaping. However, this approach forces to generate a transform-limited[14] output only, typically requiring both amplitude and phase filtering for arbitrary waveform generation. The implementation of both amplitude and phase filtering increases the complexity and cost of the OPS system; moreover, an amplitude filtering operation directly translates into energy loss of the input spectrum (as some frequency components of the input signal will need to be attenuated to conform the desired output amplitude spectrum). Since the spectral bandwidth of the output waveform is typically related with the target duration, a large portion of the input pulse spectrum (i.e., energy) may need to be filtered out to be able to synthesize a long output waveform. As illustrated in Fig. 1.8, this energy efficiency problem is particularly significant when one targets the synthesis of longer waveforms; this is an issue of critical importance for applications that require high power waveforms, such as for functionalities based on nonlinear optics phenomena, including those discussed in Section 1.2. It is important to note that the maximum temporal window that can be synthesized is inversely proportional the spectral resolution of the OPS system. In practice, pulse shapers offer limited spectral resolutions, typically above 10 GHz, which restricts the maximum duration of the optical arbitrary waveforms below 100 ps that can be synthesized with the system. Thus, the finest spectral resolution limits the maximum duration of the generated arbitrary waveforms. It should be highlighted that longer pulse durations (> 100 ps) are however needed for a range of important applications, such as for instance for time lensing of optical pulse sequences (e.g., telecom data signals etc.) [60-62], generation of user-defined coded pulse sequences [13], or photonics-based synthesis and control of microwave signals [63].

[14] A transform-limited pulse has the shortest temporal pulse duration for a given optical spectrum.

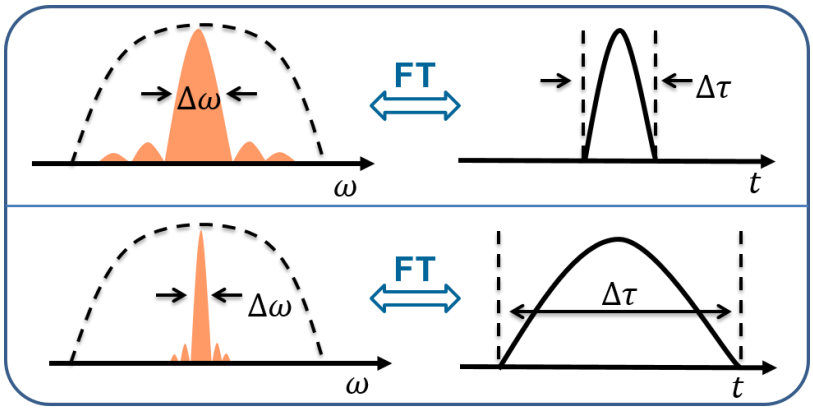

Figure 1.8 **The energy problem related to longer duration pulses in the direct Fourier synthesis method. FT stands for Fourier transformation. $\Delta\tau$ and $\Delta\omega$ stand for the temporal duration of the generated optical pulse and its corresponding spectral width, respectively.**

1.3.2 Phase-only filtering

For applications requiring the synthesis of a customized temporal intensity profile only, such as those discussed in Section 1.2, a phase-only filtering approach is more advantageous. This method reduces the complexity and cost of the experimental setup, compared to conventional full-field (amplitude and phase) control setups. More importantly, the phase-only filtering allows for design flexibility and higher energy efficiency due to the nearly zero-energy loss from the filtering process, excluding practical insertion losses. It is worth noting that this technique involves an optimal *approximation* toward the specific target intensity shape since the spectral intensity profile of the input source should be left untouched while the exact solution typically requires both amplitude and phase filtering, as discussed in the previous section (direct Fourier synthesis method). Still, many studies have demonstrated that the use of a proper phase-only filtering allows one to generate an output intensity profile that closely matches a target intensity waveform [64-67].

The technique relies on the design of an appropriate optical phase-only filter that reshapes an input spectrum to achieve the target temporal intensity waveform profile whereas the temporal phase profile is a free design parameter. The spectral response can be expressed as

$$H(\omega) \propto \exp[j\Psi(\omega)] \tag{1.4}$$

where $\Psi(\omega)$ is the required phase profile for pulse shaping as a function of angular frequency ω. The spectral response should provide a filtering function that produces an output intensity waveform $|e_{out}(t)|^2$ that is a good approximation of the target temporal intensity profile $\left|e_{target}(t)\right|^2$, in particular:

$$|e_{out}(t)|^2 = |IFT\{E_{in}(\omega)\exp[j\Psi(\omega)]\}|^2 \approx \left|e_{target}(t)\right|^2 \quad (1.5)$$

Where we recall that $IFT\{\ \ \}$ denotes the inverse Fourier transform. In pioneering work on the topic, the needed phase filtering was obtained from merely intuitive approaches, which allowed for synthesizing only basic temporal intensity waveforms [64]. Computation of the spectral phase mask $\Psi(\omega)$ for most desired waveforms is a non-trivial task, generally requiring a computer-assisted optimization algorithm, such as Simulated Annealing, a Genetic Algorithm (GA), or the Gerchberg-Saxton Algorithm (GSA) [65-67]. Recently, more complicated intensity waveforms have been successfully synthesized based on combinations of these optimization algorithms, such as symmetric pulse code sequences, flat-top shapes, etc [65-67].

To illustrate in a bit more detail the basis of an optimization algorithm in order to calculate the needed spectral phase profile to obtain a target temporal intensity waveform, I choose the case of the GA. Notice that this is the specific method used in my Thesis work, combined with the GSA for calculation of the initial generation profile, for time-domain OPS (results presented in Chapter 3).

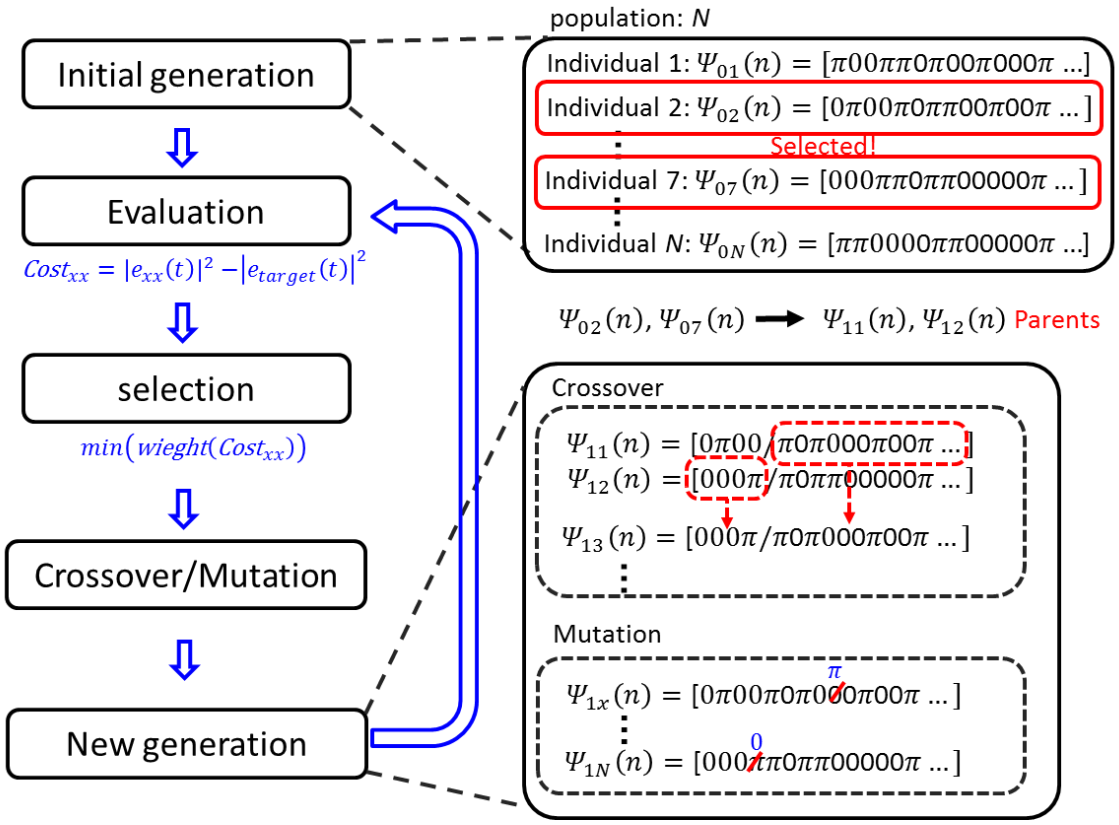

Figure 1.9 **Processing sequence of the genetic algorithm (GA). The figure illustrates the selection process to obtain a spectral phase profile that provides a target temporal intensity waveform.**

GA is an iterative global search algorithm that belongs to the larger class of evolutionary algorithms (EAs) [68]. The algorithm imitates the evolutionary processes of natural selection for optimization and search problems, as illustrated in Fig. 1.9. Many terminologies in the GA are named after genetics itself. The potential candidate for the solutions is called an individual; for the purpose of OPS enabling the synthesis of a target intensity profile, the sought-after solution is an optimal spectral phase pattern $\Psi(\omega)$. The data string of an individual is termed as a chromosome, which is then a digitized spectral phase pattern $\Psi(n) = \Psi(n\delta\omega)$, representing a properly sampled and quantized phase profile for the spectral filtering (binary levels in the example in Fig. 1.9), considering the practical spectral resolution of a pulse shaper $\delta\omega$. The sampling number n should be the ratio of the spectral bandwidth window of the pulse shaper to the spectral resolution of the optical pulse shaper. The number of the individuals in a generation is defined as population N, and the N

individuals are evaluated by the deviation between the generated temporal intensity waveform, $|e_{xx}(t)|^2 = |IFT\{E_{in}(\omega)\exp[j\Psi_{xx}(\omega)]\}|^2$ and target intensity profile $\left|e_{target}(t)\right|^2$, defined as a cost function $Cost_{xx}$. For efficient optimization, the cost function is divided into partial cost functions in order to control the different key features of each typology of target waveform, and the partial cost functions are weighted individually depending on the priority of the target features. For instance, in a flat-top pulse shape, to the features to be weighted could be the flatness, the slope of the half-width edge, and the peak intensity in the pulse pedestal, etc. [69]. From the resulting evaluation, a certain number of the spectral phase functions that provide the minimum sum of the cost function are selected as parents, and the parents breed offsprings through recombination (crossovers) and mutations to form the next generation. As illustrated in Fig. 1.9 the spectral phase profiles of offsprings are either recombination of genes from two parents or mutation from a single parent, aiming to reduce gradually a total cost function toward optimization of the spectral phase profile. This sequence continues until the cost functions reach a prescribed deviation or fitness [69].

It is important to note that more advanced waveforms such as asymmetric temporal intensity waveforms (saw tooth, completely random binary code sequences, and pulse amplitude modulation codes) require a precise and multi-level spectral phase filtering rather than the simple binary level illustrated in Fig. 1.9. Given that the phase modulation is quantized into *m*-bits levels, the size of the solution-space is increased by the power of *m* compared to the binary phase filtering case; as a result, the optimization process becomes significantly heavy [69]. The computation problem can be relaxed by combining the GA with the GSA [69], where the latest algorithm is used to obtain the initial generation in the GA. This is the combination used for the time-domain pulse shaping experiments reported in Chapter 3. The GSA is an iterative-Fourier procedure to retrieve the phase information required for the synthesis of a target temporal intensity waveform without modifying the prescribed input spectral amplitude profile. The GSA is described in more detail in Appendix B.

1.3.3 Dispersive frequency-to-time mapping

As discussed above, the spectral resolution of an optical pulse shapers (typically poorer than 10 GHz [70]) constrains the maximum temporal window that can be synthesized in practice to ~100ps.

Much longer temporal waveforms, with durations above the nanosecond regime and simultaneous,temporal resolutions in the picosecond range or better, are needed for many important applications, such as for time lensing of optical pulse sequences [60-62], synthesis of coded pulse sequences [13], or photonics-assisted microwave signal generation and processing, etc. [63]. In view of this need, strategies have been developed for photonics-based synthesis of long high-resolution waveforms. A particularly large amount of work has been carried out towards the synthesis of microwave and mm-wave waveforms using photonics-based methods, so-called photonics-assisted broadband radio-frequency (RF) arbitrary waveform generation, as desired for applications in ultrawide-bandwidth and multiple-access wireless communications, and radar systems [63,71-73]. In this context, photonics approaches are also advantageous for providing ultrawide bandwidth, low loss, and immunity to electromagnetic interference (EMI) [63,71-73]. An important and widely employed method is based on the use of *chromatic dispersion* (i.e., GVD) for mapping a re-shaped spectrum into the time-domain , what is typically referred to as dispersion-induced "frequency-to-time mapping", a process that can be interpreted as the temporal analogous of spatial Fraunhofer diffraction in the far-field. [55].

The chromatic dispersion is a well-known characteristic of a dielectric medium in optics, and its employment in optical pulse shaping (OPS) is the foundation of this Thesis. The origin of chromatic dispersion is from the frequency dependence of the refractive index, causing a variation of the group velocity as a function of frequency. Typically, a medium which has this characteristic is referred to as a dispersive medium. Notice that by refractive index here I refer either to the physical refractive index of a given bulk material, typically a dielectric material, or more generally, to the *effective refractive index* of a dielectric waveguide (for instance, an optical fiber), which considers both the material refractive index and the waveguide effect in the overall refractive index of the considered propagating optical mode [74]. Provided that a short optical pulse propagates in linear conditions along the dispersive medium, the frequency components associated with the pulse envelope travel at different speeds due to the group velocity difference, resulting in temporal broadening of the propagating pulse. Figure 1.10 (a) is an example of the pulse broadening in an anomalous dispersive medium where the higher frequencies (i.e., blue frequencies) propagate faster than the lower frequencies (i.e., red frequencies).

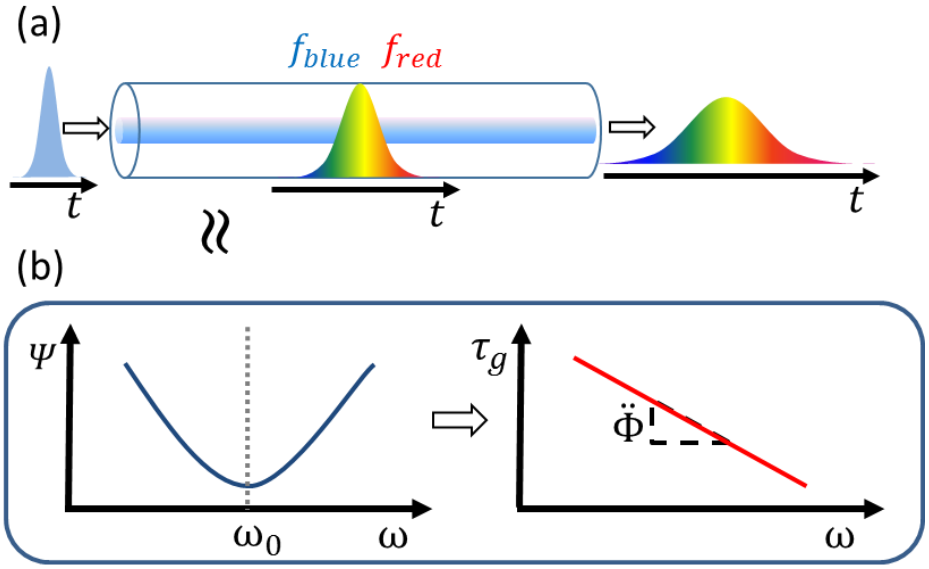

Figure 1.10 **(a) optical pulse broadening in an anomalous dispersive medium (optical fiber in telecombandwidth). f_{red} and f_{blue} stand for lower frequencies and higher frequencies, respectively. (b) the spectral quadratic phase response, Ψ, and the linear group delay response, τ_g, of a linear dispersive medium as a function of frequency. ω_0 stands for the central wavelength of an incoming optical pulse. Acronyms are defined in the text.**

Considering a pulse plane wave traveling in the z direction in a linear homogeneous, lossless, and isotropic dispersive medium with refractive index $n(\omega)$ (as mentioned above, this would refer to the effective refractive index of the relevant propagating mode in the case of propagation through an optical waveguide, e.g., optical fiber), the spectral response of the dispersive medium can be modeled as a LTI system, similarly to a phase-only linear optical filter, expressed as,

$$H(\omega) \propto \exp[j\Psi(\omega)] = \exp[-j\beta(\omega)z] \tag{1.6}$$

where $\beta(\omega)$ is a propagation constant, defined as $2\pi n(\omega)/\lambda$, where λ stands for the wavelength. The relative phase variation of the spectral response as a function of frequency can be more easily interpreted by using a Taylor series representation of the propagation constant. Assuming that ω_0 is the central angular frequency of the input pulse, the propagation constant can be mathematically expanded as

$$\beta(\omega)z = \left[\beta_0 + \beta_1\Delta\omega + \frac{1}{2}\beta_2\Delta\omega^2 + \frac{1}{6}\beta_3\Delta\omega^3 + \cdots\right]\mathrm{z}$$

$$\beta_n = \frac{\partial^n}{\partial\omega^n}\beta\Big|_{\omega=\omega_0} \tag{1.7}$$

where $\Delta\omega$ is $\omega - \omega_0$. The temporal delay induced by a spectral phase profile is determined by the first-order derivative of the spectral phase variation as a function of angular frequency, namely, $t_{delay}(\omega) = -{}^{\partial\Psi(\omega)}/_{\partial\omega}$, according to Fourier properties. Thus, the first-order term $\beta_1 z\Delta\omega$ is a linear phase shift as a function of frequency, which represents the overal group delay τ_g of the pulse envelope, and β_1 is therefore the inverse of the group velocity $1/v_g$. The second-order term, $\frac{1}{2}\beta_2 z\Delta\omega^2$ is a quadratic phase shift, inducing the linear variation of the group delay, the main reason for pulse broadening. Thus, β_2 is referred to as the group-velocity dispersion (GVD) parameter. The coefficient β_3 is defined as the third-order dispersion (TOD) parameter, which is responsible for an asymmetric temporal pulse distortion. In many dielectric media, the value of β_3 or higher-order dispersion coefficients is generally very small, and its contribution is negligible for the cases of narrow bandwidth optical pulses, e.g., picoseconds or longer pulses whose spectral bandwidths $\Delta\omega_{BW}$ are relatively small, resulting in insignificant phase values from the third-order term, i.e., $\pi \ll \frac{1}{6}\beta_3{\Delta\omega_{BW}}^3 z$ [74]. The constant term $\beta_0 z$ and arrival time (the overall group delay) of a pulse is of no importance for optical pulse shaping. Excluding all the irrelevant terms, Eq. (1.7) can be approximated as a quadratic phase term [74]:

$$H(\omega) \approx \exp\left[-j\frac{1}{2}\beta_2 z_0\Delta\omega^2\right] = \exp\left[-j\frac{1}{2}\ddot{\Phi}\Delta\omega^2\right] \tag{1.8}$$

Thus, the spectral components of the incident pulse experience approximately a linear time delay as a function of frequency, as shown in Fig. 1.10 (b). Media that have this characteristic are typically referred to as second-order linear dispersive media, and $\ddot{\Phi} = \beta_2 z_0$ is referred to as the second-order dispersion coefficient.

By exploiting the unique feature of the linear dispersive medium, the spectral components of the incident pulse can be linearly distributed in time-domain, assuming that the dispersion coefficient is sufficiently large as well as the input signal energy is confined to a sufficiently small duration $\Delta\tau_0$.

After a certain amount of propagation in the linear dispersive medium, the output temporal intensity profile is expected to be closely related to the shape of the input pulse spectrum. This is known as far-field frequency-to-time mapping (FF-FTM), which is the time-domain analogous of spatial-domain Fraunhofer diffraction in the far-field [75]. The temporal far-field condition is expressed as

$$|\ddot{\Phi}| \gg \frac{\Delta\tau_0^2}{8\pi}. \tag{1.9}$$

The detailed derivation of this far-field condition is presented in **Chapter 2**. Use of this phenomenon allows for generation of arbitrary temporal intensity waveforms by reshaping the energy spectrum of the input optical source to be proportional to the target intensity waveform, followed by a linear dispersive medium with a large second-order dispersion coefficient, as illustrated in Fig. 1.11. The output temporal intensity waveform $|a_{out}(t)|^2$ can be mathematically described as,

$$|a_{out}(t)|^2 \propto \{|A_{in}(\omega)|^2\}_{\omega=t/\ddot{\Phi}}, \tag{1.10}$$

where $|A_{in}(\omega)|^2$ is the energy spectrum of the input optical source as a function of the radial frequency variable, ω.

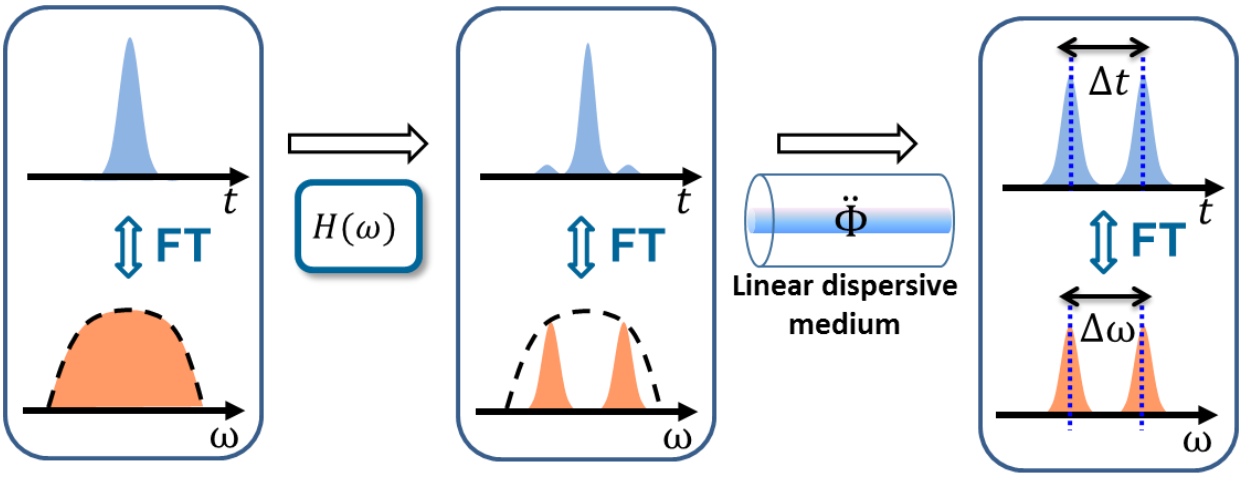

Figure 1.11 **Pulse shaping based on dispersion induced frequency-to-time mapping combined with spectral shaping. FT stands for Fourier transformation. Acronyms are defined in the text.**

It is well known that the desired linear GVD process can be provided by a simple optical fiber (e.g., conventional single mode fiber, SMF) or a linearly chirped fiber Bragg grating operated in reflection [75,76]. Particulary, the development of fiber Bragg grating (FBG) technology and its use in OPS systems as a linear dispersive medium has significantly enhanced the performance and practicality of dispersion-based OPS [75].

Typically, a FBG involves a periodic perturbation of the effective refractive index of the propagating mode along the axis of an optical fiber, with a period that is relatively short (sub-micrometer at the operation wavelength of 1.5 μm), e.g., compared to a long period grating (LPG). Assuming operation under single-mode conditions, the periodic change of the refractive index along with the optical fiber induces mode coupling between the forward-propagating mode, with its propagation constant defined as $\beta_1 = 2\pi n_{eff}/\lambda_1$, and the same mode but backward-propagating, with $\beta_2 = -\beta_1$. This translates into reflection of the propagating wave back to the input end of the optical fiber. Mode coupling is maximized when the phase-matching condition is satisfied [77], as follows

$$\beta_1 - \beta_2 = 2\pi n_{eff}\frac{2}{\lambda_1} = m\frac{2\pi}{\Lambda};\ m = 1,2,3,\ldots \tag{1.11}$$

where m is the Bragg-order, and Λ is the nominal grating period. Generally, in the first-order condition ($m = 1$) of Eq. (1.11), the Bragg wavelength (λ_B), i.e., main reflected wavelength from the FBG, is estimated as the wavelength at which the grating-induced mode coupling is dominant, according to the specific grating period, expressed as

$$\lambda_B = 2n_{eff}\Lambda \tag{1.12}$$

A linearly chirped fiber Bragg grating (LC-FBG) has a linear variation of the grating period (linear chirp), which induces that different wavelengths are reflected at different locations along the grating length, as depicted in Fig. 1.12. Said other way, a broader range of wavelengths is reflected from the device, corresponding to the range of grating periods covered by the device, and the different reflected wavelengths are delayed with respect to each other nearly in a linear fashion (considering the linear grating period variation). This enables LC-FBGs to provide a large amount of second-order dispersion over ultra-wide bandwidth while minimizing the insertion loss and device size, compared to other linear dispersive media, such as a bulky spool of standard single-mode fiber

(SMF). For instance, a ~14-m long LC-FBG used in the experiments in the Chapter 3 and 4 provides a dispersion $\ddot{\Phi}$ of ~2600 ps^2, equivalent to a length of ~120 km of conventional SMF, over a reflection bandwidth covering the whole C-Band (1530-1565nm), with a 4-dB insertion loss.

In the standard far-field frequency to time mapping (FF-FTM) based OPS, the duration of the generated arbitrary intensity waveform Δt is determined by multiplication of the reshaped spectral width $\Delta\omega$ and the amount of the dispersion [75],

$$\Delta t = \left|\ddot{\Phi}\right|\Delta\omega \tag{1.13}$$

Since the generated intensity waveform is essentially proportional to both the spectral width and the amount of dispersion ($\ddot{\Phi}$), the FF-FTM method is exempt from the restriction of the maximum pulse duration imposed by the frequency resolution of the spectral shaping device, allowing for generation of arbitrarily longer optical pulses. In addition, the approach provides a better design flexibility, compared to the direct Fourier synthesis, enabling to utilize most of the input pulse energy spectrum, regardless of the target duration or the input pulse bandwidth, through optimization of the dispersion amount only.

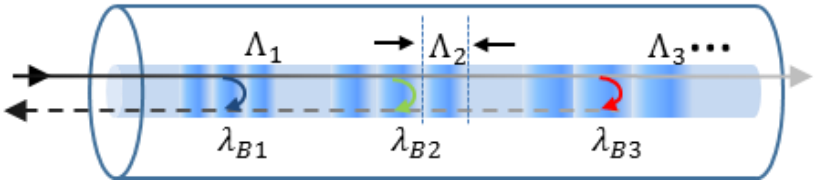

Figure 1.12 **Schematic of a linearly chirped fiber Bragg grating (LC-FBG). Λ is the nominal grating period**

However, the temporal far-field condition in Eq. (1.9) requires a large amount of dispersion, which restricts the minimum duration of an optical pulse that can be synthesized with a sufficiently high waveform fidelity. In Chapter 2, we numerically generate parabolic intensity waveforms with a temporal duration of 100 ps from a ~2 ps Gaussian input pulse using FF-FTM and noticeable waveform distortions are already observed. For this reason, this method has been mainly used for

applications where relatively longer durations of waveforms are needed, for instance for RF arbitrary waveform generation [71-73]. In my Thesis, I propose and demonstrate a novel approach for relaxing the strict far-field condition of the FF-FTM method so that arbitrary intensity waveforms can be synthesized with a temporal duration ranging from the picosecond to the nanosecond range while providing high energy efficiency.

1.4 Implementations for reconfigurable optical pulse shaping

For a photonic implementation of the optical linear filtering, various types of pulse shapers have been successfully demonstrated using optical signal processors [12-15,21,24,55]. Compared to their electronic counterparts, such as an electronic arbitrary waveform generator (E-AWG), many of the optical signal processors employed in optical pulse shaping systems are designed to perform a specific filtering function with none or very limited programmability, making it inoperative for other applications. This represents a main limitation of the OPS approach from the user's point of view. Thus, ideally, an OPS system should provide a flexible filtering function so that to enable the synthesis of various important waveforms, as required by different applications (e.g., see discussions in Section 1.2), using a single programmable configuration.

Direct modulation of a CW laser using a high-speed modulator is the most straightforward approach for optical arbitrary waveform generation (O-AWG). However, the spectral bandwidth (i.e., the temporal resolution) of the generated O-AWG is essentially proportional to the analog frequency bandwidth of the driving electric signal, typically constrained to below ~32 GHz (e.g., Keysight Technologies M8196A 92 GSa/s Arbitrary Waveform Generator) [78]. As mentioned, optical arbitrary temporal intensity profiles with resolutions in the picosecond range or faster are of great interest for a broad range of applications, such as for high-speed coding/decoding, all-optical switching, and quantum control, among many others [6,35-46,53-58,60-67,79-85]. Additionally, it is challenging to scale the direct modulation method to achieve waveforms with a relatively high pulse energy with an acceptable signal to noise ratio (SNR) as the overall energy of the synthesized waveform is limited by the average power of the modulated CW laser and the SNR is ultimately

restricted by the extinction ratio of a high-speed electro-optic intensity modulator, typically below 20 dB.

Alternatively, reconfigurable linear approaches exploiting the full utrawide bandwidth of an incident optical short pulse have been successfully demonstrated in a few platforms, based on bulk optics, fiber optics, and integrated optics. In these methods, OPS is typically achieved by use of an optical device that separates the input frequency components, enabling to have access to them either in parallel (e.g., space-domain) or in series (e.g., time-domain). This is the core process that grants synthesis of ultrafast arbitrary temporal waveforms with temporal resolution down to the femtosecond regime. In what follows, we review some of the best known methods for reconfigurable ultrafast optical pulse shaping. The main interest of this Thesis work is on optical fiber-based techniques for pulse shaping as they offer many important advantages for practical applications. These methods are relatively simple to implement and can be very cost effective; additionally, they are inherently compatible with fiber-optics systems, including very low insertion losses. For completeness, the following revision also includes pulse shaping devices implemented in free-space and integrated-waveguide technologies.

1.4.1 Space-domain pulse shapers

The design concept of the most used optical pulse shaper is based on space-domain processors, illustrated in the Fig. 1.13 [6]. The apparatus, known as a 4-f system, consists of a pair of diffraction gratings, lenses, and a spatial mask where f is the focal length of the involved thin lenses. The spectral components contained within a temporal incoming short pulse $e_{in}(t)$ are angularly decomposed by the first diffraction grating. The dispersed beams with different angles are focused into diffraction limited spots by the first lens at its back focal plane (i.e., Fourier plane), according to the incident angles. This task enables the spectral components to be spatially separated in the plane, giving an access for manipulation of the amplitude and/or phase of the individual frequency by placing a spatial mask with a desired filtering pattern. Subsequently, the output temporal waveform is obtained from the reverse processes through a second lens and diffraction grating. By using programmable spatial light modulators (SLMs), e.g., based on a liquid crystal modulator array [6,12],

or acoustic-optic modulators (AOMs) [86], reconfigurable optical pulse shapers have been successfully demonstrated with resolutions well into the femtosecond range. A key point is that because waveform synthesis is achieved by parallel modulation in the frequency domain, waveforms with effective serial modulation bandwidths exceeding a few terahertz can be easily handled and generated without requiring ultrafast modulators. This principle has been utilized in commercialized optical wave shapers, which can provide an spectral resolution up to ~10 GHz over the whole C or L band (or the whole C and L bands with ~20-GHz spectral resolution) [70]. The limitation of the spectral resolution of a space-domain pulse shaper is directly related to the insufficient amount of angular dispersion offered by a bulk grating [12]. Higher spectral resolution, up to 700 MHz over a 50 GHz free spectral range, has been achieved with a virtually imaged phased array (VIPA) device which utilizes the spectral decomposer functionality of bulk gratings combined with a Fabry–Perot etalon structure [12,87]. Still, the described method has other important drawbacks. Main restrictions of this approach include the need for efficient coupling between fiber and free-space optics, and the requirement for multiple spatially-separated modulation points, which translate into a relatively lossy and bulky configuration. Moreover, the approach is also constrained by the relatively limited update rate of SLMs, typically below the kHz range [6,12]. It is important to mention that rapid waveform updating is of growing interest in optical arbitrary waveform generation, with the ultimate target being the capability of switching the waveform shape at the repetition rate of the input pulse train (i.e., for continuous optical waveform generation).

Replacement of the SLMs by an array of fast modulators, such as $LiNbO_3$ or electro-absorption modulators, may allow for faster reconfigurable rates. However, the high-speed time-varying modulation fundamentally creates sidebands that induce undesired interference among adjacent modulation points, resulting in degradation of the generated waveform fidelity. Detailed analysis concerning the trade-off between the waveform fidelity and updating speed can be found in the literature [88,89].

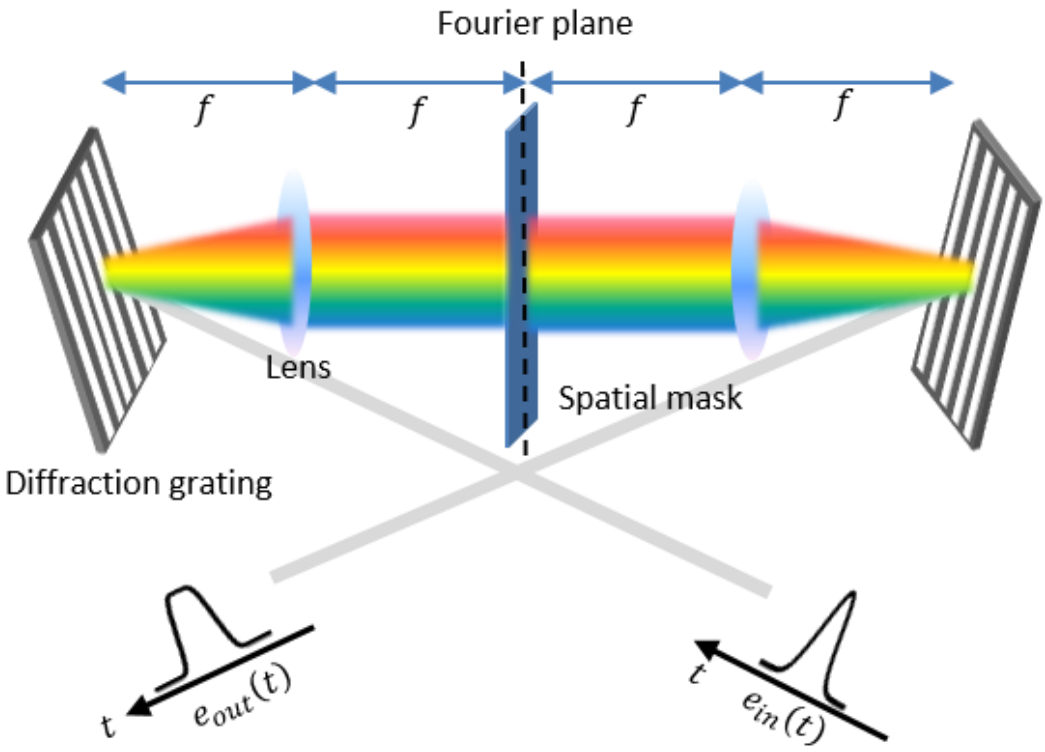

Figure 1.13 **The space-domain reconfigurable optical pulse shaper. f stands for the focal length of the lenses. $e_{in}(t)$ and $e_{out}(t)$ stand for input optical pulse and output, respectively.**

To address the size problems associated with the bulk optics approach, integrated waveguide based solutions have been proposed as an alternative method. Relevant optical pulse shaping (OPS) systems have been demonstrated using arrayed waveguide gratings (WGs) and well-defined optical frequency combs [90-95]. The arrayed WGs allow for decomposition of incident frequency components as well as recombination, analogue to the bulk diffraction gratings, yet in a more compact manner [96]. Figure 1.14 depicts the schematics of a single arrayed WG (Fig. 1.14 (a)) and an arrayed WGs-based optical pulse shaper (Fig. 1.14 (b)). An arrayed WG consists of a pair of input/output couplers and free-propagation regions, and waveguide array arms where adjacent waveguides have constant length difference. An incident light is diffracted in the first free-propagation region and distributed to the waveguide array arms. At the end of the array arms, different spectral components have different linear phase variations across the arms due to the

constant length difference, causing constructive interference at spatially separated positions after the second free-propagation region. After the demultiplexing, the amplitude and/or phase of the decomposed spectral components are manipulated by an array of modulators, generally a combination of amplitude and phase modulators or IQ modulators where "I" stands for the "in-phase" component of the waveform, and "Q" represents the "quadrature" component. Subsequently, the divided, modulated spectral components are multiplexed using the second arrayed WG, implementing the reverse process. The modulation driving signal for a target optical waveform is typically estimated from the direct Fourier-domain technique, discussed in Section 1.3.1.

Compared to the bulk optics approach, this scheme allows to reduce the device size of OPS substantially. Still, the arrayed WGs-based OPS approach is at a very early stage of development, and needs to overcome a few critical challenges for practical use. First, arrayed WGs normally offers relatively coarse spectral resolutions. The spectral resolution is inversely proportional to the constant length difference between the adjacent arms, so that a higher spectral resolution essentially requires an increase in the size of the arrayed WG, which can be extremely susceptible to fabrication errors, leading to distortions in the filtering function and spectral misalignments between the two arrayed WG passbands. In a silica platform, an arrayed WGs-based OPS has been demonstrated with a spectral resolution of 10 GHz over a spectral bandwidth of 150 GHz, with acceptable fidelity [91]. However, this technology relies on relatively slow thermo-optical effects in silica, which restricts the waveform update speed. More recent efforts for demonstrating fast reconfigurable OPSs with indium-phosphide (InP) platforms have shown to be limited from the large crosstalk in InP based arrayed WG, and the spectral misalignment problem [94-96].

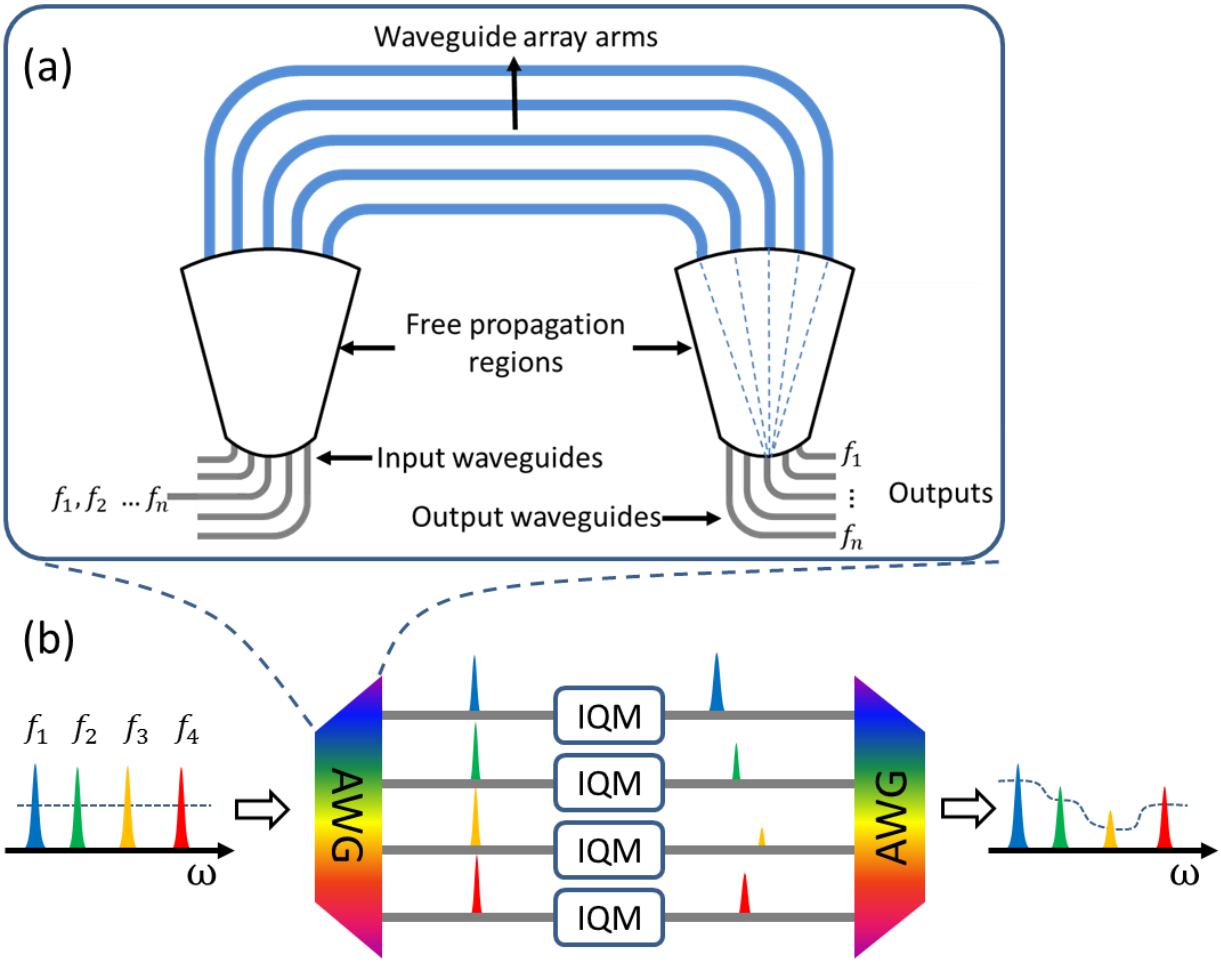

Figure 1.14 **Schematics of (a) an active-controlled arrayed waveguide grating (WG), and (b) a arrayed WGs-based optical pulse shaper. IQM stands for an IQ modulator.**

1.4.2 Time-domain pulse shapers

The intriguing space-time duality, specifically chromatic dispersion induced frequency-to-time mapping (FTM) [97], allows for the possibility of implementing the spectral multiplexing and demultiplexing processes along the time domain. This has enabled the development of optical pulse shaping (OPS) in an all-fiber simple configuration, where the filtering function is programmed directly in the time domain using high-speed electro-optic modulation (EO-M) [97]. In sharp contrast to the space-domain approaches, this time-domain optical pulse shaper provides the unique, additional capability of achieving high-speed pulse-shape update rates, into the sub-GHz range, and solid potential for integration [64,65,75,80,97].

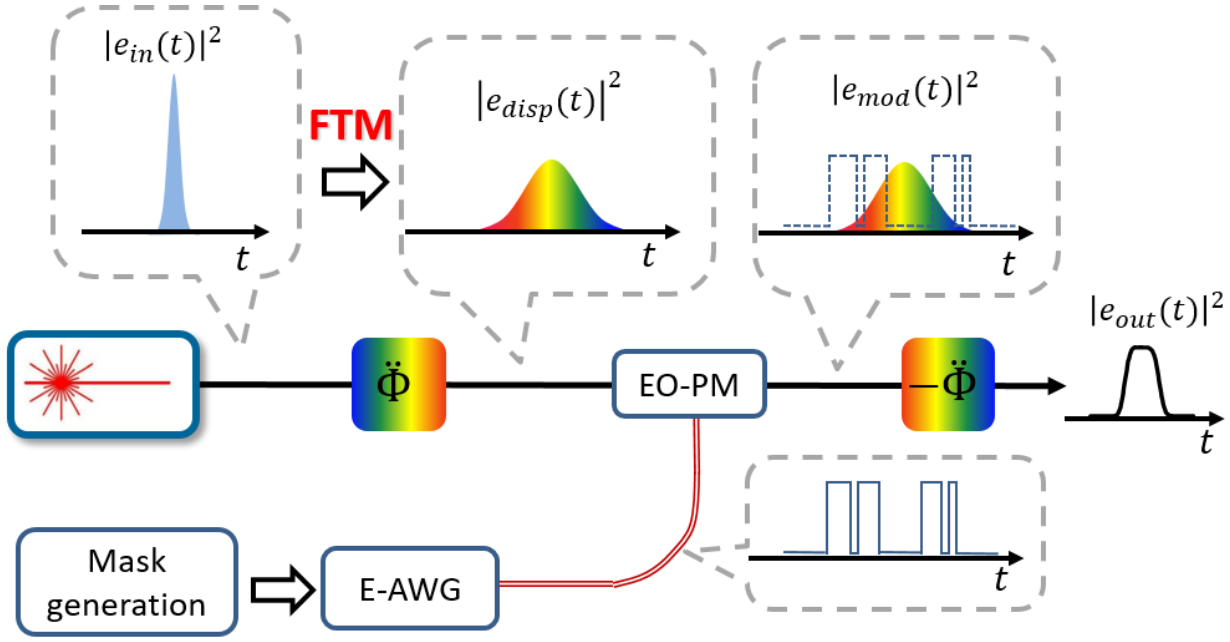

Figure 1.15 **The schematic of the time-domain reconfigurable optical pulse shaper. FTM stands for frequency-to-time mapping. $e_{in}(t)$ and $e_{out}(t)$ stand for input optical pulse and output, respectively. Acronyms are defined in the text.**

A schematic of a typical architecture for time-domain reconfigurable optical pulse shaping (OPS) is shown in Fig. 1.15. The spectral components of the incident pulse $e_{in}(t)$ are first linearly distributed in time-domain after propagation of a second-order linear dispersive medium with a sufficiently large dispersion coefficient $\ddot{\Phi}$ (defined as the first-order derivative of the medium's group delay as a function of the optical angular frequency), as discussed in Section 1.3.3. Then, the temporally stretched pulse $e_{disp}(t)$ is modulated by a high-speed single electro-optic amplitude or phase modulator, driven by a programmable electric modulation signal. In general, to achieve a degree of versatility similar to that of the space-domain OPS approach, combined amplitude and phase modulators should be used, i.e., to reshape the complex (amplitude and phase) spectral pulse profile. However, in most practical cases, a single amplitude or phase modulator is employed for experimental convenience, limiting the flexibility of the OPS method. In the most widely used scheme, e.g., as illustrated in Fig. 1.15, a single phase modulator is employed, where the desired phase modulation pattern is obtained from the phase-only filtering design method and produced from an electronic arbitrary waveform generator (E-AWG). As discussed in Section 1.3.2, this system can be designed to synthesize a desired temporal *amplitude* (or intensity) waveform profile, but cannot provide the capability of synthesizing both the amplitude and phase profles simultaneously. By subsequently compressing the stretched, phase-modulated pulse $e_{mod}(t)$ with a conjugated dispersion medium $-\ddot{\Phi}$, which compensates for the exact dispersion from the first dispersive element, the target temporal intensity profile can be directly obtained at the system output $e_{out}(t)$. Since the spectral filtering is achieved in the time-domain, this technique is referred to as time-domain spectral shaping (TDSS).

A key figure of merit for a TDSS system is the output time-bandwidth product (TBP), namely the ratio of the output spectral bandwidth to the finest spectral resolution. Alternatively, the TBP can be interpreted in the time-domain as the ratio of the duration of the output waveform to the fastest temporal feature of the waveform. In particular, the spectral resolution of the TDSS-based OPS design ($\partial\omega_{PS}$) is inversely proportional to the product of the spectral bandwidth of the modulation signal ($\Delta\omega_S$: 3-dB spectral width) and the second-order dispersion coefficient ($\ddot{\Phi}$), as follows [69]

$$\partial\omega_{PS} \propto \frac{1}{T} \propto \frac{1}{\Delta\omega_S|\ddot{\Phi}|} \tag{1.14}$$

where T is the temporal aperature of the system. The spectral resolution can be enhanced by increasing the value of the dispersion coefficient and/or the frequency bandwidth of the modulation signal, as shown in Eq. 1.14. A higher dispersion amount can be used to improve the spectral resolution without the requirement of increasing the modulation bandwidth. However, it is also important to note that the maximum value of the dispersion coefficient is limited by the pulse period of the input in order to avoid temporal overlapping between adjacent incoming pulses. The use of a lower repetition-rate input pulse allows for a larger amount of dispersion. Thus, higher spectral resolution can be achieved, according to Eq. 1.14. However, it is important to note that the repetition rate of an input pulse is equivalent to the waveform update rate in a TDSS scheme.

On the other hand, the spectral bandwidth of the output optical waveform is limited by the operation bandwidth of the linear dispersive medium. While a typical dispersive medium can process ultra-broadband signals, in most cases, the higher order dispersion parameters of the medium (beyond the needed second-order dispersion term) may become more significant as the signal bandwidth is increased, limiting the operation frequency bandwidth. This limit is below a THz for a conventional SMF at typical telecommunication wavelengths. On the other hand, a LC-FBG device can be designed to provide negligible high-order dispersion over a prescribed, wider bandwidth. A LC-FBG can also provide a larger amount of dispersion with lower insertion losses, as discussed in Section 1.3.3. In addition, the use of a LC-FBG allows for simplification of the TDSS setup since the reflection from each arm offers the exact magnitude of dispersion yet opposite signs, see detailed discussions in **Chapter 3**.

To the best of my knowledge, previously demonstrated schemes for time-domain pulse shaping (TDSS-based) phase-only filtering were limited to synthesizing purely symmetric temporal intensity waveforms. This is due to the use of a binary phase mask whereas asymmetric intensity waveforms require a multi-level phase mask. This is a highly restrictive limitation. In fact, as discussed above, asymmetric temporal intensity profiles are needed for many important applications, including arbitrary high-speed optical pulse-amplitude coding, nonlinear wavelength conversion, and time-division add–drop multiplexing with enhanced performance using asymmetric triangular pump pulses [35,36,38,41-46,81-85]. The reason for this limitation is associated with the type of modulation waveforms, i.e., spectral phase-filtering functions, used in the demonstrated setups, typically binary phase modulation patterns, which are easier to design (through the optimization

algorithms) and to implement in practice. In my doctoral work, I report the design and experimental demonstration of a TDSS-based OPS system capable of synthesizing purely arbitrary temporal intensity waveforms within a given temporal window, including asymmetric waveforms, still using a single phase modulator.

1.5 Objective and Organization of the Thesis

As a fundamental tool in optical systems, employment of optical pulse shaping (OPS) has been rapidly expanding, and multi-functionalities of an OPS system is highly desirable for practical use. In this context, ***reconfigurable*** waveform synthesis over a wide range of pulse durations has become one of the key performance factors in OPS. Various design concepts for linear optical filtering and their implementations have been demonstrate in the past, and the most relevant OPS techniques, including their main characteristics and performance limitations, have been introduced in the previous sections. Although exceptional progress has been made in the field of OPS, as discussed, important issues remain to be addressed towards the development of programmable high-performance (e.g., high resolution, high energy efficiency) arbitrary OPS platforms, according to practical requirements. My doctoral Thesis is an attempt to provide solutions to some of these remaining problems, with a focus on the use of fiber-optics platforms. As mentioned above, these platforms offer intrinsic advantages of great practical value, including their relative implementation simplicity, inherent compatibility with fiber-optics systems, including very low insertion losses, and the potential to provide cost-effective schemes. In what follows, I provide an outline of the key problems in present OPS systems to be addressed in my Thesis work, in line with the detailed discussions provided in the previous sections.

- Desired target spectral profiles for OPS are generally calculated from the direct Fourier-domain synthesis method [6,12]. However, this approach has two critical limitations: First, the maximum duration of the generated pulses is limited by the finest spectral resolution of the pulse shapers. Conventional OPS systems can offer a frequency resolution typically broader than ~10GHz, corresponding to a maximum waveform duration of the order of ~100 ps. Second, the spectral coverage of the output pulse is dictated by the target pulse duration and as such, for synthesis of long temporal waveforms, a large portion of the input

pulse spectrum, i.e., its energy, may need to be filtered out. Thus, the energy efficiency is reduced for longer pulse durations, an issue that can be of critical importance for many applications, particularly those that exploit nonlinear effects.

- Concerning specific implementations of linear OPS, the most widely used reconfigurable OPS design is based on free-space optical spectral filtering [6,12]. Central constraints of this approach include the need for efficient coupling between fiber and free-space optics, and the requirement for multiple spatially-separated modulation points, which translate into a relatively lossy and bulky configuration. Moreover, the relatively limited waveform update rate of SLMs, typically below the kHz range, represents a severe constraint for the use of the approach in applications that require rapidly reconfigurable OPS.

- Time-domain spectral shaping (TDSS) based on phase-only filtering has been proposed as an alternative to overcome the limitations of free-space optical spectral filtering discussed above [97]. However, previously demonstrated TDSS schemes have employed a simple binary phase modulation in order to avoid heavy computational design problems, allowing for the synthesis of only symmetric intensity waveforms. This is highly restrictive for practical use of TDSS based OPS in many important applications requiring more advanced intensity waveforms, e.g., saw tooth, arbitrary binary code sequences, pulse amplitude modulation codes, etc.

- The concept of incoherent time-spectrum convolution (TSC) has been previously utilized for high-speed temporal pattern recognition, as discussed in Section 1.2.2 [58]. This scheme computes a real-time correlation between the incoming temporal pattern under test (e.g., binary codes) and a spectral matching pattern, aimed for specific target applications in optical packet switching (e.g., for all-optical self-routing) and optical-code division multiple access (O-CDMA) networks, among others. However, the real-time recognition capability offered by the TSC concept has not been exploited to process spectral domain information. This includes the possibility of lightwave spectral pattern recognition, namely, to identify a

prescribed frequency-domain pattern, e.g., a spectrum absorption from a given sample, on the fly and in real time. In conventional systems, identification of a prescribed energy spectral pattern involves detection of multitude of incoming energy spectra, an inherently slow process (with update rates < kHz), and subsequent heavy numerical post-processing of the detected spectra [134]. Thus, conventional optical spectral pattern recognition methods can hardly offer operation in real time, as desired for many practical applications, while requiring the use of immense, eventually unpractical, computing resources.

The central goal of this Thesis is to develop linear-optics methods for *reconfigurable* high-speed temporal intensity OPS with temporal resolution in the picosecond regime or higher over a temporal window up to sub-nanosecond (i.e., maximum waveform duration), preferably implemented in optical fiber technologies, which can overcome the central limitations of the most conventional approaches, as defined above. Another related goal is to explore innovative applications that exploit the enhanced features offered by the newly developed OPS platforms. The different approaches explored in the Thesis are based on the concept of optical dispersion-induced FTM combined with spectral amplitude and/or phase modulation of either coherent or incoherent broadband light waves. As described, the dispersion-induced FTM is the time-domain analogous of the spatial-domain Fraunhofer diffraction effect in the far-field, in which the input signal's frequency components are linearly distributed along the time-domain. The specific contributions of this Thesis towards the defined overall goal are the following:

- In **Chapter 2**, a novel linear-optics method for reconfigurable OPS based on dispersive FTM is proposed that allows us to overcome the mentioned critical limitations of the direct Fourier-domain technique [98]. The constraints related to the minimum pulse duration of conventional FTM methods, imposed by the temporal far-field condition, are greatly relaxed by emulating a time-lens process simultaneously with the target spectral intensity filtering, using a single standard optical spectral shaping device. This method is demonstrated to provide a greatly increased flexibility to achieve a desired pulse duration, independently of the frequency resolution of the linear spectral shaping stage, as well as enabling an

optimization of the waveform energy for any target pulse duration. The focus of this work is on the synthesis and control of parabolic (quadratic-intensity) optical pulse waveforms, which are here experimentally synthesized over an unprecedented temporal duration range, from ~25ps to ~400ps, while having an output optical power up to ~4 dBm without using any amplification. High-fidelity parabolic pulses are generated from the proposed optical pulse shaper, and used for creation of an optically programmable XPM-based time-lens signal-processing platform. The optically programmable chirp factor is an unique feature of the demonstrated XPM-based time lens, directly enabled by the versatility of the developed parabolic pulse shaping technology, also avoiding the stringent phase-matching conditions of FWM-based time lensing approaches.

- Additionally, the dispersive FTM concept allows for an all-fiber simple configuration for a reconfigurable optical pulse shaper where the spectral filtering is performed in the time-domain, so-called TDSS systems. The TDSS design is a promising solution to some of the most critical limitations of space-domain approaches, as defined above, enabling high-speed pulse-shape update rates into the sub-GHz range, and solid potential for integration. **Chapter 3** presents results corresponding to the design and experimental development of a programmable fiber-optics TDSS scheme, overcoming the implementation and update-rate limitations of the conventional spatial-domain OPS approach. Additionally, the demonstrated time-domain OPS scheme enables the synthesis of fully arbitrary (including asymmetric) picosecond optical temporal pulse shapes. This is achieved through the use of *multi-level phase-only filtering*, which is programmed directly in the time-domain using a single high-speed phase modulator, driven by an electronic arbitrary waveform generator (E-AWG). The demonstrated system offers the possibilibity of synthesizing high-quality, fully arbitrary (including asymmetric) temporal intensity profiles, with resolutions in the picosecond regime and higher. In the reported proof of concept experiments, I show the synthesis of high-quality asymmetric triangular intensity waveforms, pulse code sequences with 150 Gbit/s on-off keying (OOK) modulation, and 300 Gbit/s 4-level pulse amplitude modulation (PAM-4), with a temporal resolution of ~2 ps over a time window up to ~60 ps (corresponding to a TBP of about 30).

- **Chapter 4** deals with the analysis and novel application of an incoherent-light temporal shaping system in which the temporal shape of the output waveform is determined by the convolution between the time-mapped spectral shape of a broadband incoherent light source and a temporal intensity modulation pattern, i.e., exploiting the concept of dispersion-induced time-spectrum convolution (TSC). As its main contribution, this part of the work explores the potential of this method to process light-wave incoherent spectra (rather than temporal signals), in particular, for reconfigurable real-time identification of a prescribed optical spectrum pattern. This is achieved through a suitable design of the temporal modulation signal that is programmed in an E-AWG, entirely avoiding the need for any further numerical post-processing. In the proof-of-concept experiments, I have experimentally demonstrated spectral pattern recognition at an identification rate of 650 kHz, over a 1.5-THz bandwidth with a frequency resolution of ~12 GHz in the near infrared radiation (NIR) regime.

- **Chapter 5** summarizes the presented work in this Thesis and proposes potential prospects for future work.

CHAPTER 2

CH. 2. A

Generation of high-quality parabolic pulses with optimized duration and energy by use of dispersive frequency-to-time mapping

2.1 Abstract

We propose and demonstrate a novel linear-optics method for high-fidelity parabolic pulse generation with durations ranging from the picosecond to the sub-nanosecond range. This method is based on dispersion-induced frequency-to-time mapping combined with spectral shaping in order to overcome constraints of previous linear shaping approaches. Temporal waveform distortions associated with the need to satisfy a far-field condition are eliminated by use of a virtual time-lens process, which is directly implemented in the linear spectral shaping stage.

Using this approach, the generated parabolic pulses are able to maintain most energy spectrum available from the input pulse frequency bandwidth, regardless of the target pulse duration, which is not anymore limited by the finest spectral resolution of the optical pulse spectrum shaper. High-quality parabolic pulses, with durations from 25ps to 400ps and output powers exceeding 4dBm

before amplification, have been experimentally synthesized from a picosecond mode-locked optical source using a commercial optical pulse shaper with a frequency resolution >10GHz. In particular, we report the synthesis of full-duty cycle parabolic pulses that match up almost exactly with an ideal fitting over the entire pulse period.

2.2 **Introduction**

An optical pulse with a parabolic intensity profile and a linear frequency chirp is well known for its capability to resist the deleterious effect of optical wave-breaking in a normal dispersion regime [28,99]. As such, parabolic pulses have attracted a great deal of attention over the years for a wide range of applications, including high power pulse amplification and ultrashort pulse generation [29-31,100-104], highly coherent continuum sources development [31,32,82,105], customized pulse synthesis [33], and spectral compression [34,35]. Parabolic pulses were successfully generated in normal dispersive amplifiers using rare-earth doped fiber amplification [29,30,32,99-104] or Raman amplification [106,107]. Alternative methods that do not target signal amplification are particularly interesting for applications in the context of optical telecommunications, such as time-lens-based optical regeneration methods [60,61,108] and spectral self-imaging operations [62]. In this context, generation of parabolic pulses have been proposed using dispersion varying nonlinear fibers [109-111]; however, the needed fibers are not easily accessible, and waveform distortions are induced by the impact of third-order dispersion and attenuation in the fibers [110].

Alternatively, more widely accessible linear pulse shaping techniques have been demonstrated based on the use of a super structure fiber Bragg grating (SSFBG) [82], an acousto-optic device [34], and arrayed waveguide gratings (AWGs) [112]. These methods are based on a direct Fourier-domain synthesis technique, where the spectrum of a short optical pulse is re-shaped according to the Fourier transform of the target temporal waveform. However, direct Fourier-domain synthesis of parabolic pulses has two critical limitations. First, the maximum duration of the generated pulses is limited by the finest spectral resolution of the pulse shaper. Typical pulse shaping methods offer frequency resolutions above 10-GHz [82,112] and this has restricted experimental linear generation of parabolic pulses with durations shorter than 25ps. Longer pulse durations are however needed for a range of

important applications, for instance for time lensing of optical pulse sequences [60-62,109]. Moreover, in direct Fourier-domain synthesis methods, the spectral pulse width of the output parabolic pulse is dictated by the target pulse duration and as such, a large portion of the input pulse spectrum, i.e., energy, may need to be filtered out. Again, the energy efficiency is reduced for longer pulse durations, an issue that can be of critical importance for nonlinear optics applications. The possibility of generating parabolic pulses with longer durations was also demonstrated using dispersion combined with spectral amplitude shaping [35] or temporal intensity modulation [113], but without any further discussions on the capabilities and limitations of these methodologies, and potential optimization strategies.

In this work, we propose and demonstrate a novel linear-optics method for parabolic pulse generation capable of overcoming the mentioned critical limitations of previous approaches. The proposed method provides a greatly increased flexibility to achieve a desired parabolic pulse duration, independently of the frequency resolution of the linear spectral shaping stage. This method is based on dispersion-induced frequency-to-time mapping, including the possibility of incorporating a virtual time lens so that to relax further the constraints imposed by the far-field condition [75]. Previously, similar strategies were proposed in order to increase the time-bandwidth product in ultrabroadband arbitrary RF waveform generation [114]. Here, we show how this scheme is ideally suited for parabolic pulse generation, enabling to synthesize high-quality parabolic pulses over a wide range of durations, from a few picoseconds to the sub-nanosecond range in the designs shown here, with high energy efficiency, by maintaining most of the energy spectrum available from the input pulse source.

2.3 **Principle of dispersion-induced frequency-to-time mapping**

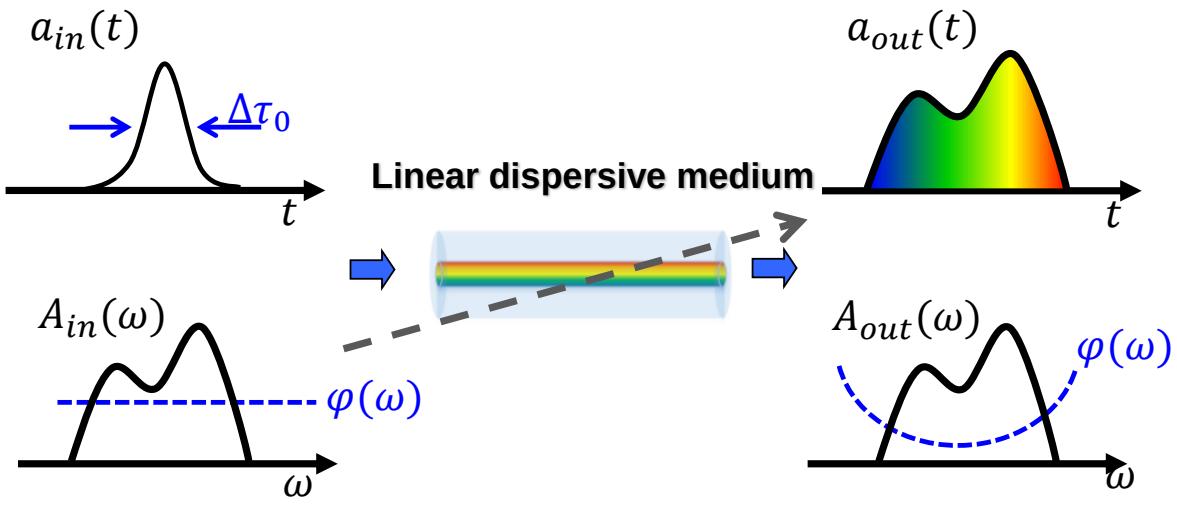

Figure 2.1 **Dispersion-induced frequency-to-time mapping in a linear second-order dispersive medium.**

Linear frequency-to-time mapping (FTM), which is the time-domain analogous of spatial-domain Fraunhofer diffraction in the far-field, essentially involves a linear distribution of the input signal's frequency components along the time domain, which is induced by the linear group velocity variation as a function of optical frequency that is characteristic of a predominantly second-order dispersive medium. After certain amount of propagation in this dispersive medium, the output temporal intensity profile is expected to be closely related to the shape of the input pulse spectrum, as illustrated in Fig. 2.1 The relationship between the input temporal waveform $a_{in}(t)$ and output waveform $a_{out}(t)$ (t is for the time variable) of an optical pulse linearly propagating through a second-order dispersive medium can be mathematically approximated as follows (obviating average group delay) [75]

$$a_{out}(t) \cong C\exp\left(\frac{j}{2\ddot{\Phi}}t^2\right)\int_{-\infty}^{\infty} a_{in}(\tau)\exp\left(\frac{j}{2\ddot{\Phi}}\tau^2\right)\exp\left(\frac{-j}{\ddot{\Phi}}\tau t\right)d\tau \tag{2.1}$$

where C is a constant in time, $j = \sqrt{-1}$, is $\ddot{\Phi}$ the second-order dispersion coefficient, defined by the first-order derivative of the medium's group delay as a function of the optical angular frequency ω, and τ is an integral variable. If the magnitude of the second-order dispersion coefficient $\ddot{\Phi}$ is large enough and the input signal energy is confined to a sufficiently small duration $\Delta\tau_0$, then the second phase term in the integral ${\Delta\tau_0}^2 \Big/ 2\ddot{\Phi}\, \Delta\tau_0{}^2/2\left|\ddot{\Phi}\right|$ becomes negligible, and therefore, Eq. (2.1) can be approximated as

$$a_{out}(t) \cong C\exp\left(\frac{j}{2\ddot{\Phi}}t^2\right)\int_{-\infty}^{\infty} a_{in}(\tau)\exp\left(\frac{-j}{\ddot{\Phi}}\tau t\right)d\tau = C\exp\left(\frac{j}{2\ddot{\Phi}}t^2\right)\left\{A_{in}(\omega)|_{\omega=t/\ddot{\Phi}}\right\} \tag{2.2}$$

where $A_{in}(\omega)$ is the Fourier transform of $a_{in}(t)$. Equation (2.2) clearly shows that under the prescribed condition, the output temporal intensity profile is a scaled replica of the input spectrum. The condition for FTM can be deduced from the above-defined phase approximation [75]:

$$\left|\ddot{\Phi}\right| \gg \frac{{\Delta\tau_0}^2}{8\pi} \triangleq TBP^2\frac{\pi}{2\Delta\omega^2} \tag{2.3}$$

where $\Delta\omega = 2\pi\Delta\nu$ is the full spectral width of $A_{in}(\omega)$ and *TBP* is a parameter than defines the time-bandwidth product, $TBP = \Delta\tau_0\Delta\nu$, of the input waveform $a_{in}(\tau)$. Recall that the *TBP* parameter strongly depends on the temporal/spectral complex shape of the waveform, but is typically much higher than 1. The relationship between the input pulse duration and the second-order dispersion coefficient in the Eq. (2.3) is the temporal far-field condition, and the linear FTM obtained in this case is usually referred to as far-field FTM (FF-FTM). The approximation in Eq. (2.3) has been also expressed as a function of the frequency bandwidth of the input pulse through its *TBP*.

2.4 **Design guide lines**

2.4.1 Far-field frequency-to-time mapping (FF-FTM)

By using this phenomenon, parabolic pulses can be simply generated by shaping the input pulse spectrum to be parabolic followed by propagation through a dispersive medium satisfying Eq. (2.3). The duration of the generated parabolic pulses Δt_0 is determined by

$$\Delta t_0 = \left|\ddot{\Phi}\right|\Delta\omega \tag{2.4}$$

where $\Delta\omega$ is the full width of the parabolic spectrum after pulse shaping. It is worth noting that the generated pulse width is proportional to both $\Delta\omega$ and $\ddot{\Phi}$. This is in sharp contrast to previous design strategies based on the use of direct spectral shaping [82,112], where the temporal width of the generated parabolic pulse is inversely proportional to the shaped spectrum width only. This translates into a lower energy efficiency for synthesizing longer parabolic pulses, as this requires filtering out a larger portion of the input pulse energy spectrum, as shown in Fig. 2.2(a). In sharp contrast, the proposed FTM method enables utilizing most of the input pulse energy spectrum, regardless of the target duration or the input pulse source bandwidth, through optimization of the dispersion amount only.

However, the far-field condition in Eq. (2.3) also restricts the minimum duration of pulses that can be generated with a sufficiently high quality using the proposed scheme. In particular, introducing the far-field condition, Eq. (2.3), into Eq. (2.4), we estimate that

$$\Delta t_0 \gg TBP^2 \frac{\pi}{2\Delta\omega^2} \tag{2.5}$$

which implies that the output pulse duration must be much longer than the transform-limited pulse time-width corresponding to the input pulse spectrum (~$1/\Delta\nu$). In regards to our specific problem, notice that the Fourier transform of a parabolic pulse is a first order Bessel function of the first kind (sinc-like shape). Thus, a high-quality parabolic spectrum requires the precise synthesis of a few sidelobes in the corresponding time-domain Bessel function, which in turns translates into an input signal of relatively high *TBP* (e.g., about 9 if 3 sidelobes at each side of the Bessel function are considered). This represents a significant constraint in regards to the minimum output parabolic pulse duration, as per Eq. (2.5).

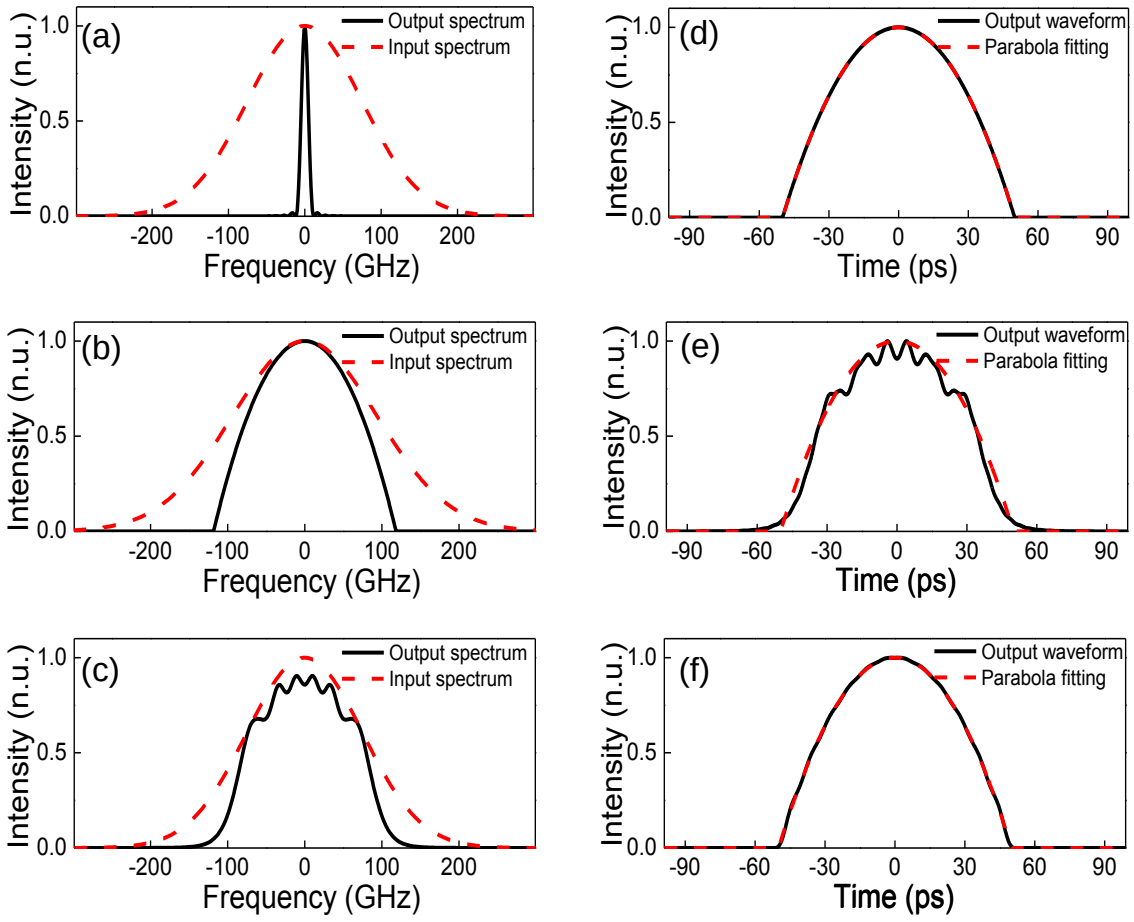

Figure 2.2 **Numerical results on the synthesis of a 100-ps parabolic pulse from a Gaussian pulse with an intensity FWHM of ~2 ps: Spectra before and after the spectral shaping stage, and numerically calculated output temporal waveforms for the direct spectral shaping ((a), (d)), FF-FTM ((b), (e)), and NF-FTM ((c), (f)) approaches. (a)-(c) black solid lines are the desired spectra after the spectral shaping stage and red dashed lines are for the initial spectrum of the input Gaussian pulse. (d)-(f) red dashed lines are for the ideal parabola fitting and black solid lines are the generated parabolic pulses.**

In order to confirm this anticipated constraint, a numerical calculation was carried out for generation of a 100-ps full-width duration parabolic pulse. A Gaussian pulse with intensity FWHM of ~2 ps was assumed as the input source. After spectral shaping, the input spectrum was modified to exhibit the desired parabolic shape, as shown in Fig. 2.2(b); the target was to use most of the input spectral bandwidth and as a result, the frequency bandwidth of the reshaped spectrum $\Delta\omega$ (zero-to-

zero full width) was $2\pi \times 237$ GHz. The corresponding second-order dispersion coefficient to achieve an output parabolic pulse duration of 100 ps, as per Eq. (2.4), was 67 ps^2. Notice that it has been previously shown that the far-field condition in Eq. (2.3) is too restrictive [115], i.e., in most cases it is sufficient that the amount of dispersion is only a few times (~2-3) higher than the right-hand side terms in the inequality. Nonetheless, our numerical simulations show that the output temporal intensity waveform, Fig. 2.2(e), still exhibits visible distortions, particularly in regards to the presence of undesirable temporal oscillations. These distortions can be directly attributed to the non-negligible quadratic phase term $\Delta\tau_0{}^2 \big/ 2\ddot{\Phi}$ in the integrand of Eq. (2.1). As predicted, this is due to the fact that the input signal (parabolic spectrum) exhibits a relatively high *TBP* (~9, in our numerical example), so that the inequality in Eq. (2.3), even in its less strict form, require the use of a notably larger dispersion; correspondingly, using the given input pulse specifications, the inequality in Eq. (2.5) indicates that one should target generation of a pulse with a duration significantly longer than 100 ps. Notice that also in line with the trend expressed by Eq. (2.5), this restriction can be relaxed by using a wider input spectral width. To give a reference, the same level of distortions as those observed in Fig. 2.2(e) would appear in a generated parabolic pulse with half the duration (50 ps) if the input parabolic spectral bandwidth was twice larger ($2\pi \times 474$ GHz). However, the fact that the required input pulse transform-limited time-width must be significantly longer (about 25-50 times longer) than the target output pulse duration represents a key limitation for practical uses of the FF-FTM methodology in the problem of parabolic pulse synthesis.

2.4.2 Near-field frequency-to-time mapping (NF-FTM)

An efficient way to overcome the described constraint of the FF-FTM method, without replacing the input pulse source, involves using a time lens process, namely the time-domain analogous of producing the desired Fourier transform in the focal plane of a spatial lens. This approach is known as near-field frequency-to-time mapping (NF-FTM).

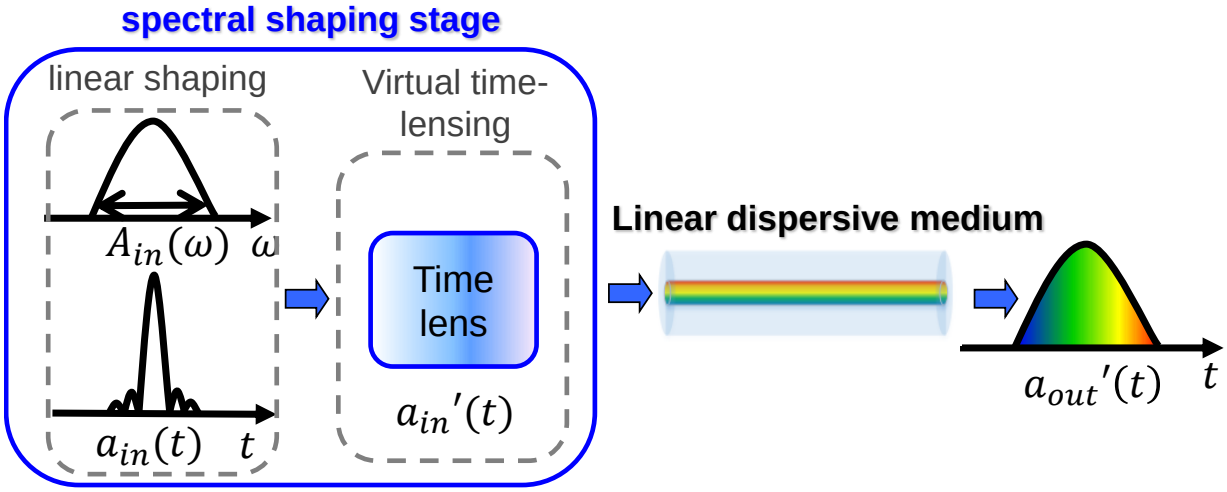

Figure 2.3 **NF-FTM by using a time lens. The time lens is virtually implemented in the linear spectral shaping stage.**

We assume that the time lens provides a phase modulation with the same magnitude but opposite sign to the quadratic phase term ${\Delta\tau_0}^2/_{2\ddot{\Phi}}$ in the integrand of Eq. (2.1) as

$$a_{in}'(t) = a_{in}(t)\exp\left(-\frac{j}{2\ddot{\Phi}}t^2\right). \tag{2.6}$$

By introducing this time-lensed signal $a_{in}'(t)$ as the input signal into Eq. (2.1), the quadratic phase term is canceled out and the output waveform is then a scaled replica of the input spectrum $A_{in}(\omega)$, regardless of the magnitude of the dispersion coefficient, which means that the generated pulse is no longer restricted by the far-field condition in Eq. (2.3). The time-lens modulation process can be 'emulated' in the linear spectral shaping stage [114]. The main idea here is to reshape linearly the original input pulse spectrum with an amplitude and phase mask that includes the parabolic spectrum reshaping process and spectral changes from the virtual time-lensing process, as shown Fig. 2.3. In particular, the desired complex spectrum after the linear spectral shaping stage should be the Fourier transform of the time-lensed signal $a_{in}'(t)$. It is important to mention that the time-lensing process generally induces spectral distortion and broadening of the original parabolic spectrum and this should be kept into account in designing the entire linear pulse shaping stage so that the resulting

frequency bandwidth after the virtual time lens does not exceed the bandwidth available from the input pulse source. To be more concrete, the spectral broadening induced by the time-lensing process is inversely proportional to the subsequent dispersion coefficient, which is directly related to the target pulse duration. Fortunately, for a fixed duration pulse, the selection of a narrower spectral width at the linear shaping stage would require a relatively higher dispersion, which in turns results in a narrower spectral broadening, and viceversa. The frequency bandwidth solely induced by the time lens should be narrower than the lens frequency chirp excursion Δf_{TL} over the entire input pulse period, *T*, in turn fixing the maximum duration of the output parabolic pulses:

$$\Delta f_{TL} = \frac{1}{2\pi}\frac{\delta\phi}{\delta t} = \frac{T}{2\pi\ddot{\Phi}} \tag{2.7}$$

In our experiments, the maximum frequency bandwidth of the time lens that can be directly estimated from Eq. (2.7) was within the input Gaussian spectral bandwidth. We reiterate that Eq. (2.7) provides an estimate for the maximum possible bandwidth to be induced by the time-lens over the entire input pulse period; in our designs, most of the energy of the signal $a_{in}(t)$ (sinc-like temporal intensity profile) is strongly concentrated near the center ($T \approx 0$) so that the estimate provided by Eq. (2.7) is usually well above the actual frequency broadening induced by the time-lensing process.

Fig. 2.2 shows the results of numerical simulations on the generation of 100-ps duration parabolic pulses from an ~2-ps input Gaussian pulse by direct spectral shaping (a, d), spectral shaping with FF-FTM (b, e), and NF-FTM (c, f). The direct spectral shaping requires the use of a pulse shaper with a very high spectral resolution, higher than 10 GHz; additionally, a large portion of the Gaussian input energy spectrum has to be filtered out in this case. This input pulse-energy loss is significantly reduced by use of the FF-FTM; however, as discussed in detail above, in this case, the output temporal waveform is significantly distorted due to the fact that the far-field condition is not fully satisfied. By using linear spectral shaping combined with NF-FTM, one can generate a parabolic intensity profile with a nearly ideal temporal shape, as shown in Fig. 2.2(f) while still using most of the input energy spectrum. Recall that the virtual time-lensing process is lossless. The spectral shape in Fig. 2.2(c) corresponds to Fourier transforming $a_{in}{}'(t)$, which is a sinc-like temporal waveform (Fourier transform of a parabolic function) modulated by the quadratic phase term from the virtual time-lensing process.

2.5 **Experimental results**

The derived design guidelines were experimentally validated. Figure 2.4 shows the experimental setup for parabolic pulse generation with durations ranging from 25ps to 400ps. Pulses below 100ps were generated using the NF-FTM approach whereas an example of generation of parabolic pulses, with a duration of 400ps, using the FF-FTM approach is also reported. The initial optical pulses were generated from an actively mode-locked fiber laser producing ~2 ps (intensity FWHM) Gaussian-like pulses at a repetition rate of ~10 GHz. The input pulse power was ~10 dBm and the central wavelength was 1550.2 nm. The input source was spectrally shaped into the desired complex spectra by using a commercial free-space optical pulse shaper (Finisar WaveShaper 4000S, resolution >10 GHz), with user-defined amplitude and phase masks for each generation case. The dispersive medium was created through a simple combination of readily available single mode optical fibers (Corning SMF-28: dispersion $\leq 18\ \mathrm{ps}/nm \cdot km$, dispersion slope $\approx 0.058\ \mathrm{ps}/nm^2 \cdot km$ at 1550 nm, and SMF-LEAF: dispersion $\leq 6\ \mathrm{ps}/nm \cdot km$, dispersion slope $\leq 0.1\ \mathrm{ps}/nm^2 \cdot km$ at 1550 nm). Given the spectral bandwidth of the input pulses and dominant second-order dispersion values of the fibers, contributions from the third-and higher-order dispersion terms are negligible. In the same context, polarization mode dispersion (maximum PMD $\leq 0.1\ \mathrm{ps}/\sqrt{km}$) can be also neglected in our analysis, considering the relatively long parabolic pulse durations (from 25ps to 400ps) and short lengths of SMF fibers used in our designs (from 0.7 km to 20 km). The input and output parabolic pulses were characterized in the spectral and temporal domains by using an Optical Spectrum Analyzer (OSA) with a wavelength resolution of 0.01 nm, and an Optical Sampling Oscilloscope (PSO-100, EXFO) with a bandwidth of 500 GHz, respectively.

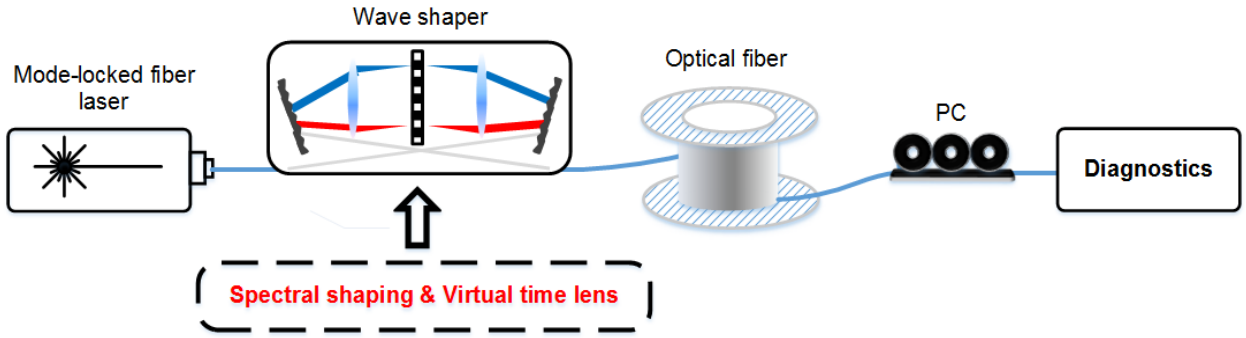

Figure 2.4 **Experimental setup used for parabolic pulse generation. A polarization controller (PC) was used to adjust the polarization state, as needed for operating the temporal diagnostic (nonlinear optical sampling oscilloscope).**

2.5.1 Far-field frequency-to-time mapping (FF-FTM)

Parabolic pulses with 400ps duration were generated using the FF-FTM approach. The original pulse repetition rate (~10 GHz) was decreased down to 2.5GHz by using a Mach-Zehnder intensity modulator (MZM) to prevent interference between consecutive output pulses. An erbium-doped fiber amplifier (EDFA) was additionally used after the dispersive medium to compensate for the losses introduced by the intensity modulation combined with propagation losses along the dispersive medium[15]. The zero-to-zero full width of the parabolic shape spectrum was adjusted to $2\pi\times147$ GHz, whereas a ~20-km long section of SMF-28 was used as the dispersive medium, introducing a second-order dispersion coefficient of -433 ps^2. The parabolic spectrum after the pulse shaper is shown in Fig. 2.5(b). The intensities of 10 GHz longitudinal modes[16] were slightly higher than the 2.5-GHz spaced spectral lines due to imperfect pulse suppression from the intensity modulation. The measured output intensity profiles are plotted in Fig. 2.5(c) (log scale) and Fig. 2.5(d) (linear scale). The experimentally generated full-duty cycle parabolic pulses matched up well with an ideal fitting; the

[15] EDFA gain: ~15 dB, intensity modulation: ~10 dB, propagation loss: ~4 dB.

[16] Standing wave patterns produced by round trips of electric waves in a resonant cavity. In this particular example, the longitudinal modes were initially formed by a 10 GHz sinusoidal modulation signal.

observed minor distortions in the synthesized pulses can be attributed to slight deviations from the strict far-field condition.

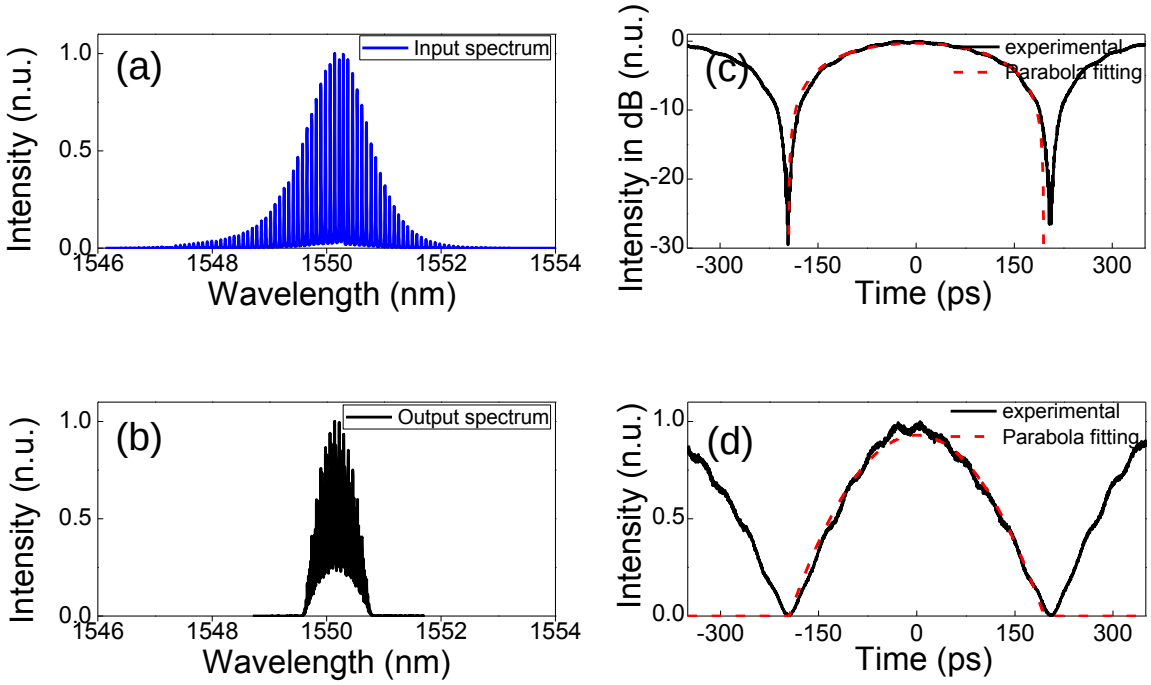

Figure 2.5 **Measured input pulse spectrum (a) and output spectrum of the 400 ps duration parabolic pulse after the pulse shaper (b), and generated temporal intensity profiles, plotted on a logarithmic scale (c) and a linear scale (d): Red dashed lines are for an ideal parabola fitting and black solid lines are the experimentally generated parabolic pulses.**

2.5.2 Near-field frequency-to-time mapping (NF-FTM)

Parabolic Parabolic pulses with durations ranging from 25 ps to 100 ps were generated using the NF-FTM technique. No amplification was used in any of the experiments reported here below. The time lens, providing the required quadratic phase variation for each dispersion coefficient, was virtually implemented into the linear spectral shaping stage. The insertion loss of the used waveshaper was ~4 dB.

For generation of 100-ps duration parabolic pulses, the dispersive medium was implemented using an ~20 km long section of SMF-LEAF fiber, for a total dispersion coefficient of ~106 ps^2, which was slightly larger than the optimal amount inferred from the numerical calculation. This required the use of a narrower spectral bandwidth than that available at the input, reducing the energy efficiency. The total frequency bandwidth (full-width of 1 % at the maximum intensity) of the output spectrum, including the time-lensing process, was ~184GHz, fitting well in the input source bandwidth (~617GHz). The input and output spectra from the pulse shaper are plotted in Figs. 2.6(a)-2.6(b), respectively. The experimentally generated full-duty cycle parabolic pulses perfectly matched up with an ideal fitting over the entire pulse period, without any sign of detrimental effects, such as pulse-to-pulse interaction in the wings, as shown in Figs. 2.6(c)-2.6(d). These specific pulse waveforms are highly desired for a range of applications [34,113]. The output average power was ~0 dBm[17], which is relatively low due to the propagation loss along the dispersive medium (~4 dB) and the selection of the narrow bandwidth in the spectral shaping stage; the obtained output power could be easily increased by replacing the dispersive medium by a ~3 km long SMF-28 fiber section.

[17] Input power: ~10 dBm, insertion loss of the pulse shaper: ~4 dB, spectral shaping loss: ~2 dB, propagation loss: ~4 dBm.

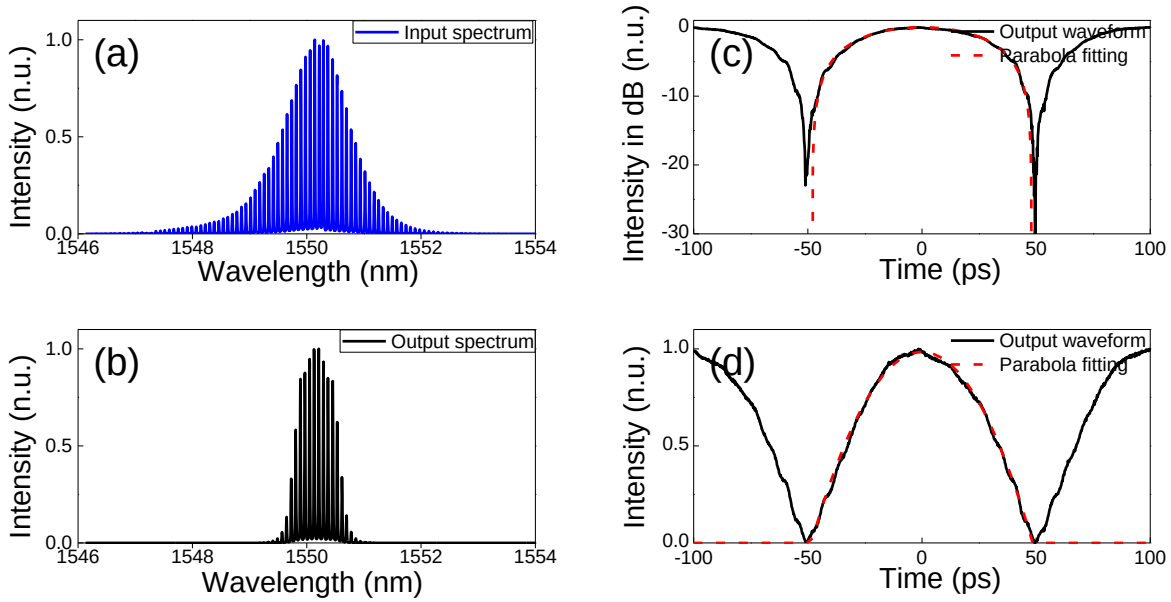

Figure 2.6 **Measured input pulse spectrum (a) and output spectrum of the 100-ps duration parabolic pulse after the pulse shaper (b), and generated temporal intensity profiles plotted on a logarithmic scale (c) and a linear scale (d): Red dashed lines are for an ideal parabola fitting and black solid lines are the experimentally generated parabolic pulses.**

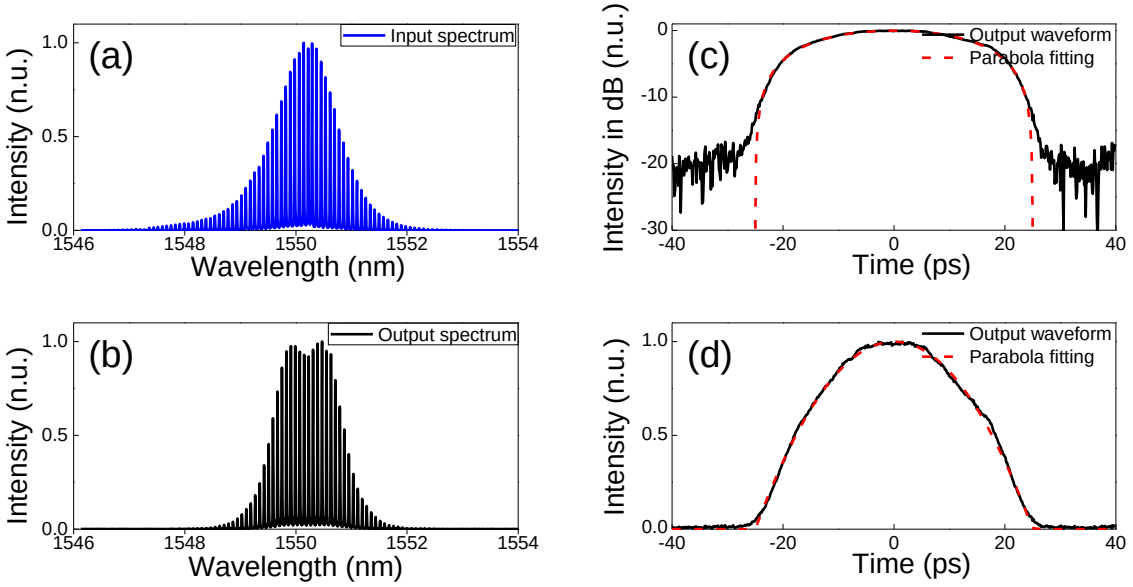

Figure 2.7 **Measured input pulse spectrum (a) and output spectrum of the 50-ps duration parabolic pulse after the pulse shaper (b), and generated temporal intensity profiles plotted on a logarithmic scale (c) and a linear scale (d): Red dashed lines are for an ideal parabola fitting and black solid lines are the experimentally generated parabolic pulses.**

In the case of 50-ps pulse duration, an ~1.8 km long SMF-28 fiber section was used as the dispersive medium, which provides a dispersion coefficient of ~37.7 ps^2. The value was optimized to minimize the input pulse-energy loss from spectral shaping while ensuring that the frequency bandwidth of the spectrum after time lensing is still within the available input spectral bandwidth. The total frequency bandwidth of the output spectrum, including the time-lens process, was estimated to be ~280 GHz. From the output spectrum in Fig. 2.7(b), it was confirmed that most of the input frequency bandwidth was utilized. Moreover, the generated pulse was a high-quality parabola, as shown in Figs. 2.7(c)-2.7(d), with a measured output average power of 3.7 dBm.

Finally, for comparative purposes, parabolic pulses with 25 ps duration were generated by using both the NF-FTM method and the direct spectral shaping, noting that this target duration is equal to the pulse duration reported in previous parabolic pulse generation experiments using the direct shaping approach [82,112]. Figure 2.8(a) shows the output spectrum for the direct spectral shaping approach, which clearly shows that a large portion of the input energy spectrum was filtered out from the spectral shaping stage. On the other hand, by using the NF-FTM, the output spectrum of the parabolic pulse was able to maintain most of the available input energy spectrum, as shown in Fig. 2.8(b). In this latest experiment, the dispersion coefficient was ~14.1 ps^2 (~700-m long SMF-28 fiber) and the total frequency bandwidth was ~405 GHz. The measured output power was ~4.2 dBm, which was about 6 dB higher than the output power of the parabolic pulse generated by the direct spectral shaping approach. The measured output temporal waveforms are illustrated in Figs. 2.8(c)-2.8(f). The generated pulses were both very close to the ideal fitting. The observed slight deviations (e.g., temporal asymmetry) in the synthesized parabolic shapes for the NF-FTM case are mainly attributed to the use of an asymmetric input pulse spectrum; this frequency-domain asymmetry was purposely not totally compensated for in the linear spectral shaping stage so that to be able to utilize a larger portion of the available input spectrum.

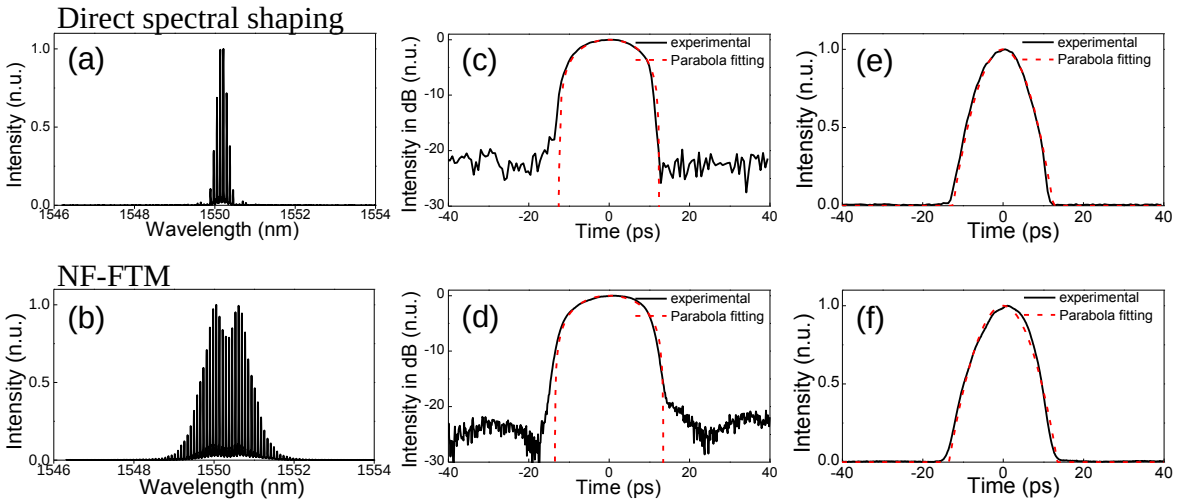

Figure 2.8 **Output spectrum of parabolic pulses generated by using a direct spectral shaping approach (a) and NF-FTM (b). The corresponding generated temporal intensity profiles are plotted on a logarithmic scale (c), (d) and a linear scale (e), (f): Red dashed lines are for an ideal parabola fitting and black solid lines are the experimentally generated parabolic pulses.**

2.6 **Summary**

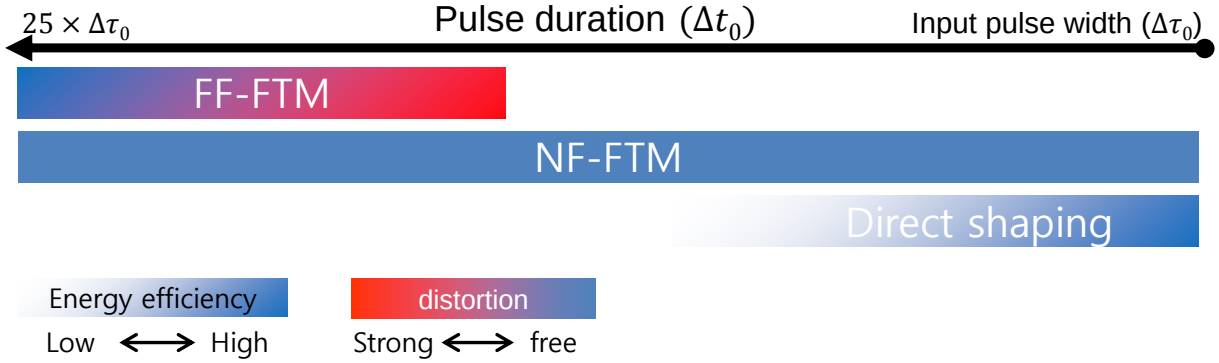

Figure 2.9 **Comparison of the direct spectral shaping, NF-FTM, and FF-FTM approaches, according to the target pulse duration from a fixed input pulse source.**

In summary, we have introduced a novel linear-optics method for parabolic pulse generation. This method is based on dispersion-induced FTM, enabling to save most of the energy spectrum available from the input pulse sources, independently of the target pulse duration. Design guidelines were provided for generation of parabolic pulses over a wide range of pulse durations, where the direct spectral shaping approach is restricted by the finest spectral resolution of the pulse shaping stage and input energy spectrum losses. The generation method based on FF-FTM was first shown to be capable of overcoming the pulse duration and energy limitations of the direct spectral shaping approach, and as proof of a concept, a 400-ps parabolic pulse was successfully synthesized from an ~2-ps input pulse source. In order to relax the waveform distortions imposed by the need to satisfy a strict far-field condition, which becomes more critical as one targets a shorter pulse duration, a virtual time lens was incorporated into the linear spectral shaping stage, effectively implementing a near-field FTM approach. Using this optimized method, generation of parabolic pulses with durations ranging from 25 ps to 100 ps was successfully demonstrated. Experimentally generated pulses were high-quality parabolic pulses with output powers as high as ~4 dBm without using any amplification. The total system losses could be further minimized through optimization of the dispersion and/or by replacing the free-space pulse shaper by an alternative, more efficient spectral shaping technique, such as a super-structured fiber Bragg grating (SS-FBG) [108]. To conclude, Fig. 2.9 summarizes the key capabilities and limitations of the three studied methods for parabolic pulse generation according to the target pulse duration from a given input pulse source.

CH. 2. B

All-Optical reconfigurable signal processing based on cross phase modulation time lensing

2.7 Abstract

A system is proposed for all-optical reconfigurable time-to-frequency (T-to-F) conversion and temporal magnification of optical waveforms using a design based on a cross phase modulation (XPM) induced time lens combined with group-velocity dispersion. In this design, the T-to-F conversion ratio and magnification factor can be easily tuned by exploiting the direct dependence of the time-lens chirp with the peak power of a parabolic pump pulse. In a proof-of-concept experiment, T-to-F conversion and temporal magnification of picosecond optical waveforms is demonstrated using a fiber-optics scheme where the T-to-F conversion and magnification factors are effectively tuned over a two-fold range by controlling the gain of an optical amplifier. The same system can be additionally adjusted to provide a time-mapped Fourier transform of the input waveform.

2.8 **Introduction**

The mathematical equivalence between paraxial diffraction of a spatial beam and chromatic dispersion of a temporal waveform, namely space-time duality, has enabled the development of important high-speed optical signal-processing functionalities [80,116,60,117,108], including temporal magnification of fast optical waveforms for their characterization using lower-bandwidth detection [116], linear and nonlinear impairment compensation in fiber-optics telecommunication links [60,117,108], and time-to-frequency (T-to-F) mapping of fast optical waveforms for time-domain measurements through spectral analysis or for telecommunication format conversion (e.g. optical time-division to wavelength-division multiplexing) [117]. A time-lens (TL), which imparts a temporal quadratic phase modulation on an incoming waveform, represents the temporal counterpart of a spatial thin lens, and it is a main element to perform the mentioned signal-processing functionalities. A simple way to create a TL utilizes an electro-optic phase modulator driven by a sinusoidal modulation waveform. However, the amount of phase modulation –and the related frequency chirp- that can be achieved by electro-optic means is relatively limited, affecting the overall performance (e.g., time resolution) of this approach [80]. Alternatively, the use of nonlinear optical phenomena has been extensively investigated to create TLs, most notably four-wave mixing (FWM) with a long, chirped optical pump pulse [118,119]. However, FWM requires precise dispersion control in the non-linear medium and stringent phase-matching conditions should be also ensured over the frequency bandwidth of interest. Perhaps more importantly, the key parameter of a TL, i.e., the frequency chirp, cannot be easily tuned in a FWM scheme as this would require controlling the frequency chirp of the pump pulse. In contrast, a TL can be also produced by XPM with a parabolic pump pulse [80]. This solution inherently offers the capability to tune the lens frequency chirp by all-optical means. In this scheme, the TL frequency chirp is directly proportional to the peak power of the parabolic pump. Nonetheless, it is generally accepted that it is challenging to produce high-quality optical parabolic pulses, with the high energy levels and long pulse durations that are needed for XPM time lensing. Recently, we reported a novel design for energy-efficient generation of such parabolic pulses, with durations ranging from the picosecond to the sub-nanosecond range, using pulse spectral shaping combined with dispersion [98]. The technique has proven to be particularly well suited for XPM time lensing applications [120].

The goal of this work is to highlight the all-optical reconfigurable capability of a XPM TL and to show how this capability can be used to create optically programmable TL-based signal processing platforms. For this purpose, we propose and demonstrate a XPM TL design -also involving a concatenated dispersive line- for reconfigurable T-to-F conversion and temporal magnification of fast optical waveforms, where one can tune the T-to-F conversion ratio and temporal magnification factor *by simply changing the peak power of the parabolic pump pulse*. The same platform could be also adjusted to produce a real-time (time-mapped) Fourier transform of the input optical waveform.

2.9 **Principle of operation**

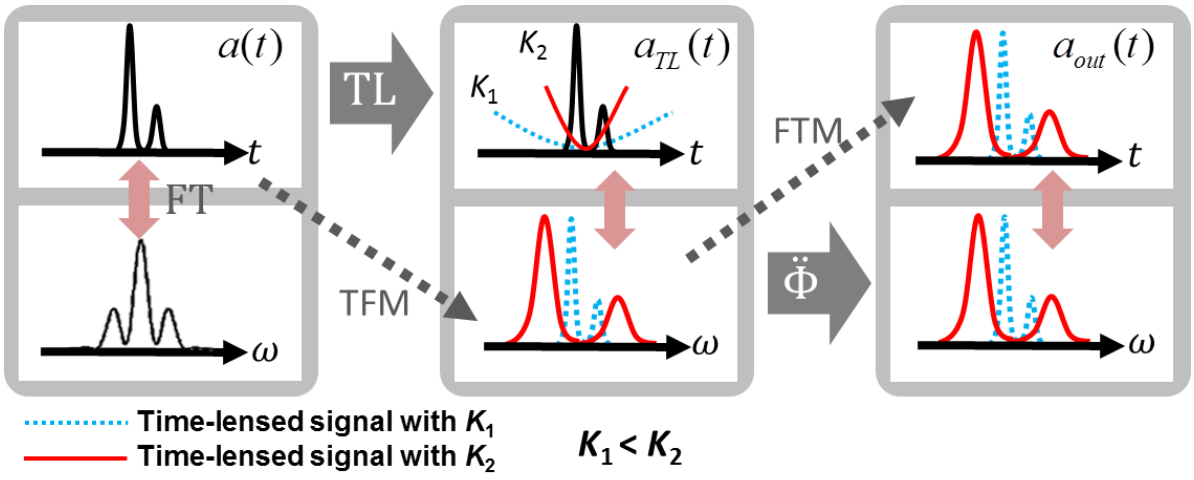

Figure 2.10 **Illustration of the proposed all-optical reconfigurable signal-processing scheme based on an XPM-TL. The parameters t and ω stand for time and radial frequency, respectively, whereas $\ddot{\Phi}$ is for second-order (group-velocity) dispersion. TFM and FTM stand for T-to-F mapping and F-to-T, respectively.**

Figure 2.10 illustrates the concept of the proposed all-optical reconfigurable signal processing scheme. The concept is based on a previously proposed design using an electro-optic TL [121], and is here adapted for an XPM TL, which leads to the important advantages mentioned above, including

all-optical reconfigurability through pump power control. Time lensing on the incoming signal (probe) $a(t)$ (temporal complex envelope modulated on an optical carrier) is achieved through XPM in a highly-nonlinear fiber (HNLF) with a parabolic optical pump pulse. Assuming that the pump pulse has a temporal intensity profile that is perfectly parabolic with its zero-crossing points positioned at $-T_0$ and T_0 (bright parabolic pulse) and no walk-off[18], a quadratic nonlinear phase shift is induced on the probe along the pump time window ($-T_0 \leq t \leq T_0$), as follows: $\phi_{XPM}(t) = -2\gamma L_{eff} P_0(1 - t^2/T_0^2)$, where γ and L_{eff} are the nonlinear coefficient and effective length of the HNLF; the last is defined as $L_{eff} = (1 - \exp(-\alpha L))/\alpha$, with L and α being the actual length and attenuation coefficient of the HNLF ($\alpha \approx \alpha_{dB/km}/4.34$, where $\alpha_{dB/km}$ is the attenuation coefficient in log scale). P_0 is the peak power of the parabolic pump pulse and the reference time, $t = 0$, is for the time corresponds to the pulse peak. This nonlinear phase shift produces the desired TL process with the following positive frequency chirp rate:

$$K = \frac{\partial \delta\omega}{\partial t} = \frac{4\gamma L_{eff} P_0}{T_0^2} \tag{2.8}$$

where $\delta\omega$ is the frequency shift induced by the nonlinear phase modulation, defined as $\delta\omega = \partial\phi_{XPM}/\partial t$. Equation (2.8) shows that the TL frequency chirp rate is directly proportional to the peak power of the parabolic pulse. The time-domain waveform of the signal at the TL input can be mapped into the frequency domain at the TL output if the chirp rate K of the TL process is sufficiently strong [121]. In particular, the Fourier transform of the time-lensed signal, $A_m(\omega)$, can be approximated as

$$A_m(\omega) \propto \exp(-j\omega^2/2K)[a(\tau)]_{\tau=\omega/K} \tag{2.9}$$

This last equation indicates that the spectral intensity profile of the probe signal at the TL output is a scaled replica of the input temporal waveform, with a T-to-F conversion ratio that is directly proportional to the TL frequency chirp rate K. Subsequently, undistorted temporal magnification of the original signal $a(t)$ can be obtained by propagating the time-lensed probe signal through a

[18] The temporal walk-off effect is induced by a group velocity difference between a probe pulse and a pump pulse due to central wavelength difference.

second-order dispersive line, with a constant dispersion coefficient $\ddot{\Phi}$ (slope of group delay as a function of ω) [121]. The resulting temporal waveform (complex envelope) at the output of the dispersive line can be expressed as

$$a_{out}(t) \propto \exp(-jt^2/2M)[a(t/M)], \tag{2.10}$$

where the temporal magnification factor is $M = 1 + K\ddot{\Phi}$. Equation (2.10) shows that the output waveforms is a temporally scaled (magnified) replica of the input with a temporal scaling factor given by *M*. Again, the temporal magnification factor in this scheme is directly dependent on *K*. The key feature of our proposed scheme is that both the T-to-F conversion ratio and temporal magnification factor are programmable by controlling *K*, which can be easily tuned by changing the peak power of the parabolic pump pulse only. In the case of dark parabolic pulses, the nonlinear phase shift within the time window ($-T_0 \leq t \leq T_0$) is given by the following equation: $\phi_{XPM}(t) = -2\gamma L_{eff} P_0(t^2/T_0^2)$, which produce the same magnitude but opposite sign (negative) of the frequency shift $\delta\omega$ and K.

Additionally, the same scheme can provide real-time Fourier transformation of the input signal $a(t)$ if the XPM stage is bypassed, i.e., by setting *K* = 0. In this case, the original signal only undergoes second-order dispersion, a process that can induce a mapping of the signal frequency spectrum onto the time domain (frequency to time mapping) if the signal is restricted to a prescribed time duration $\Delta\tau$ and the second-order dispersion $\ddot{\Phi}$ is sufficiently strong so that $|\ddot{\Phi}| \gg \Delta\tau^2/8\pi$ [98].

2.10 **Experimental demonstration**

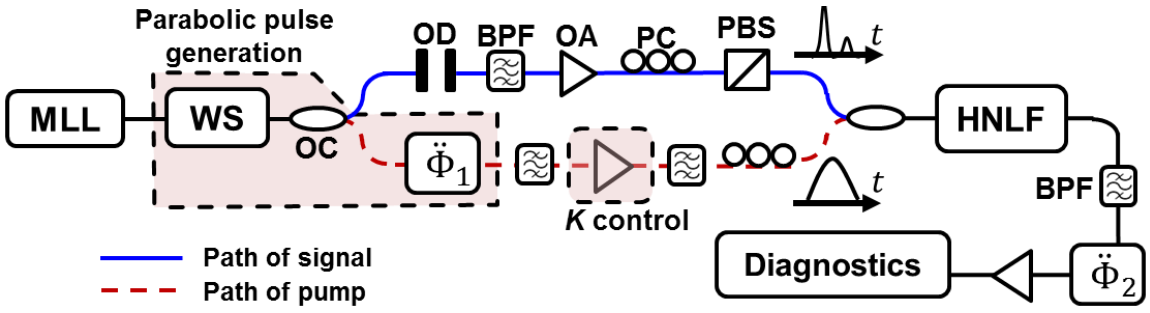

Figure 2.11 **Experimental setup of the all-optical reconfigurable XPM-TL based signal-processing system, including the parabolic pump generation part. Acronyms are defined in the text. The gain from optical amplifier (OA: PriTel, SPFA-18-300) in the path of signal is 11 dB.**

The experimental setup used for proof-of-concept is shown in Fig. 2.11. Both the pump and probe (input) signals are generated from a fiber-optics mode-locked laser (MLL) source (Menlo Systems FC1500-250-ULN), which generates a coherent optical frequency comb (OFC) with free spectral range of ~250 MHz and spectral bandwidth > 25 nm. The OFC is spectrally shaped using a linear optical waveshaper (WS: Finisar WaveShaper 4000S) with frequency resolution of ~10 GHz for generation of both the pump and the probe pulse waveforms. Each of these waveforms is synthesized over a different frequency bandwidth (pump centered at ~1550 nm and probe centered at ~1555.6 nm), and then split by a 3-dB optical coupler (OC). Tunable band-pass optical filters (BPF) are used to select the right signal (probe or pump) in each of the output coupler arms. The probe signal to be processed consists of two consecutive Gaussian optical pulses of different intensity, separated by ~21 ps, as plotted in Fig. 2.12(c). Each individual pulse has an intensity FWHM time-width of ~10 ps. High-quality 60-ps duration parabolic pump pulses are generated by using spectral shaping combined with dispersion-induced near-field frequency-to-time mapping (NF-FTM) [98]. The duration of the pump pulses are slightly wider than the total duration of the probe signal (~50ps) to enhance the time tolerance and stability of the system. This parabolic pulse generation method involves re-shaping the amplitude and phase of the input pulse spectrum so that to achieve the desired target parabolic temporal intensity profile followed by linear propagation of the re-shaped

pulse along a second-order dispersive medium. A 4.5-km long section of SMF-28 ($\ddot{\Phi} \approx -97$ ps^2) is used here as the dispersion line.

Figure 2.12 shows intensity profiles of the generated bright (Fig. 2.12 (a)) and dark (Fig. 2.12 (b)) parabolic pulses, which are designed to introduce positive and negative frequency chirps, respectively. The pump peak power -and related magnitude of the XPM-induced chirp- is altered by controlling the gain of an erbium-doped fiber amplifier (EDFA: Amonics AEDFA -33-B-FA). Polarization controllers (PC) in each signal arm, a polarization beam splitter (PBS), and an optical delay (OD) line are utilized to optimize the XPM process between the probe and pump signals. The probe signal is combined with the amplified parabolic pump signal in an OC and sent into an ~1-km long HNLF section (Huber+Suhner, HLNF-ZDW-1546). The nonlinear coefficient of the HNLF is ~11.3 $W^{-1} \cdot km^{-1}$, the attenuation coefficient $\alpha_{\mathrm{dB/km}}$ is ~1.5 dB/Km, and its zero-dispersion wavelength (ZDW) is at ~1546 nm. The dispersion of the HNLF is ~0.08 ps/nm/km, and the dispersion slope is ~0.017 ps/nm^2/km at 1550 nm. Considering the dispersion parameters, the wavelength separation between the pump and probe (~5.6 nm), and the pump pulse duration, group-delay walk-off effects are negligible. The time-lensed probe, extracted by using another BPF, is linearly propagated through a 20-km long section of SMF-28, introducing a dispersion $\ddot{\Phi}$ of –433 ps^2, for temporal magnification and optical time-domain Fourier transform. The input and output signals were characterized in the spectral and temporal domains using an Optical Spectrum Analyzer (OSA) with a resolution of 0.01 nm, a 500-GHz optical sampling oscilloscope (PSO-100, EXFO), and a 20-GHz electrical sampling oscilloscope. (after photo-detection).

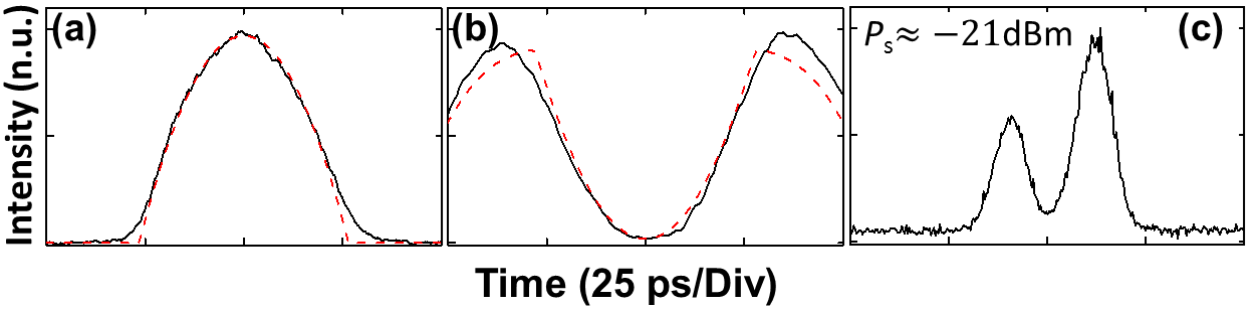

Figure 2.12 **Measured temporal intensity profiles of the bright (a) and dark (b) parabolic pumps, and the probe signal to be processed (c). The black solid lines are experimentally generated temporal waveforms and the red dashed lines are ideal bright and dark parabola fitting. P_s is average power of the probe signal at the input of the HNLF**

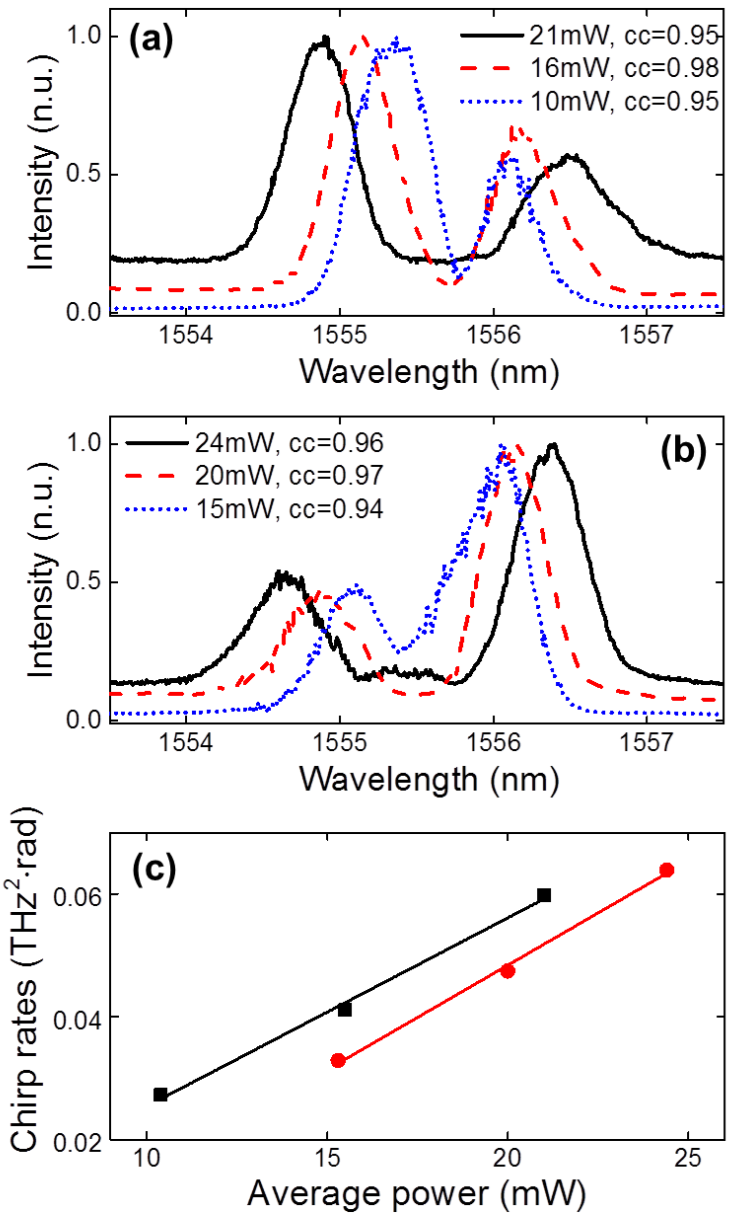

Figure 2.13 **Demonstration of T-to-F conversion with different conversion ratios by changing the average pump power P_{avr} for the cases of (a) positive and (b) negative frequency chirp rates (bright and dark parabolic pumps, respectively). Plot (c) shows a relationship graph of estimated chirp rates (from measurements) as a function of measured P_{avr} for bright (black square dots) and dark (red circle dots) parabolic pumps. Each represented spectrum is normalized with respect to its maximum spectral intensity (n.u. stands for normalized units.). Cross-correlation coefficients (cc) are estimated as the peak of the normalized correlation function between the probe signal and output spectra (mapped in time). $cc(\tau) = \int_{-\infty}^{\infty} a(t)b(t+\tau)dt/\sqrt{E_a E_b}$**

Figure 2.13(a) and (b) show measured spectra of the probe signal at the TL output for different values of pump amplification (pump average power given in the plots) for the cases of (a) bright and (b) dark parabolic pump pulses. In all cases, the measured spectra closely resemble the temporal intensity profile of the double-pulse signal under test, shown in Fig. 2.13(c), demonstrating the predicted T-to-F mapping process with an adjustable T-to-F conversion ratio. Observed deviations might be attributed to the imperfect T-to-F conversion at the cases with lowest average power and/or slightly mismatched synchronization between the probe signal and the pump. In particular, the T-to-F conversion ratio, measured from the output spectra in Fig. 2.13(a) and (b), varies from ~0.035 nm/ps (corresponding to an inter-pulse wavelength spacing of ~0.73 nm) to ~0.076 nm/ps (wavelength spacing ~1.6 nm) for the positive-chirp case (a), and it changes from ~0.042 nm/ps (wavelength spacing ~0.88 nm) to ~ 0.081 nm/ps (wavelength spacing ~1.71 nm) for the negative-chirp case (b). Figure 2.13(c) illustrates the linear relationship between the measured TL chirp rates, i.e., estimated T-to-F conversion ratios in units of THz^2/rad, and the corresponding measured average powers of bright (black square dots) and dark (blue circled dots) parabolic pumps. The peak power of the parabolic pump pulse can be calculated from the average energy per pulse E_{pulse}, which for the case of a bright parabolic pump can be expressed as: $E_{pulse} = T_{rep}P_{avr} = \int_{-T_0}^{T_0} P_0(1 - t^2/T_0^2)\, dt$, where T_{rep} is the time period of the pulse train (4ns). From the equation, the peak power of a bright parabolic pulse with a duration $2T_0$ = 60ps is about 100 times higher than the average power, $P_0 = 100P_{avr}$. Plugging this relationship into (2.8), the calculated frequency chirp rate matches fairly well the measured results in Fig. 2.13(c), e.g., estimated K from (2.8) for P_{avr} of 10mW is ~0.041 THz^2/rad, whereas the corresponding measured K is ~0.029 THz^2/rad. Deviations are attributed to a combination of imperfect polarization matching between the pump and probe for the XPM process, and the presence of amplifier spontaneous emission noise generated from the EDFA. The measured trend in the chirp rate vs. pulse power is also as predicted for the dark parabolic pump case. However, in this case, it is less straightforward to obtain a precise comparison of the calculated and measured results because the experimental parabolic pump pulse extends well beyond the time window ($-T_0$, T_0) of the theoretical pulse, making it difficult to estimate the pulse peak power from P_{avr}.

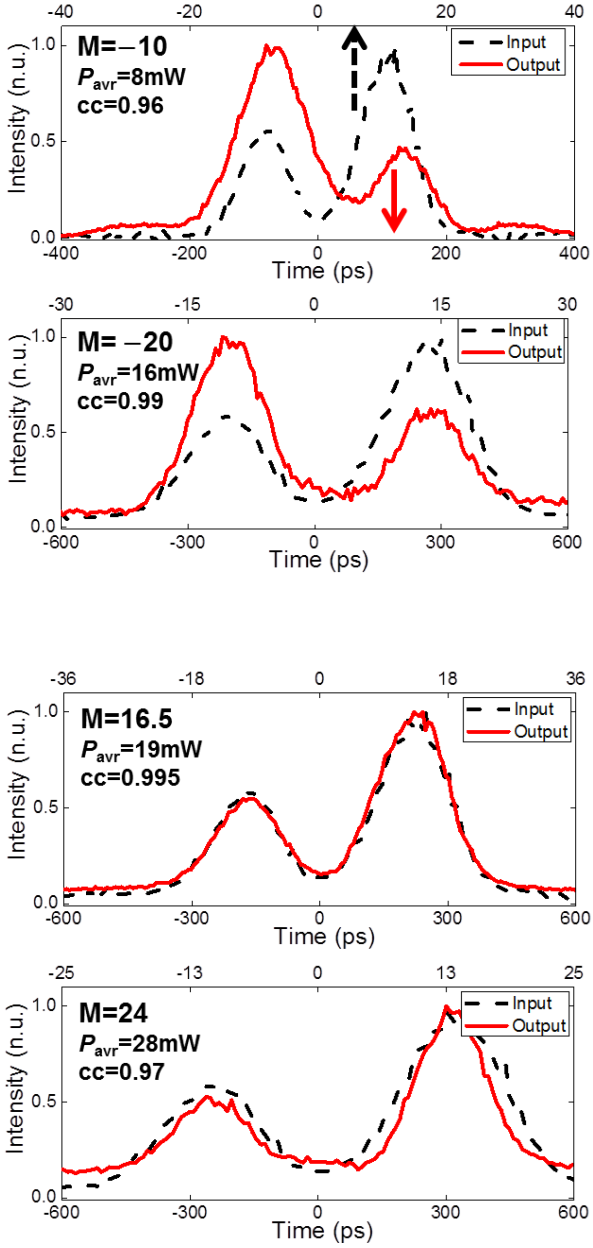

Figure 2.14 **Measured temporal intensity profiles of the input probe (black dashed lines, temporally scaled by the magnification factor *M*, with the original temporal scale shown in the top horizontal axis) and output waveform (red solid lines) for direct and reverse temporal magnification with different magnification factors, tuned by changing the pump pulse power P_{avr}. Each represented waveform is normalized with respect to its peak power.**

Figure 2.14 shows experimental results on direct and reverse temporal magnification of the input waveform after propagation through the dispersive line. Results are shown for reverse magnification by factors of −10 and −20, achieved by use of the bright pump pulse with average powers of ~8 mW and ~16 mW, respectively. Results of direct magnification by factors of 16.5 and 24 are also shown, as obtained using the dark parabolic pump pulse with average powers of ~19 mW and ~28 mW, respectively. Again, the measured output temporal waveforms are temporally magnified replicas of the input probe time-domain signal with a temporal magnification factor *M* that is tuned over an approximately twofold range by changing the gain of the pump optical amplifier. The measured magnification factors are in a fairly good agreement with those theoretically calculated considering the TL chirp that can be estimated from the results in Fig. 2.13(c) and the dispersion parameter, i.e., calculated magnifications of −9.6 and −18 for the bright pump, and of 19.9 and 32.2 for the dark pump case. The maximum average power available at the input of the HNLF is limited to 15 dBm due to the power tolerance of the BPF right after the EDFA in the experiment. However, higher *M* could be simply obtained by using a larger dispersion coefficient, only limited by the measurement noise floor.

As predicted, optical time-domain Fourier transformation of the probe signal is also successfully obtained at the system output when the XPM stage is bypassed by applying zero-gain in the pump EDFA. As shown in Fig. 2.15, the temporal intensity profile of the output waveform matches well the spectrum of the original input signal, converted in time by using the frequency-to-time conversion ratio determined by the dispersion coefficient.

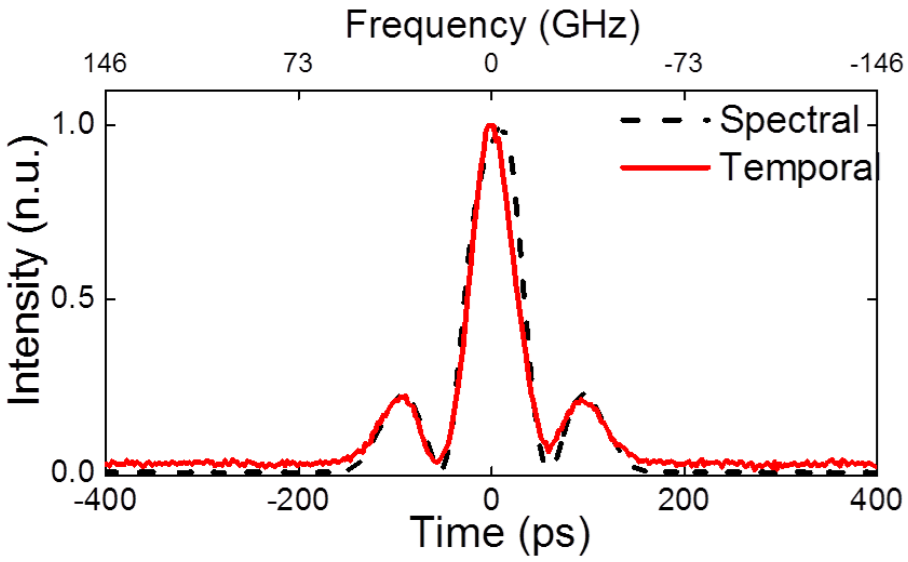

Figure 2.15 **Measured temporal intensity profile (red solid line, bottom axis) of the output waveform with zero pump power for optical time-domain Fourier transformation, and the spectrum of the original input probe signal (black dashed line, top axis). The relationship between the time and frequency scales in the plot is given by the second-order dispersion $2\pi\dot{\Phi} = 2\pi \times 433$ ps^2.**

2.11 **Conclusion**

To conclude, we have designed and demonstrated an XPM TL - based scheme for reconfigurable T-to-F conversion and temporal magnification of picosecond optical waveforms; the scheme can be also adjusted to provide the optical time-domain Fourier transform of the input signal. All functionalities are optically controlled by simply modifying the gain of an optical amplifier. This work highlights the unique capability offered by an XPM TL for realization of programmable TL-based optical signal-processing systems, which can be adapted to variable conditions in the incoming signals (e.g., time or frequency resolutions), communication link/channel (e.g., time or frequency grids), or measurement/detection specifications.

CHAPTER 3

In-fiber reconfigurable generation of arbitrary (asymmetric) picosecond temporal intensity waveforms by time-domain optical pulse shaping

3.1 Abstract

A fiber-optic programmable optical pulse shaper is experimentally demonstrated using multi-level phase-only linear filtering, capable of synthesizing arbitrary (including asymmetric) temporal intensity waveforms. The reconfigurable filtering operation is implemented in the time domain with a single electro-optic phase modulator (EO-PM) driven by a high-speed electronic arbitrary waveform generator (AWG). The required multi-level modulation signal is calculated from a combination of optimization algorithms, namely the Gerchberg–Saxton algorithm (GSA) and a genetic algorithm (GA). We report the synthesis of high-quality, arbitrary temporal intensity profiles, including asymmetric triangular waveforms and ~150 Gbaud random on–off keying (OOK) pulse and pulse amplitude-modulation (PAM) code sequences, with a temporal resolution of ~2 ps over a maximum time window of ~60 ps.

3.2 **Introduction**

Broadband arbitrary optical waveforms, with resolutions in the picosecond regime and faster, need to be synthesized for a wide range of applications, including high-speed optical communications and information processing, quantum control and computing etc. [6,83,66]. A photonic generation approach based on programmable optical pulse shaping offers a promising solution since it enables overcoming the severe bandwidth limitations of digital-to-analog converters in electronic arbitrary waveform generators (AWGs) [83]. The design concept of the most extensively used approach to date is as follows: the spectral components of an incident optical pulse are first decomposed angularly (e.g., by bulk-optics diffraction gratings), focused, and then linearly modulated by spatial amplitude and/or phase masks. By using programmable spatial light modulators (SLMs), reconfigurable optical pulse shapers have been successfully demonstrated with resolutions well into the sub-picosecond range [6]. Central constraints of this approach include the need for efficient coupling between fiber and free-space optics, and the requirement for multiple spatially-separated modulation points, which translate into a relatively lossy and bulky configuration. The approach is also constrained by the relatively limited update rate of SLMs, typically below the kHz range. Previous works have demonstrated faster updating speeds based on wavelength switching [122] or multi-wavelength injection locking [89]. However, in these techniques, waveform reconfigurability is severely constrained either by the number of light sources [122] or by compromising waveform fidelity [89]. Alternatively, so-called time-domain spectral shapers (TDSS) [97], where the spectral filtering function is programmed in the time domain using a single high-speed electro-optic modulator (EO-M) between two opposite-dispersion media, have attracted a great deal of attention due to their all-fiber simple configuration, capability to achieve high-speed pulse-shape update rates, into the sub-GHz range, and solid potential for integration. In sharp contrast to direct time-domain pulse shaping approaches [123], where temporal intensity profiles are directly crafted using electro-optic intensity modulators (EO-IM), TDSS enables re-shaping ultrashort optical pulses into arbitrary intensity waveforms with a temporal resolution that is not restricted by the frequency bandwidth of the temporal modulation process (typically limited by the electronic AWG[19] bandwidth). However, to the best of our knowledge, all previously demonstrated schemes for TDSS

[19] Arbitrary waveform generator.

were limited to synthesizing purely symmetric temporal intensity waveforms. This is a highly restrictive limitation of TDSS, and in fact, asymmetric temporal intensity profiles are needed for a wide range of important applications, including arbitrary high-speed optical pulse-amplitude coding, and nonlinear wavelength conversion and time-division add–drop multiplexing with enhanced performance using asymmetric triangular pump pulses [124,125].

In previously demonstrated schemes [66,126], binary (two-level) phase-only filtering was used, leading to the mentioned symmetric temporal waveform limitation. Whereas the possibility of overcoming this limitation by use of multi-level phase filtering was theoretically studied [69], to date, no experimental demonstration of such a potential has been reported (to our knowledge). In this work, a fiber-optic programmable picosecond pulse shaper is experimentally demonstrated using *multi-level* phase-only linear filtering in the time-domain, which enables the synthesis of high-quality, fully arbitrary (including asymmetric) temporal intensity profiles. The proposed technique employs an EO phase modulator (EO-PM) driven by a high-speed AWG in between two conjugated fiber-optics dispersive lines, which are here implemented using a single linearly-chirped fiber Bragg grating (LC-FBG) consecutively operated from its two ends. The method is highly energy efficient, thanks to the use of phase-only linear filtering. The needed spectral phase filtering function is obtained through a combination of the Gerchberg-Saxton algorithm (GSA) and a genetic algorithm (GA) [69]. By programming the modulating pattern from a high-speed AWG with a temporal resolution of ~150 ps, we report here the synthesis of asymmetric triangular pulse shapes, and high-speed (~150 Gbaud) random on-off-keying (OOK) pulse and pulse-amplitude-modulation (PAM) code sequences, with a resolution of ~2 ps over a maximum temporal window of ~60 ps, corresponding to an estimated frequency resolution of ~16 GHz.

3.3 **Principle of operation**

The proposed technique relies on the design of a phase-only linear optical filter to achieve the desired re-shaping of the temporal intensity waveform profile, leaving the temporal phase as a free design parameter. The phase-only spectral transfer function is then [66]

$$H(\omega) \propto \exp[j\Psi(\omega)] \tag{3.1}$$

where ω is the base-band angular frequency variable (around the pulse carrier optical frequency), and $\Psi(\omega)$ is the required phase profile for pulse shaping. The filtering process should enable to achieve an output intensity waveform $|u_{out}(t)|^2$ that is approximately proportional to the target temporal intensity profile $\left|u_{target}(t)\right|^2$, so that

$$|u_{out}(t)| = |IFT\{U_{in}(\omega) \cdot \exp[j\Psi(\omega)]\}| \propto \left|u_{target}(t)\right| \tag{3.2}$$

where $U_{in}(\omega)$ is the complex amplitude of the input spectrum, and $IFT\{\ \ \}$ denotes the inverse Fourier transform. To achieve arbitrary (including asymmetric) temporal waveform generation, $\Psi(\omega)$ must be a multi-level function [69]. It is well known that certain asymmetric intensity profiles, such as triangles with different slopes, can be also obtained by use of cubic spectral phase filtering, which is more straightforward for a practical implementation [126]. Nonetheless, in this case, the synthesized waveforms are only a rough approximation of the target pulse shape, typically having undesired strong oscillations. By using an optimization algorithm, not only can one target the synthesis of any desired, arbitrary intensity waveform, but additionally, one can get to generate the target profile with a much higher precision, e.g., minimizing undesired oscillations. Nonetheless, the computation of the required spectral phase function is not trivial and we use the calculation strategy first reported in Ref. [69] based on a suitable combination of well-known optimization algorithms. Briefly, first, the required multi-level phase profile is approximately estimated by using GSA [126].

The algorithm is based on an iterative-Fourier procedure to retrieve the phase information that is required to achieve the known amplitude profiles in the temporal domain (i.e., target temporal amplitude waveform after pulse shaping) and spectral domain (i.e., spectral amplitude profile of the input pulse before pulse shaping). The key idea here is to update the temporal and spectral phase profiles every iteration after switching between the conjugate Fourier domains while keeping both

known amplitudes. An acceptable intermediate solution is obtained following only a few tens of iterations of the GSA. According to the specification of the AWG[20], the obtained analog spectral phase profile is then sampled, quantized, and transferred to the GA. In the algorithm, the deviations in the generated output intensity waveform, with respect to the target one, are evaluated and weighted individually as partial cost functions in order to control the different key features of each typology of pulse target; the aim is to reduce gradually a total cost function toward optimization of the spectral phase profile [69].

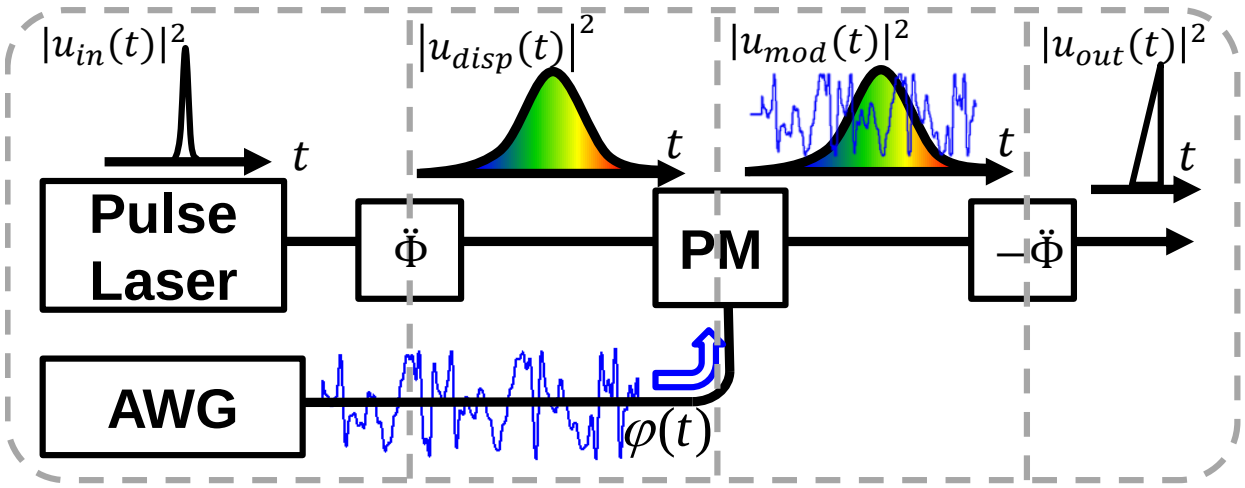

Figure 3.1 **Scheme of the fiber-based programmable optical pulse shaping system. PM: phase modulation.**

The schematic of the time-domain pulse shaping system is shown in Fig. 3.1. In order to implement the computed spectral filtering of the pulse's phase profile, the input pulse's frequency components are first linearly distributed along the time domain by linear propagation through a dispersive medium with a high second-order dispersion coefficient $\ddot{\Phi}$ (defined as the slope of the medium's group delay as a function of ω). The temporally stretched pulse is then phase-modulated by using an EO-PM driven by a time-domain modulation signal that maps the desired phase spectral-

[20] Arbitrary waveform generator

transfer function, $\phi(t) = \Psi(\omega)|_{\omega=t/\ddot{\Phi}}$. By subsequently compressing the stretched, phase-modulated pulse with a dispersion compensator providing the exact conjugated dispersion of the first dispersive element, the target temporal intensity profile, as per Eq. (3.2), can be directly obtained at the system output. Note that the output temporal phase profile is generally an irregular pattern with rapid variations. As discussed in previous works [69], the output time resolution is determined by the inverse of the input pulse frequency bandwidth unless the spectral pass-band of the dispersive medium is narrower than the input pulse bandwidth; in this latest case, the output time resolution is directly given by the inverse of the dispersive medium's frequency pass-band. On the other hand, the maximum output waveform time duration T –inverse of output frequency resolution $\delta\omega_{PS}$– depends on the product of the optical dispersion amount and frequency bandwidth of the modulating signal:

$$T \propto \frac{1}{\delta\omega_{PS}} \propto \Delta\omega_S \left|\ddot{\Phi}\right| \propto \frac{2\pi|\ddot{\Phi}|}{\delta t_s} \tag{3.3}$$

where $\Delta\omega_S$ is an estimate of the full spectral width of the modulation signal and δt_s is the corresponding modulation temporal resolution.

3.4 **Experimental demonstration**

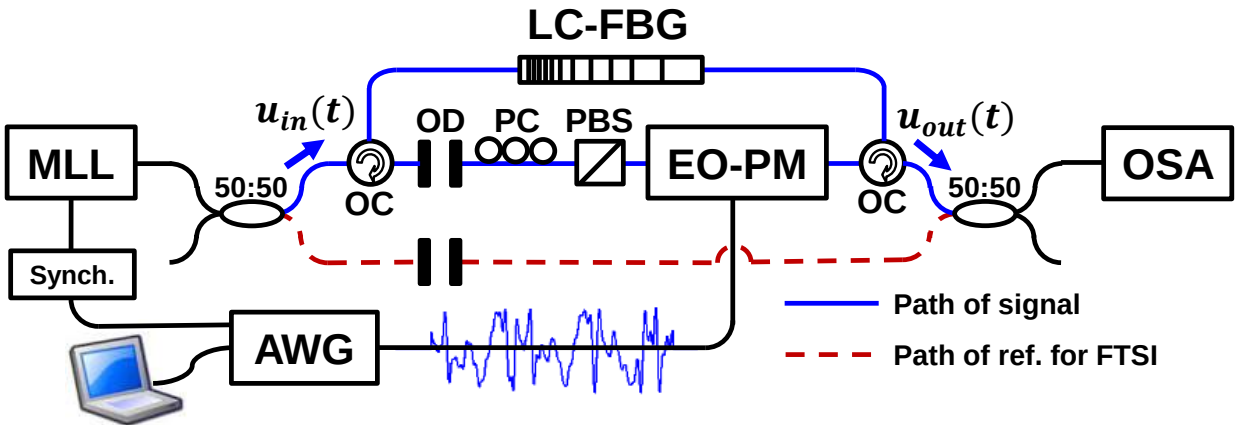

Figure 3.2 **Experimental setup of the demonstrated fiber-based programmable optical pulse shaping system, including an interferometry configuration for FTSI-based output pulse characterization. OC: optical circulator. Acronyms are in the text.**

The experimental setup is shown in Fig. 3.2. The initial optical pulses were generated from a passively mode-locked fiber laser (MLL) producing ~2 ps (intensity FWHM) nearly transform-limited Gaussian-like pulses with average power of ~3 dBm at a repetition rate of ~16MHz, spectrally centered at ~1554.5 nm. The input pulses were temporally stretched by reflection from a LC-FBG, providing a dispersion $|\ddot{\Phi}|$ of ~2600 ps^2 over the whole C-Band (1530-1565nm). The dispersed pulses were linearly polarized from a polarization beam splitter (PBS), and modulated by a 40-GHz EO-PM driven by the optimized time-domain modulation signal $\phi(t)$, obtained from the described numerical algorithms, which was generated by a high-speed AWG (Tektronix AWG7122C, Sampling rate: ~20-Gsample/s). The modulation signals were programmed with a temporal resolution of ~150 ps (corresponding to 3 identical samples per time slot), designed to clearly distinguish the modulation signal point by point. The clock signal for the AWG was obtained from the optical input pulse (secondary output) using an amplified photodetector (PD) with 3dB bandwidth of ~75 MHz combined with a low-pass filter (LPF) with 3dB bandwidth of ~14 MHz in order to suppress higher-order harmonics of the photodetected signal. An optical delay line (OD) was used for precise synchronization between the pulses with the modulation signals. The stretched, phase-

modulated pulses were exactly compressed back through reflection from the same LC-FBG in the opposite direction. No optical amplification was used in any of the experiments reported here below, and the output power was measured to be ~-7 dBm in all these experiments. Generated waveforms were characterized by using a Fourier transform spectral interferometry (FTSI) setup [127], since the output intensity profiles required diagnostics with a picosecond temporal resolution. The temporal intensity profile of the signal is retrieved from the input pulse spectrum and spectral interference pattern between the output optical waveform (blue solid lines in Fig. 3.2) and the optical input pulse used as the reference (red dashed lines in Fig. 3.2); all spectra were measured by an optical spectrum analyzer (OSA) with a resolution of 0.01 nm. It is important to note that there is a residual, undesired signal that is transmitted through the LC-FBG to the system output, ~5 % of the input pulse power. This residual signal could be discriminated from the desired output waveform using an additional polarization controller (PC) and a PBS at the output of the setup, as in [69]. In our experiments, the residual signal is well separated in time from the output waveform (>4 ns): this translates into a much faster variation of the corresponding spectral interference pattern (combination of the output with the reference pulse) than the OSA resolution, so that the residual signal simply adds to the energy spectrum rather than generating an undesirable interference. The produced effect can be simply canceled out by including the residual signal in the reference spectrum used in the FTSI phase-recovery process.

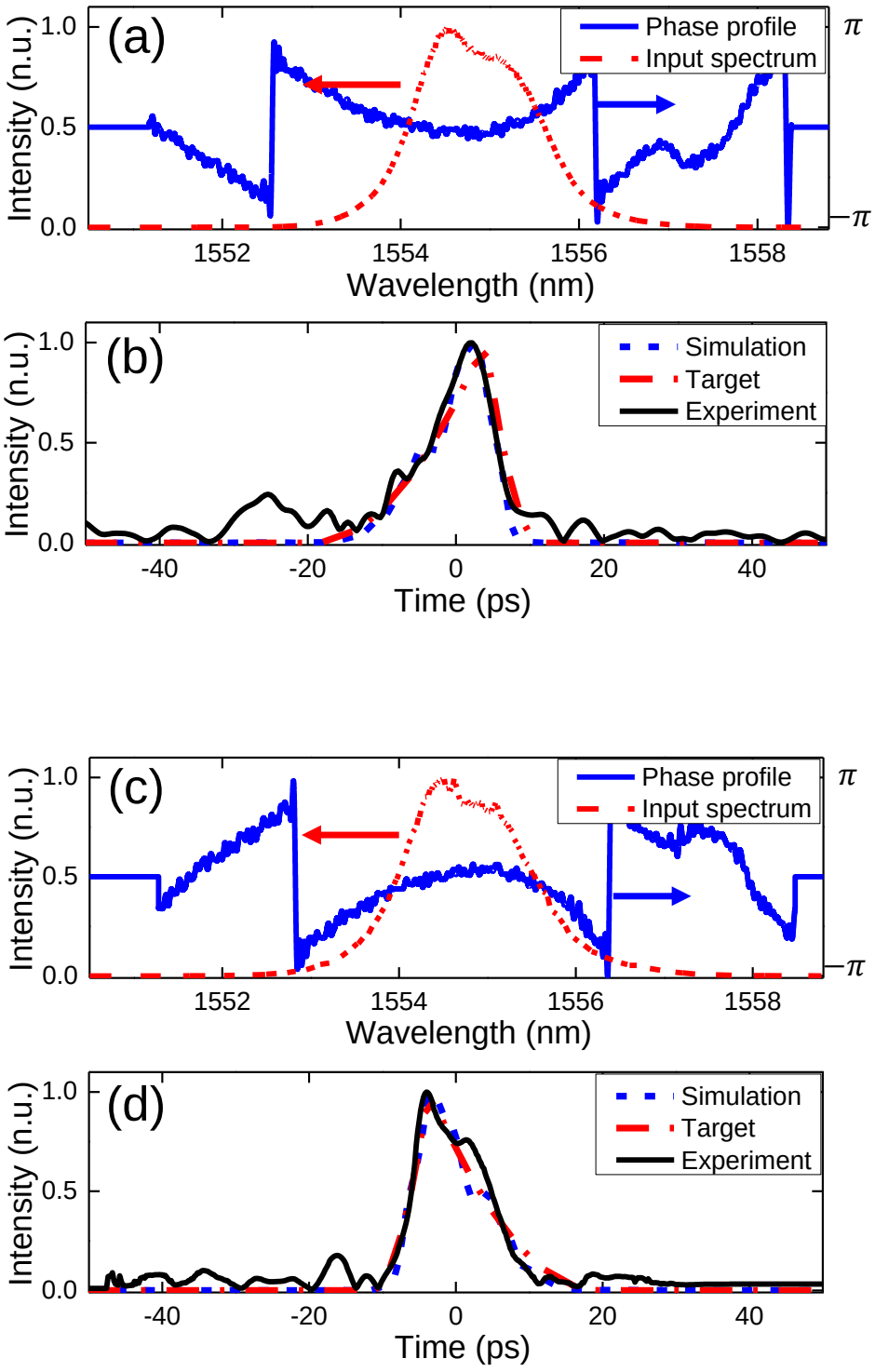

Figure 3.3 **Input pulse spectrum and the calculated spectral phase profile ((a), (c)), and measured (vs. simulated and target) output temporal intensity profiles ((b), (d)) of the synthesized asymmetric triangle waveforms with customized slopes. n.u. stands for normalized units with respect to the waveform peak.**

Figure 3.3 presents the results for two examples of generation of asymmetric temporal triangular waveforms with different, customized raising and decaying slopes, for a total pulse duration of ~30 ps (full-width at 1 % of the maximum intensity). Figs. 3.3(a) and 3.3(c) show the input optical pulse spectrum and calculated phase spectral-transfer functions for generation of the target waveforms. The normalized output intensity profile matched up well with the simulated and ideal target waveforms, as reported in Fig. 3.3(b) and 3.3(d). In the numerical calculation, the measured spectrum of the Gaussian-like pulse from the MLL was used as the input pulse source, assuming an ideal uniform spectral phase, and then the entire process was simulated according to the conditions of the experiment. The amplitude and group delay ripples from the LC-FBG were not considered in the simulations. The observed deviations in the experimentally synthesized waveforms and noise outside the pulse-shape temporal windows are mainly attributed to artifacts of the employed indirect characterization technique (FTSI), which requires very stable measurements over the entire sweep time of the OSA, with a high resolution ($\geq$ 0.01nm) for the spectral interference patterns. In addition, the amplitude and group delay ripples of the LC-FBG, and slight variations of the input pulse spectrum during the experiment, may have had an impact on the observed deviations.

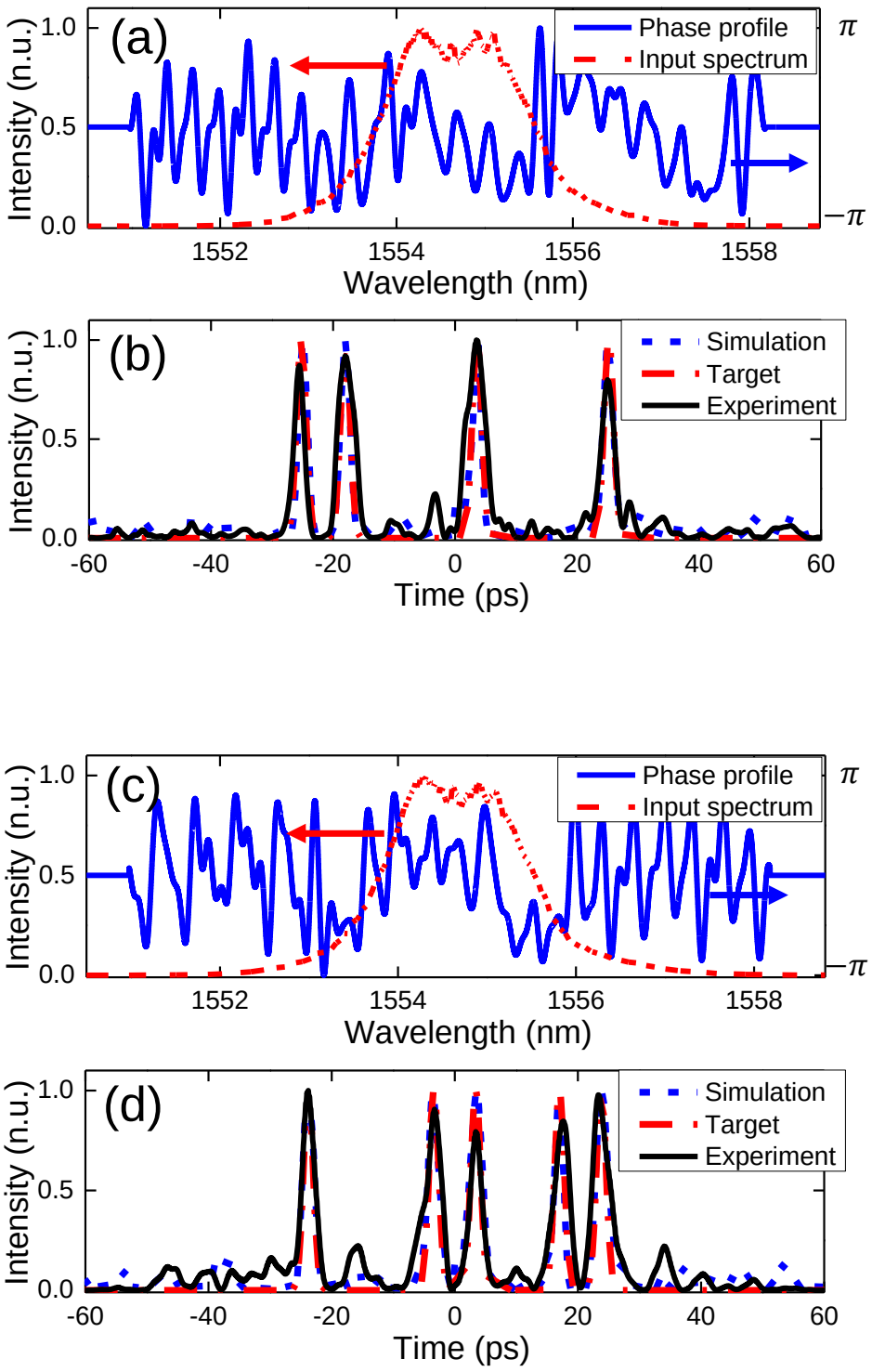

Figure 3.4 **Input pulse spectrum and the calculated spectral phase filtering profile ((a),(c)), and measured (vs. simulated and target) output temporal intensity profiles ((b),(d)) of the synthesized 8-bits random OOK pulse codes.**

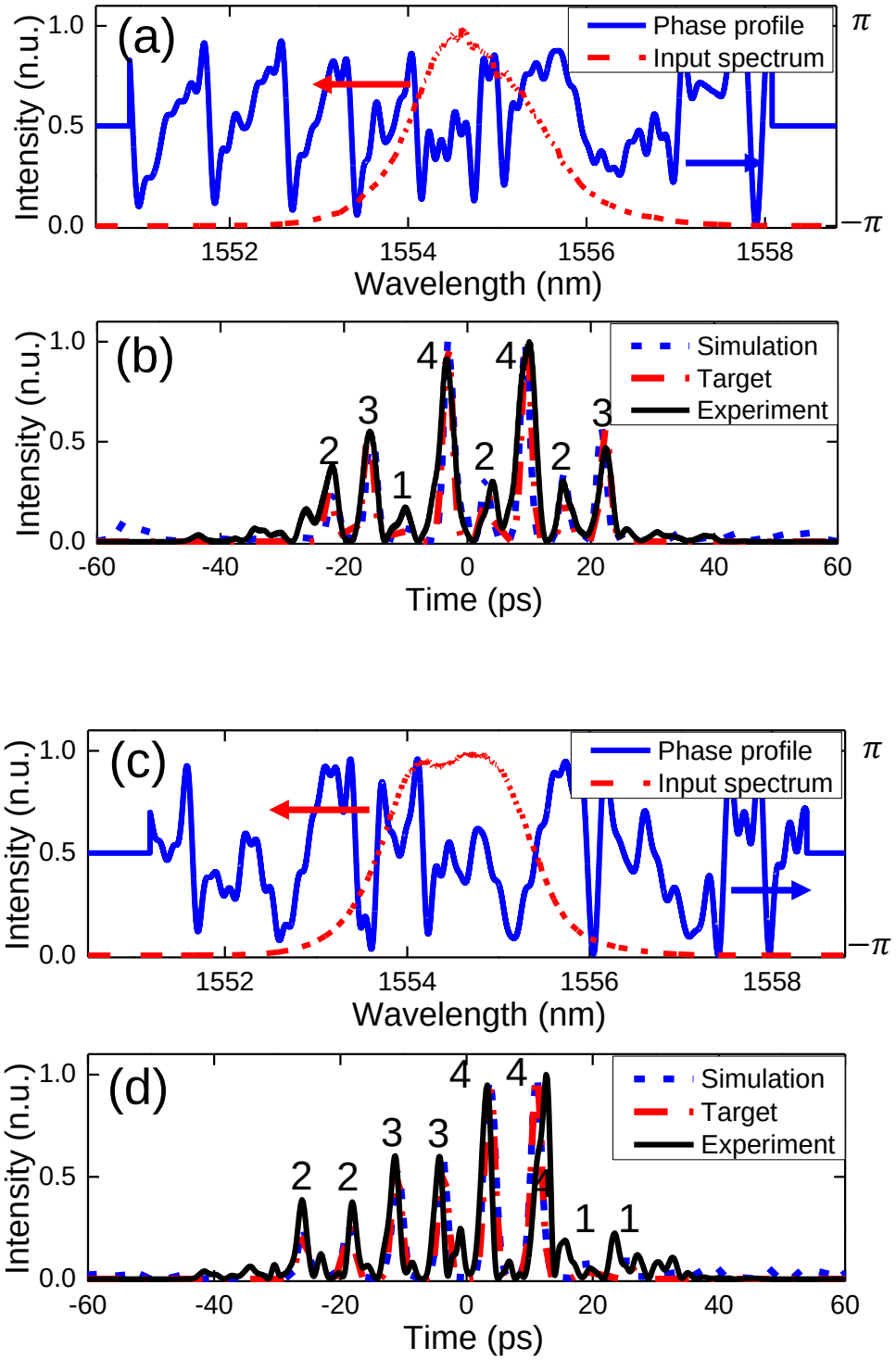

Figure 3.5 **Input spectrum and the calculated spectral phase profile ((a), (b)), and measured (vs. simulated and target) output temporal intensity profiles ((b), (d)) of the synthesized 8-bits PAMs with 5 different pulse intensity levels.**

The next target waveforms were 8-bits random 150-GHz OOK pulse codes. The phase spectral-transfer functions were relatively more complex (Fig. 3.4(a) and 3.4(c)) than the phase profiles needed for the synthesis of triangular waveforms (Fig. 3.3). The measured output temporal intensity profiles are again in excellent agreement with the numerically calculated and ideal target shapes, as plotted in Fig. 3.4(b) and 3.4(d). Consistently with the designed specifications and theoretical predictions outlined above, the intensity FWHM of the individual pulses (time resolution) was ~2 ps, the pulse-to-pulse spacing in the pulse codes was ~6.7 ps (corresponding bit rate ~150 GHz), and the overall time window of each synthesized sequence was ~60 ps.

Finally, 8-bits 150-GHz PAM sequences with 5 different, equi-spaced pulse intensity levels (including the zero level) were targeted in order to demonstrate further the capability of fully arbitrary waveform intensity generation. The calculated spectral phase filtering profiles in Fig. 3.5(a) and 3.5(c) exhibit a similar level of complexity as those of the OOK pulse sequences (Fig. 3.4). Again, the measured output intensity profiles were in excellent agreement with the numerical simulated and ideal waveforms. The target and experimentally obtained specifications for the PAM pulses are similar to the OOK pulse sequences (2 ps individual pulses, separated by ~6.7ps, over a duration of ~60 ps), except for the intensity-level variations among pulses.

As discussed above, the temporal resolution of the synthesized shapes could be further improved by use of a broader bandwidth optical pulse source. In our specific setup, resolutions down to ~200 fs (femtosecond) could be achieved by exploiting the full reflection bandwidth of the employed LC-FBG. Similarly, the output temporal aperture could be also further increased using higher-bandwidth modulation signals and/or a higher amount of dispersion in the system. The same setup could provide a longer output temporal aperture by use of the shortest time features of the AWG, as described in Eq. (3.3), but at the expense of degrading the quality of the synthesized pulse shapes. Finally, it should be also noted that the temporal shape of the synthesized waveforms could be reconfigured pulse to pulse with an update rate that is dictated by the input pulse repetition rate, namely up to ~16-MHz in the scheme reported here.

3.5 **Summary**

In summary, we have experimentally demonstrated a low-loss, fiber-based programmable optical pulse shaper using phase-only linear filtering with a single EO-PM driven by a multi-level modulation function. The approach enables the synthesis of high-quality, fully arbitrary temporal intensity profiles with a resolution just limited by the input pulse o ptical bandwidth, ~2 ps in the shown examples, and over a temporal window (up to ~60 ps in our reported scheme) that directly depends on the product of dispersion and modulation frequency bandwidth. Thus, the demonstrated setup provides a time-bandwidth product (TBP) of ~30, measured as the ratio of the shaping time window to the temporal resolution [69]. The technique should prove useful for ultrafast optical switching and wavelength conversion, high-speed optical coding, signal/device characterization and measurements, as well as for non-linear fiber-optics studies and applications.

CHAPTER 4

In-fiber high-speed recognition of incoherent-light broadband energy-spectrum patterns

4.1 Abstract

A fiber-optic system is proposed and experimentally demonstrated for real-time, on-the-fly identification of an incoherent-light energy spectrum pattern based on dispersion-induced time-spectrum convolution. In the proposed system, the incoming frequency-spectrum patterns to be identified are modulated by a time-mapped version of the target intensity profile. Following propagation through a suitable fiber-optic dispersive medium, the measured output temporal waveform provides a correlation of the incoming spectra with the programmed target pattern. This enables direct, real-time detection of the matching energy spectra, without any further numerical post-processing. We experimentally demonstrate successful recognition of a target infrared spectral pattern, extending over a bandwidth of 1.5 THz with a resolution of ~12 GHz, with sub-megahertz update rates. A path for further performance improvements is also suggested.

4.2 Introduction

Identification of a prescribed energy spectral pattern, such as the spectral signature produced from the interaction between a broadband electromagnetic wave and a material, device or system, is essential for a wide variety of applications, including environmental and biomedical monitoring and analysis [128-130], classification of optical telecommunication paths [131] and quality control in the pharmaceutical and agricultural industries [132,133]. In most of these applications, a fast (real-time) analysis of the incoming spectra is highly desired.

The identification process typically involves detection of multitude of incoming energy spectra from the probed material, device or system using conventional spectrometers, and subsequent numerical post-processing of the detected spectra using digital signal processing (DSP) to identify and extract the desired pattern(s). The use of conventional optical spectrum analysis (OSA), involving spatial dispersion of the incoming optical spectrum, is inherently slow, with typical updated rates in the kHz range. As such, this is unsuited for many applications, particularly those aimed towards the analysis of a sample or target with rapidly changing specifications, such as for monitoring or sensing dynamic chemical or physical phenomena [128-134]. As a solution to this problem, real-time spectroscopy has been demonstrated, with coherent [134] and incoherent [55] optical sources, using frequency-to-time mapping induced by second-order chromatic (temporal) dispersion. These methods enable the acquire of the desired energy spectra using fast time-domain measurement instrumentation, at speeds orders of magnitude higher than with conventional OSAs, e.g. at MHz rates. However, the captured spectra still need to be processed off-line to be able to identify and extract the desired spectral pattern(s). This task requires heavy and time-consuming DSP, as well as storage of the massive digitalized spectral data. Interestingly, the deterministic nature of the target spectral pattern(s) can be exploited to achieve the desired identification process on the fly, through a direct all-optical correlation between the reflected/transmitted light from the sample and the matching pattern. This principle has been exploited in a real-time optical correlation system based on time-domain spectral filtering of coherent-light spectra, with a successful demonstration of a correlation rate up to 36.7MHz [135]. However, this previous schematic can be applied for recognition of *coherent* lightwave spectra only, while requiring a precise synchronization between the time-mapped spectra to be identified and the target temporal intensity pattern. These are two important limitations for practical application of the method. In this work, we propose and

experimentally demonstrate a fiber-optics scheme for high-speed, on-the-fly recognition of a prescribed incoherent-light energy spectral pattern, avoiding numerical post-processing. The scheme is based on the concept of time-spectrum convolution (TSC) in a dispersive fiber grating [25]. The system directly computes a real-time correlation of the incoming spectra with the target pattern that is programmed in a temporal modulator, with no need for synchronization between the incoming light spectra and the modulation pattern. This can be interpreted as the frequency-domain counterpart of a previously reported temporal pattern recognition system based on the TSC concept, aimed at identification of time-domain phase-shift-keying (PSK) coded sequences [58].

4.3 **Principle of operation**

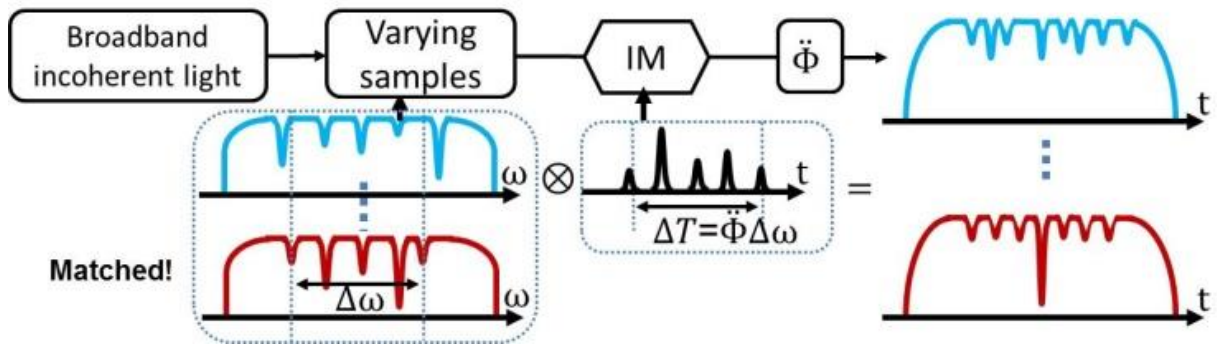

Figure 4.1 **Illustration of the proposed real-time energy spectrum recognition scheme. The parameters t and ω stand for time and radial frequency, respectively, whereas ⊗ is for convolution. Acronyms are defined in the text.**

The scheme for the proposed real-time spectral recognition system is illustrated in Fig. 4.1. A broadband incoherent light source is spectrally linearly filtered to emulate the absorption spectrum of a given sample. The shaped lightwave spectra to be identified are first temporally modulated using an electro-optic intensity modulator (IM) driven by the matching pattern. This is calculated as the time-mapped version of the target energy spectrum, e.g., the absorption spectral response of a target material. Subsequently, the modulated optical signal propagates linearly through a second-order chromatic dispersive medium, characterized by a predominantly linear group delay profile. The

averaged temporal intensity waveform at the output of the dispersive medium is proportional to the time-domain convolution between the time-mapped version of the incoming energy spectrum and the temporal modulation target[21] [25]. The relationship between the frequency axis of each spectral pattern (e.g., spacing $\Delta\omega$) and temporal axis of its corresponding time-mapped version (e.g., spacing ΔT) is determined by the second-order dispersion coefficient $\ddot{\Phi}$ (slope of the group delay as a function of radial frequency ω) of the linear dispersive medium, expressed as $\Delta T = \ddot{\Phi}\Delta\omega$. This scheme computes the cross-correlation between the time-mapped version of the energy spectrum and the *temporally inverted* modulation pattern (or vice versa), updated at the repetition rate of the modulation signal. As illustrated in Fig. 1, the averaged output power will reach above a prescribed threshold (or below, depending on the form of the incoming energy spectrum) only when the incoming spectrum matches the programmed pattern in the modulator (autocorrelation peak), with no need for any further post-processing.

4.4 **Experimental demonstration**

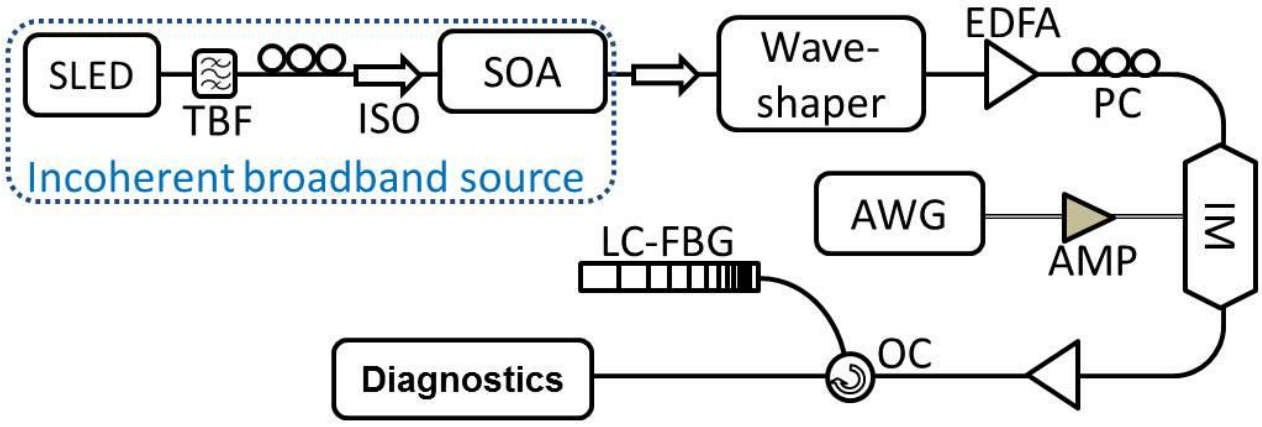

Figure 4.2 **Experimental setup for proof-of-concept demonstration of the proposed real-time energy spectrum recognition system. Acronyms are defined in the text.**

[21] This is mathematically described in Appendix A.

The experimental setup is shown in Fig. 4.2. The broadband incoherent light is generated from a super-luminescent diode (SLED) with output power of ~5 dBm followed by a tunable bandpass filter (TBF, 3-dB bandwidth of 20 nm) and a saturated semiconductor optical amplifier (SOA), providing an optical gain of ~15 dB with improved noise performance [136]. The energy-spectrum patterns to be identified, emulating transmitted absorption spectra from potential samples, are carved by a spectral wave shaper (Finisar WaveShaper 4000S) with a frequency resolution of ~10 GHz. The shaped energy spectra are first measured by an optical spectrum analyzer (OSA) with a resolution of 0.02 nm. Figure 4.3 shows the measured spectra for three different tested cases, including the target absorption spectral pattern (Fig 4.3(b)), the same absorption pattern with a re-scaled frequency axis, 10% wider than the target (Fig 4.3(c)), and the target pattern, keeping the original frequency scaling (i.e., peak spectral separation), but with a different magnitude of the absorption peaks (Fig 4.3(d)). The carved signal is optically amplified by an Erbium-doped fiber amplifier (EDFA) with an optical gain of ~10 dB in order to compensate for the loss from the spectral shaping process (10~23 dB). The amplified signal is temporally modulated by the target pattern (Fig. 4.3(a)) using a 40-GHz electro-optic Mach-Zehnder intensity modulator (IM) driven by an amplified (AMP) high-speed electronic arbitrary waveform generator (AWG) with a sampling rate of 20-GSample/s. The DC bias of the IM is controlled to have the minimum transmission point at the output with zero-voltage input (the DC component of the modulation signal from the AWG[22] is filtered out by the AMP). We highlight that the driving modulation pattern in Fig. 4.3(a) is calculated as the temporally inverted copy of the time-mapped version of the target energy spectrum in Fig. 4.3(b). The modulated light is re-amplified with an optical gain of ~12 dB, and then reflected from a linearly chirped fiber Bragg grating (LC-FBG) that provides a second-order dispersion coefficient $\ddot{\Phi}$ of $+2600$ ps^2 over a reflection bandwidth covering the whole C-Band (1530-1565nm). Finally, the signal received at the output of the dispersive grating is characterized by a 20-GHz electrical sampling oscilloscope following photo-detection (3-dB bandwidth of 10 GHz and sensitivity of -19 dBm at 10Gb/s). The measured output temporal waveforms are averaged 32 times in the experiments.

[22] Arbitrary waveform generator

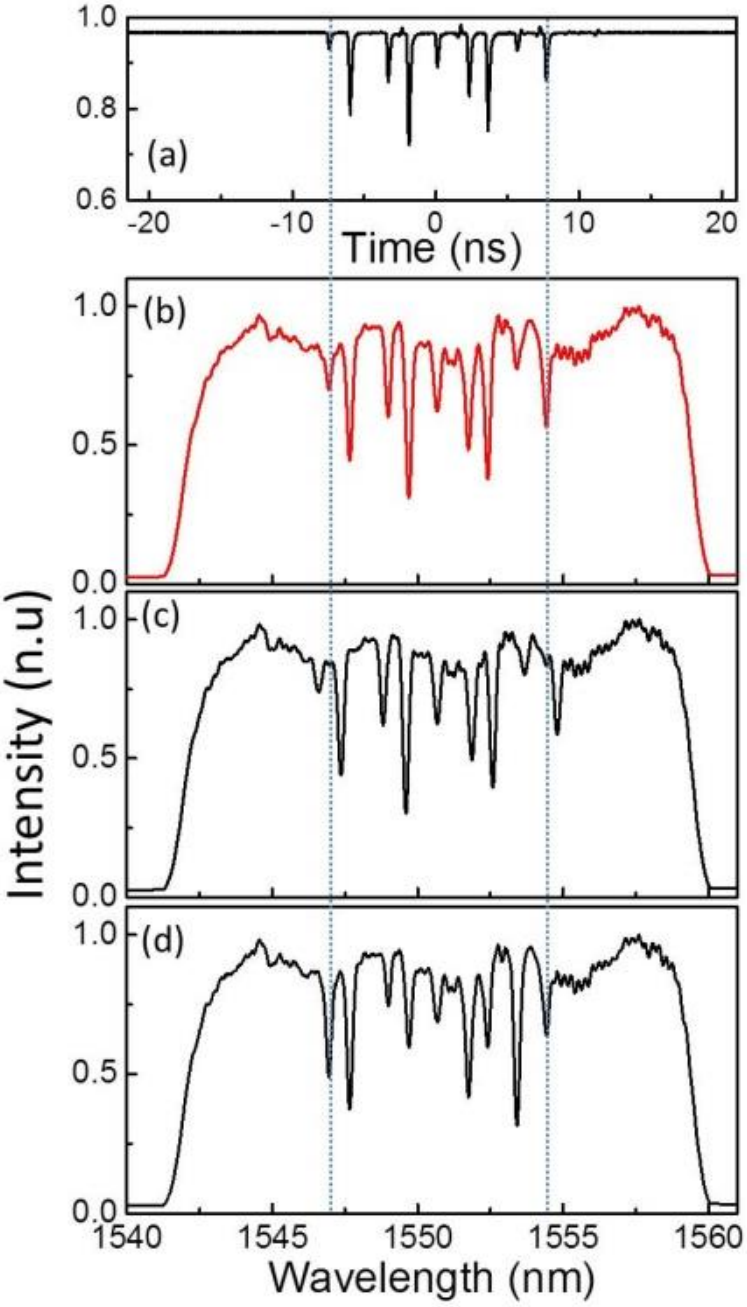

Figure 4.3 **Measured temporal target pattern from the AWG (a), and emulated absorption spectral patterns for three different tests, including the target spectral pattern (b), the same pattern but with 10 % wider spectral spacing (c), and the target pattern but with different magnitude of the absorption peaks (d). The spectra are carved from a broadband light source using a wave shaper. n.u. stands for normalized units. Notice that the spectra are represented as a function of wavelength, thus being temporally inverted with respect to the modulation pattern in (a) when mapped to the time domain through a positive dispersion medium ($\ddot{\Phi} > 0$).**

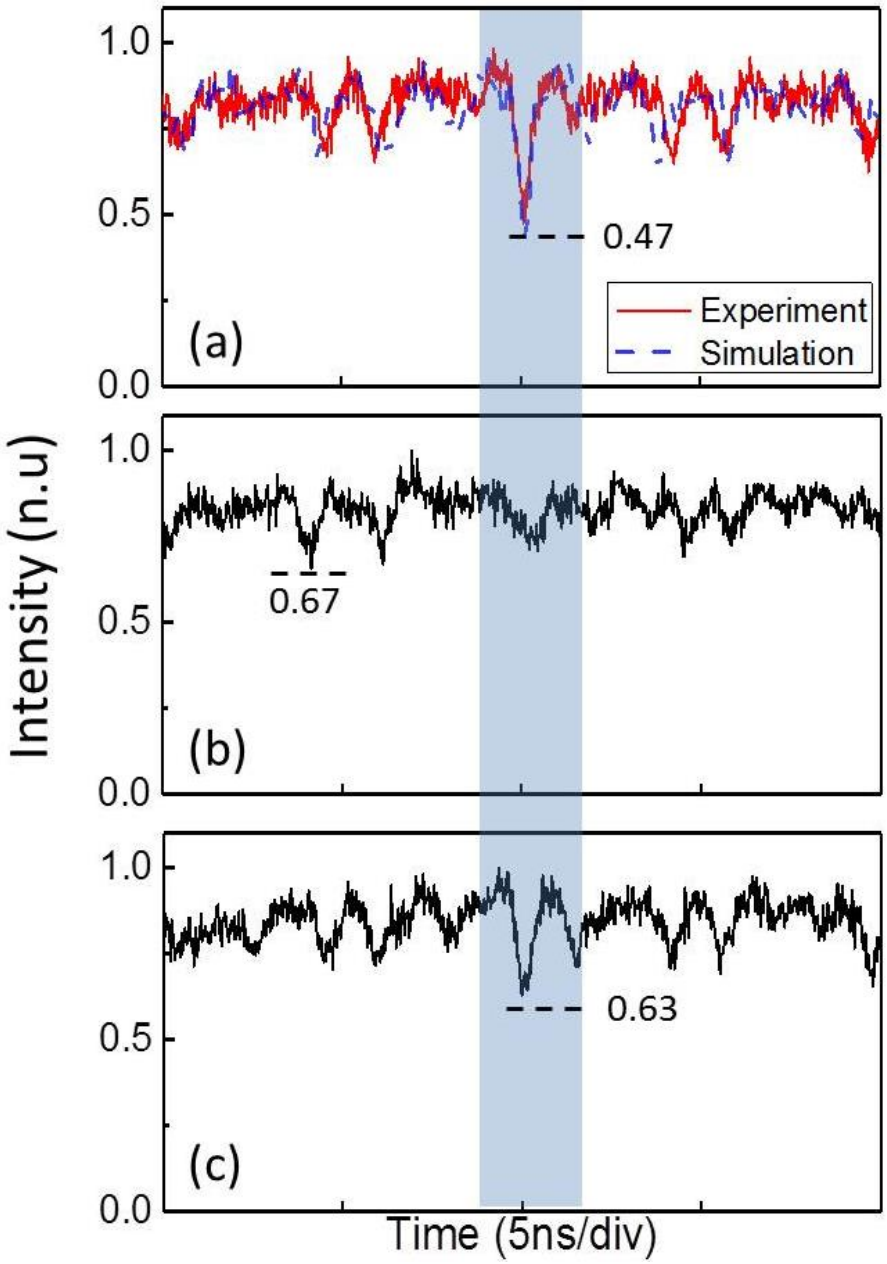

Figure 4.4 **Measured output temporal waveforms (averaged 32 times) when the incoming spectrum is the target pattern (a), the pattern with 10% wider spectral spacing (b), and the pattern with different magnitude of absorption peaks (c). In the case of the target spectrum, the experimentally measured intensity profile (red line) is compared to the simulated autocorrelation (blue dashed line).**

Fig. 4.4 shows the measured averaged output temporal waveforms corresponding to the absorption spectra in Fig. 4.3. Figure 4.4(a) shows the experimental result (red line) and the corresponding numerical simulation (blue dashed line) when the absorption spectrum shape matches the programmed pattern. There is an excellent agreement between the measured temporal waveform and the theoretically calculated one. As predicted, the highest dip for this waveform, corresponding to the autocorrelation peak, is observed at the center of the temporal background waveform, repeating at the rate of the temporal modulation signal. In the case corresponding to the spectral pattern with a frequency spacing ($\Delta\omega$) that is 10% wider than the target (results in Fig. 4.4(b)), the largest dip is significantly lower than the autocorrelation dip observed in Fig. 4.4(a). This demonstrates the high sensitivity of the proposed system to variations in the frequency spacing of the target absorption profile. Such a sensitivity is a desired feature for applications where a given target is identified by recognizing its vibrational/rotational frequencies and their overtones [128-130]. Additionally, we test the capability of the proposed system for recognition of the relative magnitude of the absorption peaks. This test is conducted by changing the relative amplitude of the absorption peaks while keeping their same frequency location as well as the total sum of the magnitudes of the peaks. A relatively smaller dip is again observed in the cross-correlation temporal output waveform, shown in Fig 4.4(c).

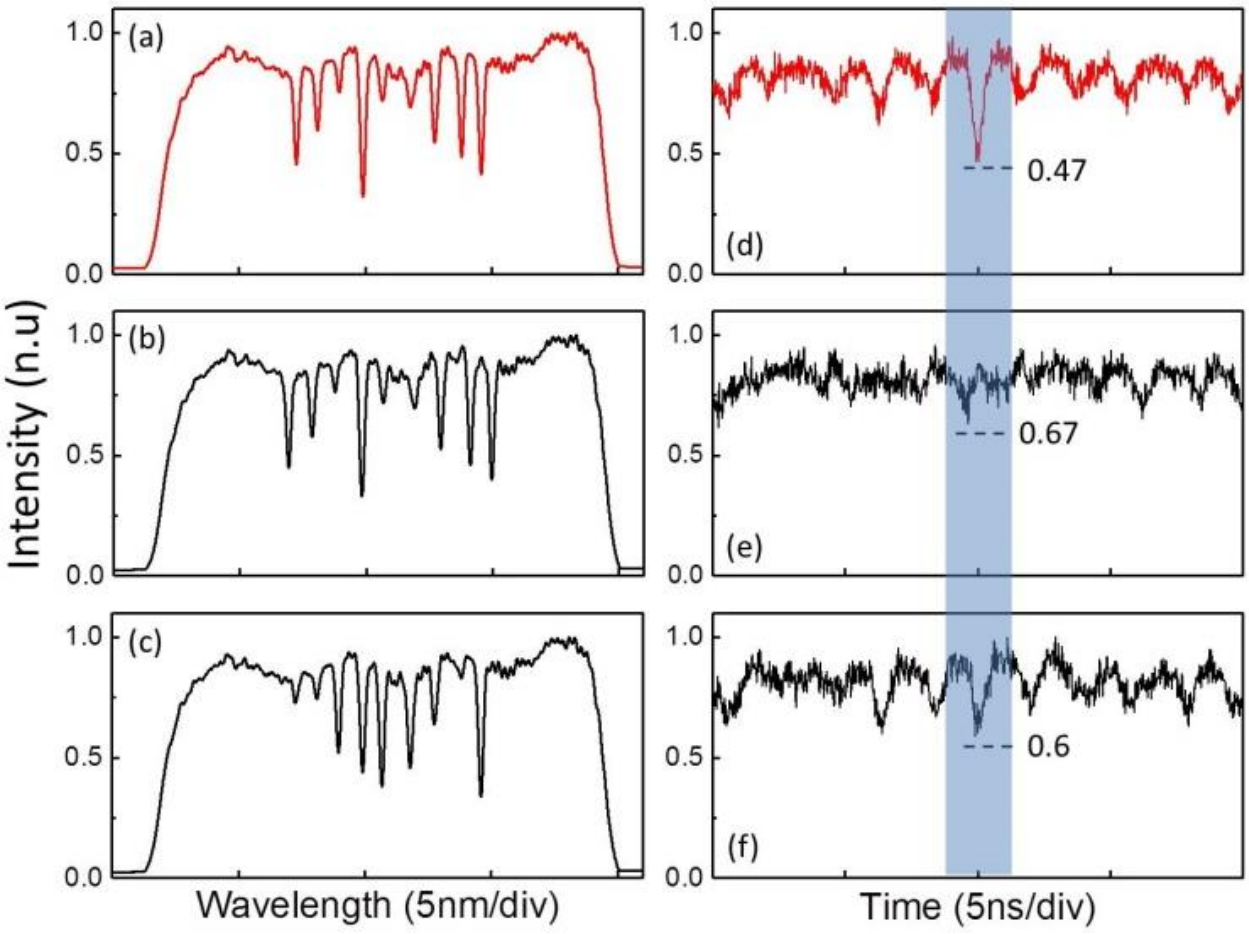

Figure 4.5 **Measured, emulated absorption spectral patterns and their corresponding output temporal waveforms (averaged 32 times), for three different tests, including the target spectral pattern ((a), (d)), the same pattern but with 10% wider spectral spacing ((b), (e)), and the target pattern but with different magnitude of the absorption peaks ((c), (f)), respectively.**

Fig. 4.5 shows additional experimental results for the case of a different target absorption spectrum. Similarly to the previous case, the tested absorption spectra include the exact target spectral pattern (Fig. 4.5(a)), a pattern that has a 10% wider spectral spacing (Fig. 4.5(b)), and a pattern that has different relative intensity levels in between the same spectral absorption peaks (Fig. 4.5(c)). The obtained averaged output temporal waveforms corresponding to these different tested spectra are shown in Fig. 4.5(d)-5(f). Again, the experimentally measured output temporal waveforms match very well the theoretically calculated ones, and the intensity levels of the observed cross-correlation dips for the different spectral patterns follow a similar trend to that of the first experiment, with the highest dip being clearly distinguishable for the target spectrum.

In the previous experiments, the emulated absorption spectra are spectrally carved into the input broadband light wave using a relatively slow wave shaper[23], which restricts the possibility to test the capabilities of the method to identify rapidly changing spectral patterns with a fast update rate. In the following experiment, different spectral patterns are emulated by accordingly modifying the driving temporal modulation signal (from the AWG) while the incoming energy spectrum is kept unchanged to a 16-bit binary spectral pattern (1000100001100001), again carved by the wave shaper on the input light spectrum. The temporal modulation patterns are modified every 24 ns, evaluating the following cases: i) the matching pattern corresponding to the target spectral response, ii) a pattern that is just 1 bit different from the matching pattern (0100100001100001), and iii) 3 other random patterns. For a fair comparison, the total energy of the each modulation pattern is set to be equal. The experimental results and corresponding numerical simulations are shown in Fig. 4.6. The experimentally measured output temporal waveform (Fig. 4.6(b), averaged 32 times) matches well with the theoretically calculated one (Fig. 4.6(a)). As expected, the autocorrelation peak (highest peak power) is obtained when the energy spectrum under test matches the driving modulation pattern; a noticeable lower peak is recovered even when there is only 1-bit difference between the spectral and modulation patterns. Figure 4.6(c) shows a close-up of the output temporal intensity profile of the experiment (red solid) and simulation (blue dashed). Again, the measured temporal waveform matched very well with the theoretically calculated one.

[23] A commercial space-domain wave shaper.

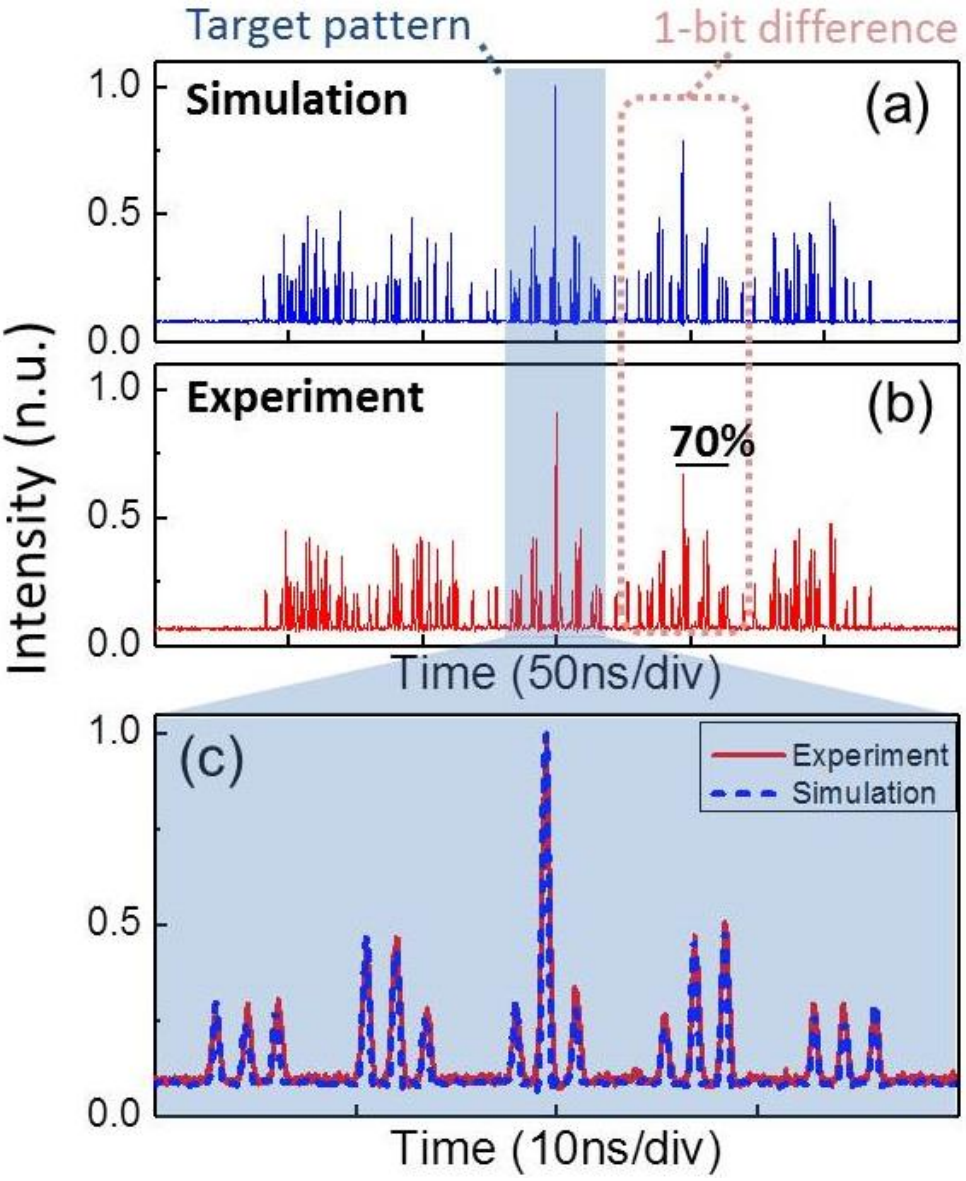

Figure 4.6 **Demonstration of energy-spectrum recognition with a fast update date. Simulation (a) and experimental (b) averaged output temporal patterns (cross-correlation) as the temporal modulation pattern is changed every 24 ns. The plot in (c) shows a close-up of the output temporal intensity profile in the experiment (red solid) and simulation (blue dashed) around the autocorrelation peak.**

The presented results show that the output correlation can be measured with a refreshing rate that is only limited by the duration of the resulting temporal convolution patterns, about twice the duration of the matching temporal modulation pattern (e.g., 2×24 ns in our example), and the needed 32 averaging in detecting the output waveforms. This enables direct spectral pattern identification at sub-MHz rates ($1/(32\times 48\,\mathrm{ns})$~650 kHz, demonstrated here), without the requirement for any further post-processing. The duration of the modulation signal ($\Delta T \approx 24\mathrm{ns}$) is determined by the product of the full analysis spectral bandwidth ($\Delta\omega \approx$~$2\pi\times 1.5\mathrm{THz}$) and the magnitude of the dispersion coefficient ($|\ddot{\Phi}| = 2600\,\mathrm{ps}^2$). This implies that the identification rate (R) is inversely proportional to the dispersion coefficient, expressed as R=1/($2N\times|\ddot{\Phi}|\Delta\omega$), where N is the averaging number. Therefore, a higher identification rate could be achieved by use of a lower dispersion coefficient, but this translates into a degraded detection frequency resolution. In particular, the spectral resolution of the system ($\delta\omega$) is inversely proportional to the dispersion coefficient, expressed as $\delta\omega = \delta t/|\ddot{\Phi}|$, where δt is an estimate of the temporal resolution of the modulation signal (dictated by the modulation bandwidth). This analysis assumes that the photodetection system at the system output has sufficient bandwidth to resolve accurately the modulation time resolution δt. In our experiment, the modulation resolution is designed to be ~200ps, so that the corresponding frequency resolution (~$2\pi\times 12$ GHz,) fits very closely the spectral resolution of the spectral waveshaper used in the experiment. Considering the outlined trade-offs between spectral resolution, analysis bandwidth, and the identification rate, we define a figure of merit (*FOM*) for the proposed system as the number of spectral points that can be identified in a second, as follows:

$$FOM = R\frac{\Delta\omega}{\delta\omega} \approx \frac{1}{2N\delta t} \tag{4.1}$$

From Eq. (4.1), the *FOM* of our system is calculated to be ~78 MPoints/s. It is important to note that for many applications, a possible temporal overlapping between consecutive output correlation patterns may be tolerated as long as the individual correlation peaks do not interference with each other. Most importantly, previous studies have demonstrated that the proposed scheme can provide the desired time-spectrum convolution in a single-shot measurement (N =1) using a suitable multi-wavelength laser, rather than a broadband incoherent light source [137]. In particular, the multi-wavelength laser should exhibit a free spectral range (FSR) wider than the photo-detection bandwidth, itself larger than the modulation signal bandwidth. By employing this alternative laser source, the *FOM* in Eq. (4.1) can be increased up to $FOM = 1/(2\times\delta t)$. In this case, the FOM of our specific

setup could potentially perform at ~3.8 GPoints/s (e.g., using a source with a FSR of ~12 GHz to keep the same frequency resolution), ultimately constrained by the frequency bandwidth of the high-speed AWG used in our experiments (~7.5 GHz).

4.5 **Summary**

In summary, we have proposed and experimentally demonstrated a fiber-optics system for real-time recognition of a prescribed incoherent-light energy spectrum pattern. The scheme involves temporal modulation of the broadband light waves under analysis with a suitable time-domain scaled version of the target spectral pattern, followed by chromatic dispersion and averaged photo-detection. This system directly computes the cross-correlation of the incoming light energy spectra with the target pattern, with no needed temporal synchronization or any additional numerical post-processing. Proof-of-concept experimental demonstrations are reported, including successful recognition of ~120-points spectral patterns at an update rate of ~650 kHz. The performance of the proposed system can be potentially improved by employing a multi-wavelength laser, relaxing the need for averaging the photodetected waveforms. The technique should prove useful for real-time identification, sensing and/or monitoring tasks in the analysis of a variety of physical or chemical samples or events.

CHAPTER 5

CONCLUSION

5.1 Conclusion of the Thesis

Various linear optical pulse shaping techniques are discussed as a powerful tool to exploit the ultra-wide bandwidth of photonics coherent/incoherent sources. Two main topics of optical pulse shaping, a design concept for a filtering function and its implementation, are focused in this Thesis. The employment of the simple passive dispersive medium allow to develop novel linear approaches for fiber-optics programmable optical pulse shaping methods and their innovative applications for all optical signal processing. Generally, proposed techniques are based on dispersion-induced frequency-to-time mapping (FTM) combined with spectral amplitude and/or phase modulation of both coherent and incoherent lights. The proposed methods provide a greatly increased flexibility to achieve a desired arbitrary pulse duration and minimized energy loss from the filtering process, independently of the frequency resolution of the operating linear optical pulse shaper.

In **Chapter 2**, we have proposed and demonstrated a novel linear-optics method for parabolic pulse generation. The method is based on dispersion-induced frequency-to-time mapping (FTM), allowing to preserve most of the energy spectra available from the input optical sources, regardless of the target pulse duration. This is in contrast to the conventional direct Fourier synthesis method where the pulse durations are essentially restricted by energy spectrum losses of the pulse shaping stage, or ultimately by the finest spectral resolution of the pulse shaper. Design guidelines based on far-field FTM (FF-FTM) and near-field FTM (NF-FTM) are suggested for generation of optical parabolic pulses over a broad range of target durations. First, the pulse synthesis based on FF-FTM combined with spectral shaping prove to be capable of overcoming the limitations of the direct spectral shaping approach. As a proof of a concept, a 400-ps

parabolic pulse was successfully generated from an ~2-ps input mode-locked laser source with the average power of ~10 dBm. As the pulse duration gets shorter, the waveform distortions imposed by the requirement for satisfying a strict far-field condition become more critical. This restriction was relaxed by use of a virtual time lens, incorporated into the linear spectral shaping stage, effectively implementing a NF- FTM approach. This method allowed generation of parabolic pulses with durations ranging from ~25 ps to ~400 ps, and the experimentally synthesized pulses were high-quality parabolas with output powers as high as ~4 dBm without using any amplification. In the experiments for the generation of 25ps parabolic pulses, the measured system losses were ~6 dB and ~12 dB for the NF-FTM method and direct Fourier synthesis method, respectively. This demonstrates the significant improvement provided by the proposed method in terms of energy efficiency.

The generated parabolic pulses are used as a pump for creation of a high-quality time-lens (TL) though XPM. This approach does not require to satisfy stringent phase-matching conditions and provide additional all-optical programmable capabilities, exploiting the feature that the lens chirp factor (i.e., focal length of the time-lens) is dependent on the peak power of the parabolic pump pulse. In order to demonstrate the capability, we have designed and demonstrated an XPM TL -based scheme for reconfigurable T-to-F conversion and temporal magnification of picosecond optical waveforms; the scheme can perform the optical time-domain Fourier transform of the input signal when the XPM stage is bypassed. All functionalities are optically controlled by simple gain tuning an optical amplifier.

In **Chapter 3**, we have experimentally demonstrated a low-loss, fiber-optic programmable optical pulse shaper using a single EO-PM, implementing phase-only linear filtering. The multi-level modulation function is calculated from a combination of optimization algorithms, namely the Gerchberg–Saxton algorithm (GSA) and a genetic algorithm (GA), and generated from electronic arbitrary waveform generator. The method allows the synthesis of high-quality, fully arbitrary temporal intensity profiles with a temporal resolution just limited by the optical bandwidth of input pulse (~2 ps in the shown examples), and a temporal window directly depending on the product of dispersion and modulation frequency bandwidth (up to ~60 ps in our reported scheme). As a proof-of-concept, we report the synthesis of asymmetric triangular waveforms and ~150 Gbaud random on–off keying (OOK) pulse and pulse amplitude-modulation (PAM) code sequences, with a temporal

resolution of ~2 ps over a maximum time window of ~60 ps, which provides a time-bandwidth product (TBP) of ~30, measured as the ratio of the shaping time window to the temporal resolution.

In **Chapter 4**, we have proposed and experimentally demonstrated a fiber-optics system for real-time, on-the-fly identification of an incoherent-light energy spectrum pattern. The scheme is based on dispersion-induced time-spectrum convolution (TSC), which involves temporal modulation of the broadband incoherent lightwaves under analysis with a time-domain scaled version of the target spectral pattern, followed by suitable dispersive medium. The averaged output temporal waveform is a correlation of the incoming spectra with the programmed target pattern. This system directly computes the cross-correlation of the incoming light energy spectra with the target pattern, without the requirement for temporal synchronization or any additional numerical post-processing. In the proof-of-concept experiments, we have demonstrated infrared spectral pattern recognition at an update rate of 650 kHz, over a bandwidth of 1.5 THz with a spectral resolution of ~12 GHz.

5.2 **Future perspectives**

Next, we briefly discuss several potential lines of future research considered to be of higher relevance by the author:

1. The proposed design guidelines based on dispersion-induced FTM and NF-FTM in **Chapter 2** allow one to generate high-fidelity arbitrary optical intensity waveforms over a wide range of pulse durations with optimized energy efficiency. As illustrated in Fig. 2.9, the previous techniques provide a narrow length of output pulse durations due to the constraints associated with the increasing energy losses from the filtering process and the degradation of the waveform quality. The improved pulse duration flexibilities combined with the high energy-efficiency and waveform-fidelity should broaden the range of applications of the dispersive FTM based optical pulse shaping in many important applications. As a highly relevant application, the important time-lensing functionality has been successfully demonstrated by using high-quality bright/dark parabolic pump pulses generated from the proposed method. As an extension of the work, other important temporal intensity waveforms (e.g., saw tooth, flat-top) can be generated to implement different functionalities, such as for wavelength

conversion, optical switching, optical regenerations, etc. For this purpose, the design equations of the NF-FTM approach should be generalized to the synthesis of waveforms with time resolutions down to the femtosecond range; this is a regime that is challenging to achieve with conventional FF-FTM methods but it may be possible to approach by exploiting the enhanced versatility offered by the NF-FTM concept.

2. In **Chapter 2**, high-quality bright/dark parabolic pulses are synthesized as pump pulses for the creation of a XPM-based time lens (XPM-TL) using the proposed NF-FTM method. Our work highlights the all-optical reconfigurable capability of a XPM-TL through the design and experimental demonstration of an optically programmable TL-based signal processing platform, namely a system aimed at imaging high-speed temporal waveforms with a temporal magnification factor that can be programmed over a wide range of values by simply tuning the pump pulse power. The XPM-TL scheme can provide a femtosecond response time simultaneously with the programmable chirp rate. Moreover, it does not require to satisfy the stringent phase-matching conditions of FWM-based methods while also avoiding undesired wavelength shifts. These unique features should be beneficial for realization of other important time-domain signal-processing applications, including ultrafast waveform characterization, OTDM-to-WDM conversion, impairment (e.g., dispersion and nonlinearity) compensation in communication links, etc. However, in order to realize some of these functionalities, XPM-TL should offer an increased chirp rate, with respect to the values reported in my experiments here. For instance, the conversion from a 640-Gbit/s OTDM data to a 50-GHz grid DWDM data requires a chirp rate of ~0.2 THz^2/rad whereas the maximum chirp reported in **Chapter 2** is ~0.07 THz^2/rad. This was mainly due to the maximum average power available at the input of the HNLF (15 dBm) which was restricted by the increasing spontaneous emission noise from the EDFA, and the power tolerance of the bandpass filter after the EDFA in the experiment. Strategies to overcome these limitations should be explored so that to be able to enhance the performance of the XPM-TL mechanism (e.g., to increase chirp rates) according to the needed specifications for practical applications
3. The time-domain spectral shaping (TDSS) systems based on multi-level phase-only filtering using a single electro-optic phase modulator is capable of synthesizing fully arbitrary (including asymmetric) temporal intensity waveforms in the picosecond regime. The increased waveform flexibility of the TDSS-based optical pulse shaper should allow us to

explore the advantages of TDSS systems for extended applications, including ultrafast optical channel add/drop, nonlinear wavelength conversion, high-speed optical code division multiple access (OCDMA), and signal/device characterization and measurements. The frequency resolution of the time-domain pulse shaper demonstrated here (i.e., temporal aperture) is ~16 GHz, and this could be further increased using higher-bandwidth modulation signals and/or a higher amount of dispersion in the system. It is important to note that the use of larger dispersion requires long pulse periods for the input broadband optical source to implement the TDSS, resulting in a lower waveform update rate. In our specific setup, temporal resolutions of the target pulses down to ~200 fs could be achieved by exploiting the full reflection bandwidth of the employed LC-FBG.

4. In **Chapter 4**, I have proposed and experimentally demonstrated an innovative fiber-optics system design for real-time recognition of a prescribed incoherent-light energy spectrum pattern. The proposed system directly computes the cross-correlation of the incoming light spectra with the target pattern, without the need for (unpractical) time synchronization or any additional numerical post-processing. The technique should prove particularly useful for real-time identification, sensing and/or monitoring tasks in the analysis of a variety of physical or chemical samples or events. In the experimental demonstration, optical spectral patterns with >100 points are recognized at sub-MHz update rates. Potentially, the requirement for temporal averaging can be relaxed by employing a multi-wavelength laser source, which would result in great performance improvements, e.g. increased recognition rate of up to 21 MHz in the specific demonstrated setup.

REFERENCES

[1] T. Maiman, "Stimulated optical radiation in ruby," Nature **187**, 493-494 (1960).

[2] Lockheed Martin, "Lockheed martin to deliver world record-setting 60kW laser to U.S. army," [Online]. Available: https://news.lockheedmartin.com/2017-03-16-Lockheed-Martin-to-Deliver-World-Record-Setting-60kW-Laser-to-U-S-Army?_ga=2.129860300.1748624792.1520889089-336625012.1515479529. [Accessed 12 03 2018].

[3] A.M. Weiner, Ultrafast Optics, Hoboken, NJ, USA: Wiley (2009).

[4] J. C. Diels and W. Rudolph, Ultrashort laser pulse phenomena, San Diego, CA, USA: Academic, 2nd edn. (2006).

[5] F. Krausz and M. Ivanov. "Attosecond physics," Rev. Mod. Phys. **81**, 163-234 (2009).

[6] A. M. Weiner, "Femtosecond pulse shaping using spatial light modulators," Rev. Sci. Instrum. **71**, 1929-1960 (2000).

[7] J. P. Callan, A. M.-T. Kim, L. Huang, and E. Mazur, "Ultrafast electron and lattice dynamics in semiconductors at high excited carrier densities," Chem. Phys. **251**, 167-179 (2000).

[8] T. Richter, E, Palushani, C. Schmidt-Langhorst, R. Ludwig, L. Molle, M. Nölle, and C. Schubert, "Transmission of single-channel 16-QAM data signals at terabaud symbol rates," J. Lightwave Technol. **30**, 504-511 (2012).

[9] A. V. Andrianov, V. M. Mylnikov, M. Y. Koptev, S. V. Muravyev and A. V. Kim, "Broadband femtosecond fiber laser with ultrahigh repetition rate in the telecommunication range," in *2016 International Conference Laser Optics* (LO), St. Petersburg, Russia, paper R8-10.

[10] B. W. Tilma, M. Mangold, C. A. Zaugg, S. M. Link, D. Waldburger, A. Klenner, A. S. Mayer, E. Gini, M. Golling, and U. Keller, "Recent advances in ultrafast semiconductor disk lasers," Light Sci. Appl. **4**, e310 (2015).

[11] C. L. Hoy, O. Ferhanoğlu, M. Yildirim, K. H. Kim, S. S. Karajanagi, K. M. Chan, J. B. Kobler, S. M. Zeitels, and A. Ben-Yakar "Clinical ultrafast laser surgery: recent advances and future directions," IEEE J. Sel. Top. Quantum Electron. **20**, 242-255 (2014).

[12] A. M. Weiner, “Ultrafast optical pulse shaping: a tutorial review,” Opt. Commun. **284**, 3669-3692 (2011).

[13] H. P. Bazargani, M. Burla, Z. Chen, F. Zhang, L. Chrostowski and J. Azaña, "Long-duration optical pulse shaping and complex coding on SOI," IEEE Photon. J. **8,** 1-7 (2016).

[14] C. Dorrer, W. A. Bittle, R. Cuffney, M. Spilatro, E. M. Hill, T. Z. Kosc, J. H. Kelly, and J. D. Zuegel, "Characterization and Optimization of an Eight-Channel Time-Multiplexed Pulse-Shaping System," J. Lightwave Technol. **35**, 173-185 (2017).

[15] A. J. Metcalf, H. Kim, D. E. Leaird, J. A. Jaramillo-Villegas, K. A. McKinzie, V. Lal, A. Hosseini, G. E. Hoefler, F. Kish, and A. M. Weiner, "Integrated line-by-line optical pulse shaper for high-fidelity and rapidly reconfigurable RF-filtering," Opt. Express **24**, 23925-23940 (2016).

[16] M. C. Fischer, J. W. Wilson, F. E. Robles, and W. S. Warren, “Invited review article: pump-probe microscopy,” Rev. Sci. Instrum. **87**, 031101 1-21 (2016).

[17] S. Wabnitz and B. J. Eggleton, All-optical signal processing: data communication and storage applications, Berlin, Germany: Springer (2015).

[18] E. B. Treacy, “Optical pulse compression with diffraction gratings,” IEEE J. Quantum Electron. **QE-5**, 454-458 (1969).

[19] T. K. Gustafson, J. P. Taran, H. A. Haus, J. R. Lifsitz, and P. L. Kelley, “Self-modulation, self-steepening, and spectral development of light in small-scale trapped filaments,” Physical Review, **177**, 306-313 (1969).

[20] E. B. Traecy, “Compression of picosecond light pulses,” Phys. Lett. A **28**, 34-35 (1969).

[21] V. Binjrajka, C.-C. Chang, A. W. R. Emanuel, D. E. Leaird, and A. M. Weiner, "Pulse shaping of incoherent light by use of a liquid-crystal modulator array," Opt. Lett. **21**, 86-87 (1996).

[22] L. Wang and A.M. Weiner, “Programmable spectral phase coding of an amplified spontaneous emission light source,” Opt. Comm. **167**, 211-224 (1999).

[23] C. Dorrer, “Temporal van Cittert-Zernike theorem and its application to the measurement of chromatic dispersion,” J. Opt. Soc. Am. B **21**, 1417-1423 (2004).

[24] V. Torres-Company, J. Lancis, and P. Andrés, “Arbitrary waveform generator based on all-incoherent pulse shaping,” IEEE Photon. Technol. Lett. **18**, 2626-2628 (2006).

[25] Y. Park and J. Azaña, “Optical signal processors based on a time-spectrum convolution,” Opt. Lett. **35**, 796-798 (2010).

[26] S. Boscolo, F. Chaussard, E. Andresen, H. Rigneault, and C. Finot, “Impact of initial pulse shape on the nonlinear spectral compression in optical fibre,” Optics & Laser Technol. **99**, 301-309 (2018).

[27] G. P. Agrawal Nonlinear fiber optics, San Diego, CA, USA: Academy, 3rd edn. (2001).

[28] D. Anderson, M. Desaix, M. Karlson, M. Lisak, and M. L. Quiroga-Teixeiro, "Wave-breaking-free pulses in nonlinear optical fibers," J. Opt. Soc. Am. B **10**, 1185-1190 (1993).

[29] M. E. Fermann, V. I. Kruglov, B. C. Thomsen, J. M. Dudley, and J. D. Harvey, "Self-similar propagation and amplification of parabolic pulses in optical fibers," Phys. Rev. Lett. **84**, 6010-6013 (2000).

[30] J. P. Limpert, T. Schreiber, T. Clausnitzer, K. Zöllner, H. J. Fuchs, E. B. Kley, H. Zellmer, and A. Tünnermann, "High-power femtosecond Yb-doped fiber amplifier," Opt. Express **10**, 628-638 (2002).

[31] D. Krcmarik, R. Slavik, Y. Park, and J. Azana, "Nonlinear pulse compression of picosecond parabolic-like pulses synthesized with a long period fiber grating filter," Opt. Express **17**, 7074-7087 (2009).

[32] Y. Ozeki, Y. Takushima, K. Aiso, and K. Kikuchi, "High repetition-rate similariton generation in normal dispersion erbium-doped fiber amplifiers and its application to multi-wavelength light sources," IEICE Trans. Electron. **88**, 904-911 (2005).

[33] C. Finot and G. Millot, "Synthesis of optical pulses by use of similaritons," Opt. Express **12**, 5104-5109 (2004).

[34] E. R. Andresen, J. M. Dudley, C. Finot, D. Oron, and H. Rigneault, “Transform-limited spectral compression by self-phase modulation of amplitude shaped pulses with negative chirp,” Opt. Lett. **36**, 707-709 (2011).

[35] J. Fatome, B. Kibler, E. R. Andresen, H. Rigneault, and C. Finot, "All-fiber spectral compression of picosecond pulses at telecommunication wavelength enhanced by amplitude shaping,” Appl. Opt. **51**, 4547-4553 (2012).

[36] A. W. Lohmann and D. Mendlovic, “Temporal filtering with time lenses,” Appl. Opt. **31**, 6212-6219 (1992).

[37] E. Agrell, M. Karlsson, A. Chraplyvy, D. J. Richardson, P. M. Krummrich, P. Winzer, K. Roberts, J. K. Fischer, S. J. Savory, B. J. Eggleton, M. Secondini, F. R. Kschischang, A. Lord, J. Prat, I. Tomkos, J. E. Bowers, S. Srinivasan, M. Brandt-Pearce, and N. Gisin, “Roadmap of optical communications,” J. Opt. **18**, 063002 (2016)

[38] E. Palushani, H.C.H. Mulvad, M. Galili, H. Hu, L.K. Oxenløwe, A. Clausen, and P. Jeppesen, “OTDM-to-WDM conversion based on time-to-frequency mapping by time-domain optical Fourier transformation,” IEEE J. Sel. Top Quantum Electron. **18**, 681-688 (2011).

[39] P. J. Winzer and A. H. Gnauck, “112-Gb/s polarization-multiplexed 16-QAM on a 25-GHz WDM grid,” in *34th European Conference on Optical Communication* (ECOC 2008), Brussels, Belgium, paper Mo.4.C.

[40] N. Cvijetic, "OFDM for next-generation optical access networks," J. Lightwave Technol. **30**, 384-398 (2012).

[41] L. Zheng, J. Ding, S. Shao, L. Zhang, and L. Yang, "Silicon PAM-4 optical modulator driven by two binary electrical signals with different peak-to-peak voltages," Opt. Lett. **42**, 2213-2216 (2017).

[42] C. Xiong, D. M. Gill, J. E. Proesel, J. S. Orcutt, W. Haensch, and W. M. J. Green, "Monolithic 56 Gb/s silicon photonic pulse-amplitude modulation transmitter," Optica **3**, 1060-1065 (2016).

[43] A. E. Willner, S. Khaleghi, M. R. Chitgarha and O. F. Yilmaz, "All-optical signal processing," J. Lightwave Technol. **32**, 660-680 (2014).

[44] F. Parmigiani, T. T. Ng, M. Ibsen, P. P. Petropoulos and D. J. Richardson, "Timing jitter tolerant all-optical TDM demultiplexing using a saw-tooth pulse shaper," IEEE Photon. Technol. Lett. **20**, 1992-1994 (2008).

[45] F. Parmigiani, M. Ibsen, T. Ng, L. Provost, P. Petropoulos and D. Richardson, "An efficient wavelength converter exploiting a grating-based saw-tooth pulse shaper," IEEE Photon. Technol. Lett. **20**, 1461-1463 (2008).

[46] F. Parmigiani, M. Ibsen, P. Petropoulos and D. Richardson, "Efficient all-optical wavelength-conversion scheme based on a saw-tooth pulse shaper," IEEE Photon. Technol. Lett. **21**, 1837-1839 (2009).

[47] R. Tucker and K. Hinton, "Energy consumption and energy density in optical and electronic signal processing," IEEE Photonics J. **3**, 821-833 (2011).

[48] V. Eckhouse, I. Cestier, G. Eisenstein, S. Combrié, P. Colman, A. De Rossi, M. Santagiustina, C. G. Someda, and G. Vadalà, "Highly efficient four wave mixing in GaInP photonic crystal waveguides," Opt. Lett. **35**, 1440-1442 (2010).

[49] A. R. Motamedi, A. H. Nejadmalayeri, A. Khilo, F. X. Kärtner, and E. P. Ippen, "Ultrafast nonlinear optical studies of silicon nanowaveguides," Opt. Express **20**, 4085-4101 (2012).

[50] T. Yang, E. Wang, H. Jiang, Z. Hu, and K. Xie, "High birefringence photonic crystal fiber with high nonlinearity and low confinement loss," Opt. Express **23**, 8329-8337 (2015).

[51] H. Zhang, S. Virally, Q. Bao, L. K. Ping, S. Massar, N. Godbout, and P. Kockaert, "Z-scan measurement of the nonlinear refractive index of graphene," Opt. Lett. **37**, 1856-1858 (2012).

[52] J. Wang and X. Hu, "Recent advances in graphene-assisted nonlinear optical signal processing," J. Nanotechnol. **2016**, 1-18 (2016).

[53] Y. Park, M. Kulishov, R. Slavík, and J. Azaña, "Picosecond and sub-picosecond flat-top pulse generation using uniform long-period fiber gratings," Opt. Express **14**, 12670-12678 (2006).

[54] L. Oxenlowe, R. Slavik, M. Galili, H. Mulvad, A. Clausen, Y. Park, J. Azana and P. Jeppesen, "640 Gb/s timing jitter-tolerant data processing using a long-period fiber-gratingbased flat-top pulse shaper," ," IEEE J. Quantum Electron. **14**, 566-572 (2008).

[55] V. Torres-Company, J. Lands, and P. Andres, "Incoherent frequency-to-time mapping: Application to incoherent pulse shaping," J. Opt. Soc. Am. A **24**, 888-894 (2007).

[56] C. Dorrer, "Statistical analysis of incoherent pulse shaping," Opt. Express **17**, 3341-3352 (2009).

[57] J. Capmany, J. Mora, I. Gasulla, J. Sancho, J. Lloret and S. Sales, "Microwave photonic signal processing," J. Lightwave Technol. **31**, 571-586 (2013).

[58] A. Malacarne, R. Ashrafi, Y. Park, and J. Azaña, "Reconfigurable optical differential phase-shift-keying pattern recognition based on incoherent photonic processing," Opt. Lett. **36**, 4290-4292 (2011).

[59] A. V. Oppenheim and A. S. Willsky, Signals and systems, Upper Saddle River, NJ, USA: Prentice-Hall, 2nd edn. (1997).

[60] T. T. Ng, F. Parmigiani, M. Ibsen, Z. Zhang, P. Petropoulos, and D. J. Richardson, "Compensation of linear distortions by using XPM with parabolic pulses as a time lens," IEEE Photon. Technol. Lett. **20,** 1097-1099 (2008).

[61] C. Finot, S. Pitois, and G. Millot, "Regenerative 40 Gbit/s wavelength converter based on similariton generation," Opt. Lett. **30**, 1776-1778 (2005).

[62] R. Maram and J. Azaña, "Spectral self-imaging of time-periodic coherent frequency combs by parabolic cross-phase modulation" Opt. Express **21**, 28824- 28835 (2013).

[63] A. Rashidinejad, Y. Li and A. M. Weiner, "Recent advances in programmable photonic-assisted ultrabroadband radio-frequency arbitrary waveform generation," IEEE J. Quantum Electron. **52**, 1-17 (2016).

[64] J. Azaña, N. K. Berger, B. Levit, and B. Fischer, "Reconfigurable generation of high-repetition-rate optical pulse sequences based on timedomain phase-only filtering," Opt. Lett. **30**, 3228-3230 (2005).

[65] S. Thomas, A. Malacarne, F. Fresi, L. Potì, A. Bogoni, and J. Azaña, " Programmable fiber-based picosecond optical pulse shaper using time-domain binary phase-only linear filtering," Opt. Lett. **34**, 545-547 (2009).

[66] A. M. Weiner, S. Oudin, D. E. Leaird, and D. H. Reitze, ''Shaping of femtosecond pulses using phase-only filters designed by simulated annealing,'' J. Opt. Soc. Am. A **10**, 1112-1120 (1993).

[67] Andy Rundquist, Anatoly Efimov, and David H. Reitze, "Pulse shaping with the Gerchberg–Saxton algorithm," J. Opt. Soc. Am. B **19**, 2468-2478 (2002)

[68] R. L. Haupt and S. E. Haupt, Practical genetic algorithms, New York, NY, USA: Wiley, 2nd ed. (2004).

[69] S. Thomas, A. Malacarne, F. Fresi, L. Poti, and J. Azaña, "Fiber-based programmable picosecond optical pulse shaper," J. Lightwave Technol. 28, 1832-1843 (2010).

[70] Finistar, “ Finistar 4000S,” [Online]. Available: https://www.finisar.com/sites/default/files/downloads/waveshaper_12page_product_brochure_09_16_3.pdf [Accessed 12 03 2018].

[71] J. Capmany D. Novak "Microwave photonics combines two worlds" Nat. Photonics **1**, 319-330 (2007).

[72] A. Seeds "Microwave photonics," IEEE Trans. Microwave Theory Tech. **50**, 877-887 (2002).

[73] J. Yao "Microwave photonics," IEEE J. Lightwave Technol. **27**, 314-335 (2009).

[74] B. E. A. Saleh and M. C. Teich, Fundamentals of photonics, New York, NY, USA: Wiley, 2nd edn. (2013).

[75] J. Azana and M. A. Muriel, “Real-time optical spectrum analysis based on the time-space duality in chirped fiber gratings,” IEEE J. Quantum Electron. **36**, 517-526 (2000).

[76] J. Chou, Y. Han, and B. Jalali, “Adaptive RF-photonic arbitrary waveform generator,” IEEE Photon. Technol. Lett. **15**, 581-583 (2003).

[77] R. Kashyap, Fiber Bragg gratings, New York, NY, USA: Academic, 2nd edn. (2009).

[78] Keysight Technologies, “M8196A 92 GSa/s Arbitrary waveform generator” [Online]. Available: http://literature.cdn.keysight.com/litweb/pdf/5992-0971EN.pdf [Accessed 10 07 2018].

[79] B. H. Kolner, "Space-time duality and the theory of temporal imaging," IEEE J. Quantum Electron. **30**, 1951-1963 (1994).

[80] R. Salem, M. A. Foster, and A. L. Gaeta, “Application of space–time duality to ultrahigh-speed optical signal processing,” Adv. Opt. Photonics **5**, 274-317 (2013).

[81] X. Fang, D. N. Wang and S. Li, "Fiber Bragg grating for spectral phase optical code-division multiple-access encoding and decoding," J. Opt. Soc. Am. B **20**, 1603-1610 (2003).

[82] J. A. Salehi, A. M. Weiner and J. P. Heritage, "Coherent ultrashort light pulse code-division multiple access communication systems," J. Lightwave Technol. **8**, 478-491 (1990).

[83] Z. Jiang, D. S. Seo, S.-D. Yang, D. E. Leaird, R. V. Roussev, C. Langrock, M. M. Fejer and A. M. Weiner, "Four-user, 2.5-Gb/s, spectrally coded OCDMA system demonstration using low-power nonlinear processing," J. Lightwave Technol. **23**, 143-158 (2005).

[84] P. C. Teh, M. Ibsen, J. H. Lee, P. Petropoulos and D. J. Richardson, "Demonstration of a four-channel WDM/OCDMA system using 255-chip 320-Gchip/s quarternary phase coding gratings," IEEE Photon. Technol. Lett. **14**, 227-229 (2002).

[85] X. Lu and R. T. Chen, "Polymeric optical code-division multiple-access (CDMA) encoder and decoder modules," Polymers **3**, 1554-1564 (2011).

[86] M. A. Dugan, J. X. Tull, and W. S. Warren, "High-resolution acousto-optic shaping of unamplified and amplified femtosecond laser pulses," J. Opt. Soc. Am. B **14**, 2348-2358 (1997).

[87] M. Shirasaki, "Large angular dispersion by a virtually imaged phased array and its application to a wavelength demultiplexer" Opt. Lett. **21**, 366-368 (1996).

[88] 8. J. T. Willits, A. M. Weiner, and S. T. Cundiff, "Theory of rapid-update line-by-line pulse shaping," Opt. Express **16**, 315-327 (2008).

[89] M. Akbulut, S. Bhooplapur, I. Ozdur, J. Davila-Rodriguez, and P. J. Delfyett, "Dynamic line-by-line pulse shaping with GHz update rate," Opt. Express **18**, 18284-18291 (2010).

[90] S. Feng, C. Qin, K. Shang, S. Pathak, W. Lai, B. Guan, M. Clements, T. Su, G. Liu, H. Lu, R. P. Scott, and S. J. Ben Yoo, "Rapidly reconfigurable high-fidelity optical arbitrary waveform generation in heterogeneous photonic integrated circuits," Opt. Express **25**, 8872-8885 (2017).

[91] N. K. Fontaine, R. P. Scott, C. Yang, D. J. Geisler, J. P. Heritage, K. Okamoto, and S. J. B. Yoo, "Compact 10 GHz loopback arrayed-waveguide grating for high-fidelity optical arbitrary waveform generation," Opt. Lett. **33**, 1714-1716 (2008).

[92] N. K. Fontaine, D. J. Geisler, R. P. Scott, T. He, J. P. Heritage, and S. J. B. Yoo, "Demonstration of high-fidelity dynamic optical arbitrary waveform generation," Opt. Express **18**, 22988-22995 (2010).

[93] J. Wang H. Shen L. Fan R. Wu B. Niu L. T. Varghese Y. Xuan D. E. Leaird X. Wang F. Gan A. M. Weiner, and M. Qi, "Reconfigurable radio-frequency arbitrary waveforms synthesized in a silicon photonic chip," Nature Commun. **6**, 5957 (2015).

[94] N. K. Fontaine, R. P. Scott, S.J.B. Yoo, "Dynamic optical arbitrary waveform generation and detection in InP photonic integrated circuits for Tb/s optical communications," Opt. Commun. **284**, 3693-3705 (2011).

[95] A. J. Metcalf, H. Kim, D. E. Leaird, J. A. Jaramillo-Villegas, K. A. McKinzie, V. Lal, A. Hosseini, Gloria E. Hoefler, F. Kish, and A. M. Weiner, "Integrated line-by-line optical pulse shaper for high-fidelity and rapidly reconfigurable RF-filtering," Opt. Express **24**, 23925-23940 (2016).

[96] H. Takahashi, S. Suzuki, K. Kato, and I. Nishi, "Arrayed-waveguide grating for wavelength division multi/demultiplexer with nanometre resolution," Electron. Lett. **26**, 87-88 (1990).

[97] R. E. Saperstein and Y. Fainman, "Information processing with longitudinal spectral decomposition of ultrafast pulses," Appl. Opt. **47**, A21-A31 (2008).

[98] J. Huh and J. Azaña, "Generation of high-quality parabolic pulses with optimized duration and energy by use of dispersive frequency-to-time mapping," Opt. Express **23**, 27751-27762 (2015).

[99] K. Tamura and M. Nakazawa, "Pulse compression by nonlinear pulse evolution with reduced optical wave breaking in erbium-doped fiber amplifiers," Opt. Lett. **21**, 68-70 (1996).

[100] A. Malinowski, A. Piper, J. H. V. Price, K. Furusawa, Y. Jeong, J. Nilsson, and D. J. Richardson, "Ultrashort-pulse Yb3+-fiber-based laser and amplifier system producing > 25-W average power," Opt. Lett. **29**, 2073-2075 (2004).

[101] C. Billet, J. M. Dudley, N. Joly, and J. C. Knight, "Intermediate asymptotic evolution and photonic bandgap fiber compression of optical similaritons around 1550 nm," Opt. Express **13**, 3236-3241 (2005).

[102] T. Schreiber, C. K. Nielsen, B. Ortac, J. P. Limpert, and A. Tünnermann, "Microjoule-level all-polarization-maintaining femtosecond fiber source," Opt. Lett. **31**, 574-576 (2006).

[103] P. Dupriez, C. Finot, A. Malinowski, J. K. Sahu, J. Nilsson, D. J. Richardson, K. G. Wilcox, H. D. Foreman, and A. C. Tropper, "High-power, high repetition rate picosecond and femtosecond sources based on Yb-doped fiber amplification of VECSELS," Opt. Express **14**, 9611-9616 (2006).

[104] D. N. Papadopoulos, Y. Zaouter, M. Hanna, F. Druon, E. Mottay, E. Cormier, and P. Georges, "Generation of 63 fs 4.1 MW peak power pulses from a parabolic fiber amplifier operated beyond the gain bandwith limit," Opt. Lett. **32**, 2520-2522 (2007).

[105] J. W. Nicholson, A. Yablon, P. S. Westbrook, K. S. Feder, and M. F. Yan, "High power, single mode, all-fiber source of femtosecond pulses at 1550 nm and its use in supercontinuum generation," Opt. Expres **12**, 3 3025-3034 (2004).

[106] K. Hammani, C. Finot, S. Pitois, J. Fatome, and G. Millot, "Real-time measurement of long parabolic optical similaritons," Electron. Lett. **44**, 1239-1240 (2008).

[107] C. Finot, G. Millot, C. Billet, and J. M. Dudley, "Experimental generation of parabolic pulses via Raman amplification in optical fiber," Opt. Express **11**, 1547-1552 (2003).

[108] F. Parmigiani, P. Petropoulos, M. Ibsen, and D. J. Richardson, "Pulse retiming based on XPM using parabolic pulses formed in a fiber Bragg grating," IEEE Photon. Technol. Lett. **18**, 829-831 (2006).

[109] T. Hirooka and M. Nakazawa, "Parabolic pulse generation by use of a dispersion-decreasing fiber with normal group-velocity dispersion," Opt. Lett. **29**, 498-500 (2004).

[110] A. Latkin, S. K. Turitsyn, and A. Sysoliatin, "Theory of parabolic pulse generation in tapered fibre," Opt. Lett. **32**, 331-333 (2007).

[111] S. Zhang, G. Zhao, A. Luo, and Z. Zhang, "Third-order dispersion role on parabolic pulse propagation in dispersion-decreasing fiber with normal group-velocity dispersion," Appl. Phys. B **94**, 227-232 (2008).4.

[112] T. Hirooka, M. Nakazawa, and K. Okamoto, "Bright and dark 40 GHz parabolic pulse generation using a picosecond optical pulse train and an arrayed waveguide grating," Opt. Lett. **33**, 1102-1104 (2008).

[113] D. Nguyen, M. U. Piracha, D. Mandridis, P. J. Delfyett, "Dynamic parabolic pulse generation using temporal shaping of wavelength to time mapped pulses," Opt. Express **19**, 12305-12311 (2011).

[114] A. Dezfooliyan and A. M. Weiner, "Photonic synthesis of high fidelity microwave arbitrary waveforms using near field frequency to time mapping," Opt. Express **21**, 22974-22987 (2013).

[115] V. Torres-Company, D. E. Leaird, and A. M. Weiner, "Dispersion requirements in coherent frequency-to-time mapping," Opt. Express **19**, 24718- 24729 (2011).

[116] V. J. Hernandez, C. V. Bennett, B. D. Moran, A. D. Drobshoff, D. Chang, C. Langrock, M. M. Fejer, and M. Ibsen, "104 MHz rate single-shot recording with subpicosecond resolution using temporal imaging," Opt. Express **21**, 196-203 (2013).

[117] O. Kuzucu, Y. Okawachi, R. Salem, M. A. Foster, A. C. Turner-Foster, M. Lipson, and A. L. Gaeta, "Spectral phase conjugation via temporal imaging," Opt. Express **17**, 20605-20614 (2009).

[118] P. Guan, K. M. Rege, T. Morioka, and L. K. Oxenløwe, "Time lens based optical Fourier transformation for advanced processing of spectrally-efficient OFDM and N-WDM signals," in *2016 Optical Fiber Communication conference* (OFC), Anaheim, CA, USA, paper Th3H.1.

[119] Z. Wu, L. Lei, J. Dong, J. Hou and X. Zhang, "Reconfigurable temporal fourier transformation and temporal Imaging," J. Lightw. Technol. **32**, 4565-4570 (2014).

[120] L. Lei, J. Huh, L. R. Cortés, R. Maram, B. Wetzel, D. Duchesne, R. Morandotti, and J. Azaña, "Observation of spectral self-imaging by nonlinear parabolic cross-phase modulation," Opt. Lett. **40**, 5403-5406 (2015).

[121] J. Azaña, N. K. Berger, B. Levit, and B. Fischer, "Simplified temporal imaging systems for optical waveforms," IEEE Photon. Technol. Lett. **17**, 94-96 (2005).

[122] C. B. Huang, D. E. Leaird, A. M. Weiner, "Time-multiplexed photonically enabled radio-frequency arbitrary waveform generation with 100 ps transitions," Opt. Lett. **32**, 3242-3244 (2007).

[123] P. K. Kondrotko, A. Leven, Y. K. Chen, J. Lin, U. V. Koc, K. Y. Tu, and J. Lee, "12.5-GHz Optically sampled interference-based photonic arbitrary waveform generator," IEEE Photon. Technol. Lett. **17**, 2727-2729 (2005).

[124] F. Parmigiani, P. Petropoulos, M. Ibsen, P. J. Almeida, T. T. Ng, and D. J. Richardson, "Time domain add-drop multiplexing scheme enhanced using a saw-tooth pulse shaper," Opt. Express **17**, 8362-8369 (2009).

[125] J. P. Heritage and A. M. Weiner, "Advances in spectral optical code division multiple-access communications," IEEE J. Sel. Top. Quantum Electron. **13**, 1351-1369 (2007).

[126] R. W. Gerchberg and W. O. Saxton, "A practical algorithm for the determination of phase from image and diffraction plane pictures," Optik **35**, 237-246 (1972).

[127] Y. Park, F. Li and J. Azaña, "Characterization and optimization of optical pulse differentiation using spectral interferometry," IEEE Photon. Technol. Lett. **18**, 1798-1800 (2006).

[128] J. R. Quagliano, P. O. Stoutland, R. R. Petrin, R. K. Sander, R. J. Romero, M. C. Whitehead, C. R. Quick, J. J. Tiee, and L. J. Jolin, "Quantitative chemical identification of four gases in remote infrared (9–11 μm) differential absorption lidar experiments," Appl. Opt. **36**, 1915-1927 (1997).

[129] J. Hult, R. S. Watt, and C. F. Kaminski, “High bandwidth absorption spectroscopy with a dispersed supercontinuum source.” Opt. Express **15**, 11385-11395 (2007).

[130] A. Sakudo, “Near-infrared spectroscopy for medical applications: Current status and future perspectives,” Clin. Chim. Acta **455**, 181-188 (2016).

[131] S. J. B. Yoo, “Optical packet and burst switching technologies for the future photonic Internet,” J. Lightwave. Technol. **24**, 4468-4492 (2006).

[132] H. Cen, Y. He, “Theory and application of near infrared reflectance spectroscopy in determination of food quality,” Trends Food Sci. Technol. **18**, 72-83 (2007).

[133] J. Luypaert, D.L. Massart, Y. Vander Heyden, “Near-infrared spectroscopy applications in pharmaceutical analysis,” Talanta **72**, 865-883 (2007).

[134] D. R. Solli, J. Chou, and B. Jalali, “Amplified wavelength-time transformation for real-time spectroscopy,” Nat. Photonics **2**, 48-51 (2008).

[135] S. Kim, K. Goda, A. Fard, and B. Jalali, "Optical time-domain analog pattern correlator for high-speed real-time image recognition," Opt. Lett. **36**, 220-222 (2011).

[136] S. Shin, U. Sharma, H. Tu, W. Jung, and S. A. Boppart, “Characterization and analysis of relative intensity noise in broadband optical sources for optical coherence tomography,” IEEE Photon. Technol. Lett. **22**, 1057-1059 (2010).

[137] A. Malacarne, R. Ashrafi, M. Li, S. LaRochelle, J. Yao, and J. Azaña, "Single-shot photonic time-intensity integration based on a time-spectrum convolution system," Opt. Lett. 37, 1355-1357 (2012).

APPENDIX A

Time-spectrum convolution

The operation principles of the time-spectrum convolution (TSC) with mathematical derivation are also well-explained in the Ref. [28]. The complex electric field of an individual angular frequency component of an incoming incoherent light source $a_{in,\omega}(t)$ can be mathematically described as follows [56]

$$a_{in,\omega}(t) = \sqrt{S_{inc}(\omega)}\exp[j\phi_{inc}(\omega)]\exp[j\omega t], \tag{A.1}$$

where $S_{inc}(\omega)$ is the spectral density of the incoherent light source, $\phi_{inc}(\omega)$ is the random phase variable, representing the random correlation among the frequency components associated with the light source. The amplitude of the incoming light is temporally modulated by a RF signal $m(t)$, and then the modulated signal propagates a linear dispersive medium with dispersion coefficient $\ddot{\Phi}$, which provides the spectral phase response of $\exp\left[-j\frac{1}{2}\ddot{\Phi}\omega^2\right]$, as discuussed in Section 1.3.3. The output complex electric field of a single frequency component can be expressed as

$$a_{out,\omega}(t) = m_{chirp}(t-\tau_g(\omega))\sqrt{S_{inc}(\omega)}\exp[j\phi_{inc}(\omega)]\exp[j\omega t], \tag{A.2}$$

where $m_{chirp}(t) = \frac{1}{2\pi}\int M(\omega)\exp\left[-j\frac{1}{2}\ddot{\Phi}\omega^2\right]\exp[j\omega t]d\omega$, which stands for the chirped modulation signal after the dispersion. $\tau_g(\omega)$ represents the group delay of the corresponding frequency, i.e.,

$$\tau_g(\omega) = -\left.\partial\left(-\frac{1}{2}\ddot{\Phi}\omega^2\right)\right/_{\partial\omega} = \ddot{\Phi}\omega. \tag{A.3}$$

Then, the averaged/photodetected output signal $I_{PD}(t)$ is an intensity sum of Eq. (A.2) for all frequency components associated with the incoherent light, which can be expressed as

$$I_{PD}(t) = \int_{-\infty}^{\infty} S_{inc}(\omega)\left|m_{chirp}(t-\ddot{\Phi}\omega)\right|^2 d\omega, \tag{A.4}$$

Given that the waveform distortion of the modulation signal is negligible due to the relatively narrow-band modulation signal ω_m, i.e., $m_{chirp}(t) \approx m(t)$. Similar to frequency-to-time mapping in

Section 1.3.3, the dispersion-induced group delay τ_g linearly distributes the frequency components in the temporal domain, and then the Eq. (A.4) can be rewritten as

$$I_{PD}(t) \approx \frac{1}{\ddot{\Phi}} \int_{-\infty}^{\infty} S_{inc}\left(\frac{t'}{\ddot{\Phi}}\right) |m(t-t')|^2 dt'$$
$$\propto S_{inc}\left(\frac{t'}{\ddot{\Phi}}\right) \otimes |m(t-t')|^2, \quad \text{(A.5)}$$

where $\otimes$ denotes the convolution. Thus, the averaged temporal intensity waveform at the output of the dispersive medium is proportional to the time-domain convolution between the time-mapped version of the energy spectrum of the incoherent light and the temporal intensity modulation signal.

APPENDIX B

Gerchberg-Saxton algorithm

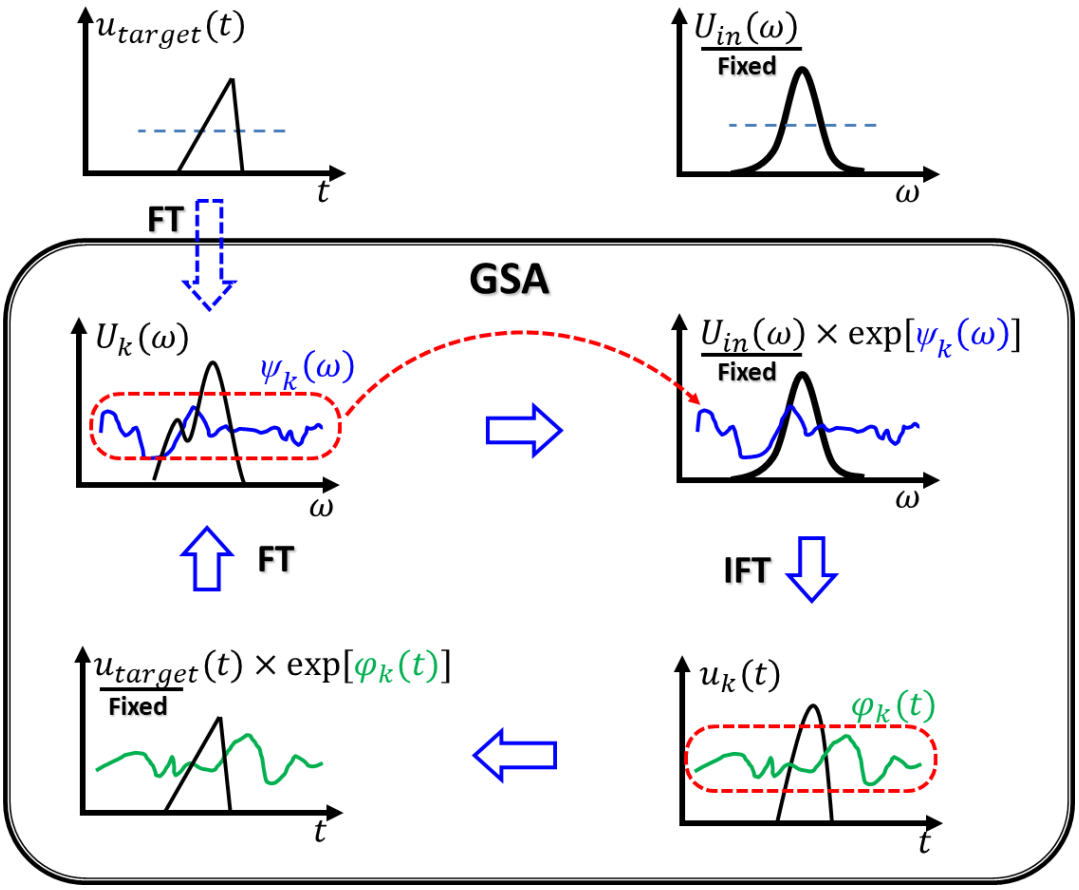

Figure B.1 **Illustration of Gerchberg-Saxton algorithm (GSA) based optical pulse shaping.**

As discussed, GSA enables to retrieve the required phase information for the synthesis of target temporal intensity profile $\left|u_{target}(t)\right|^2$ based on an iterative-Fourier technique when the input spectral amplitude and phase $U_{in}(\omega)$ are given [69]. In this technique, the required spectral phase profile is obtained by continuously switching between the conjugate Fourier domain while updating a temporal/spectral phase profile to the fixed target temporal amplitude profile and the input spectral amplitude. For instance, the initial spectral phase profile $\psi_k(\omega)|_{k=1}$ is obtained from the Fourier

transform of the target amplitude and then transferred to the input spectral amplitude, namely $U_{in}(\omega)\exp[\psi_k(\omega)]$. The initial temporal phase profile $\varphi_k(t)|_{k=1}$ is retrieved from the inverse Fourier transform of the phase filtered input spectrum and then transferred to the target amplitude profile, i.e., $u_{target}(t) \times \exp[\varphi_k(t)]$. This process should be repeated until a synthesized amplitude profile $u_k(t)$ matches well with the target amplitude profile. In **Chapter 3**, only a few tens of iterations were sufficient to develop an acceptable intermediate spectral phase profile (initial generation used in the subsequent optimization GA).